



Skolkovo Institute of Science and Technology

ERGODIZATION DYNAMICS OF  
THE GROSS-PITAEVSKII EQUATION  
ON A LATTICE

*Doctoral Thesis*

by

ANDREI E. TARKHOV

DOCTORAL PROGRAM IN PHYSICS

Supervisor

Associate Professor Dr. Boris V. Fine

Moscow — 2020

©Andrei E. Tarkhov 2020

I hereby declare that the work presented in this thesis was carried out by myself at Skolkovo Institute of Science and Technology, Moscow, except where due acknowledgment is made, and has not been submitted for any other degree.

Candidate (Andrei E. Tarkhov)

Supervisor (Associate Prof. Dr. Boris V. Fine)

# Abstract

The dynamical foundations of statistical physics are based on the assumptions that a typical interacting many-particle system is chaotic and ergodic. The classical definitions of chaos and ergodicity rely on the notion of phase space trajectories. This definition is impractical for diagnosing chaos experimentally in many-particle systems because it is impossible to track all phase space coordinates of the system in a physical experiment. It therefore remains unclear how to demonstrate chaoticity of an interacting many-particle system. In addition, there are conceptual problems with generalizing the notions of chaos and ergodicity to quantum systems. In the broader context of dynamic thermalization, there is a consensus that a typical interacting many-particle system does equilibrate after a sufficiently long time. However, the quantitative description of this process is still a challenge for relaxation from a far-from-equilibrium state (quench). The above issues are addressed in the present Thesis in the context of the dynamics of the discrete Gross-Pitaevskii equation on a lattice. This equation can describe coupled Bose-Einstein condensates on optical lattices, and other systems with mathematically similar order parameters, such as superconductors or charge-density-wave materials.

In this Thesis:

1. We propose an experimentally realizable method for demonstrating the primary characteristic of chaos, namely the Lyapunov instability. The method is based on monitoring equilibrium noise of virtually any observable quantity before and after time reversal of dynamics (Loschmidt echo), from which, following the proposed procedure, one can extract the value of the largest Lyapunov exponent of the system.
2. We introduce a new characteristic time of ergodization as the time required to detect the largest Lyapunov exponent of the system. We further show that the quantity that needs to be monitored in order to extract this measure is the classical counterpart of the so-called quantum “out-of-time-order correlators” (OTOCs). Thereby, we show that the exponential growth rate of an OTOC

systematically exceeds the largest Lyapunov exponent, and further demonstrate that the difference between the two becomes smaller with the increase of the dimensionality of the lattice. We investigate this difference and show that it is proportional to the ergodization time of the system. We also propose a practical ergodicity test that can be implemented with the help of a Loschmidt echo.

3. We numerically study dynamical thermalization after thermal quenches across the second-order phase transition associated with a spontaneous symmetry breaking in the DGPE lattice. We show that topological defects significantly slow down the process of dynamical thermalization. At the same time, the dynamics of the system remains ergodic. Our simulations are used to describe laser-induced melting of the charge-density-wave order in a solid. The results are found to be in a good agreement with a recent experiment in  $\text{LaTe}_3$ .

The above results are obtained by a combination of analytical considerations and numerical simulations.

## Publications

1. Andrei E Tarkhov, Sandro Wimberger, and Boris V Fine. “Extracting Lyapunov exponents from the echo dynamics of Bose-Einstein condensates on a lattice”. In: *Physical Review A* 96 (2017), p. 023624
2. Andrei E Tarkhov and Boris V Fine. “Estimating ergodization time of a chaotic many-particle system from a time reversal of equilibrium noise”. In: *New Journal of Physics* 20.12 (2018), p. 123021
3. Andrei E. Tarkhov, Alexander Rozhkov, Alfred Zong, Anshul Kogar, Nuh Gedik, and Boris V. Fine. “The role of topological defects in the slowing down of recovery of a charge-density wave after laser-induced melting”. In: *in preparation* (2020)

*Dedicated to my mother*

## Acknowledgments

First of all, I would like to thank my parents for raising me in the harsh post-Soviet crisis times of Russia, and for securing for me the freedom of choice in what I want to be and what future I see for myself. I can imagine how hard it was to let me follow the chosen path, whose outcome neither you nor I could fully understand or predict. I am indebted to my parents for not tightening the screws and letting me be a shy thoughtful kid, and for supporting me and inflating my interest in exploring the world around me. I would not have been where I am now without my father, who taught me perseverance. I would also like to thank my siblings Dmitry, Pavel, Irina, niece Diana and nephew Lev, for always being around, believing in me and supporting me all this time. I love you all, and hope I have been doing well enough up to this point, and I know that you are and will be proud of me no matter what.

I am thankful to all the brilliant teachers I had, especially of my lyceum years—Oksana R. Mazurskaya, Svetlana L. Bazhenova, Vladimir I. Govyrin and Vladimir V. Sharkov—for having laid a solid multidisciplinary foundation for my future research. And to my research advisor at Moscow State University, the late Prof. Vladimir I. Emelyanov, who inspired and encouraged me to pursue my postgraduate studies and without whom I might have stepped off the scientific path after graduation. To Peter O. Fedichev for mentoring me in my move from physics towards a biotechnological career path.

I have been fortunate to have Prof. Boris V. Fine as my research advisor during the four years of my PhD. With his guidance, I have finally started gaining insights into how physics actually works. He has really spent a lot of time and made every effort to help me *understand* physics, which, from time to time, turned out to be excruciatingly slow and arduous, especially to restless me. His calm and consistent interest and assistance rendered our regular discussions a safe haven for my turbulent four-year journey into PhD, and helped redirect my anxiety to productive work.

I'd like to thank my co-authors and colleagues, Prof. Sandro Wimberger, Alexander Rozhkov, Prof. Nuh Gedik, Alfred Zong, Emre Ergeçen, Edoardo Baldini, Batyr Ilyas and Anshul Kogar for helpful discussions and insightful critique.

I am also happy to have worked along with my academic peers: Pavel Dolgirev, Asya Aristova, Grigory Starkov, Walter Hahn, Vivek Bhartiya, Egor Skorokhodov and Igor Ermakov. It was relaxing and fun to have all those discussions during the walks round the pond, it really helped overcome the feeling of isolation.

I don't think I would have come this far without my friends' support and acceptance: Anna Danilina, Nadya Belyaeva, Dima Doronin, Olga Gavrilenko, Ksenia Kiseleva, Alexander and Varya Sologub, Ivan and Yulia Kozhevnikov, Lena and Vladimir Avetyan, Yuri Pogorelov, Alexey Radkevich, Darya Ponomareva, Evgeny Bykov, Denis Bikkulov, Lyuda Kudryashova, Brandon Walker, Fabrice Le Blanc (also thanks for your help with proofreading the drafts of my Thesis) and many others. To Kirill Danilov for having been there for me for so long, even when I had messed up and hadn't really deserved it—I appreciate all what you've done for me, and I am sorry it ended up so painful. To my sweetheart, Vladimir Ternovykh for his constant love and support in the last year of my PhD while I've been balancing on the edge of a mental breakdown under the pressure of a recent break-up, towering workload, the uncertainty of my future academic and scientific career path: altogether complicated by my personal mental health issues.

Last but not least, I am grateful to Skoltech and its faculty for the given opportunity to learn, teach and carry out research.

This work was supported by a grant of the Russian Science Foundation (Project No. 17-12-01587).

# Contents

<b>1</b>	<b>Introduction</b>	<b>14</b>
1.1	Foundations of Statistical Physics . . . . .	14
1.2	Classical chaos and Lyapunov exponents . . . . .	17
1.3	Loschmidt echoes and out-of-time-order correlators (OTOCs) . . . . .	18
1.4	Microcanonical thermodynamics . . . . .	22
1.5	Discrete Gross-Pitaevskii equation (DGPE) . . . . .	23
1.6	Dynamic and thermodynamic properties of the DGPE . . . . .	26
1.7	Topological defects in lattice systems . . . . .	27
1.8	Thesis structure . . . . .	29
<b>2</b>	<b>Experimentally realizable method for extracting Lyapunov exponents in an interacting many-particle system</b>	<b>30</b>
2.1	Lyapunov exponent from Loschmidt echo: general idea . . . . .	31
2.2	Formulation of the problem . . . . .	34
2.3	Numerical algorithm . . . . .	35
2.3.1	Direct calculation of the largest Lyapunov exponent . . . . .	36
2.3.2	Loschmidt echo simulations . . . . .	38
2.4	Applicability of DGPE as a constraint on experimental implementation	39
2.5	Experimental Proposal . . . . .	40
2.5.1	Measurement of the quantity of interest . . . . .	40
2.5.2	Initial and final conditions . . . . .	41
2.5.3	Time-reversal of dynamics . . . . .	42
2.5.4	Lattice geometry . . . . .	43
2.6	Discussion . . . . .	43
<b>3</b>	<b>Extracting ergodization time from the Lyapunov process</b>	<b>44</b>
3.1	Ergodization time . . . . .	45
3.1.1	Definition of ergodization time based on the Lyapunov process	45
3.1.2	Ergodization time from Loschmidt echoes . . . . .	48
3.1.3	Independence of the choice of an observable . . . . .	50
3.1.4	Relation to OTOCs in quantum systems . . . . .	51
3.2	Extracting the ergodization time of DGPE lattices . . . . .	53
3.3	Criterion of ergodicity . . . . .	54
3.4	Numerical experiments . . . . .	56
3.5	Discussion . . . . .	58

---

<b>4 Investigation of non-equilibrium quenches across a second-order phase transition</b>	<b>59</b>
4.1 Experimental motivation . . . . .	59
4.2 Mapping charge-density wave dynamics to DGPE . . . . .	61
4.3 Model system . . . . .	67
4.4 Quenching protocol . . . . .	69
4.5 Simulation of non-equilibrium quenches . . . . .	70
4.6 Topological defects induced by the quench . . . . .	72
4.6.1 Definition of vorticity for the 3D DGPE lattice . . . . .	72
4.6.2 Monitoring the vorticity in the course of the quench . . . . .	74
4.7 Ergodization time estimates . . . . .	77
4.8 Discussion . . . . .	78
<b>5 Conclusions and outlook</b>	<b>82</b>
<b>Bibliography</b>	<b>84</b>

# List of Figures

1-1	Sketch of a slightly imperfect noise reversal with the illustrated behavior of an observable quantity of interest . . . . .	20
2-1	Sketch of a typical Loschmidt echo response . . . . .	33
2-2	Illustrations of the numerical routine for computing the largest Lyapunov exponent . . . . .	37
2-3	Loschmidt echo simulations for extracting the largest Lyapunov exponent . . . . .	38
3-1	Fluctuations of instantaneous stretching rates and the number of sites participating in the Lyapunov eigenvector . . . . .	46
3-2	Autocorrelation functions for instantaneous stretching rates . . . . .	47
3-3	Numerical test of an empirical conjecture required for extracting the ergodization time from monitoring a few observables . . . . .	53
3-4	Results of Loschmidt echo simulations for estimating the ergodization time . . . . .	55
3-5	Results of ergodicity tests for lattices of different dimensionality . . . . .	56
4-1	Time evolution of integrated intensity of the CDW electron diffraction peak after photo-excitation. Reproduced from an experimental paper . . . . .	60
4-2	Acoustic phonon dispersion relation for a CDW material . . . . .	62
4-3	Spontaneous symmetry breaking in the 3D DGPE lattice: energy density, specific heat and the order parameter as functions of temperature . . . . .	68
4-4	Spontaneous symmetry breaking in the 3D DGPE lattice: temperature, specific heat and the order parameter as functions of the energy density . . . . .	69
4-5	The non-equilibrium quench protocol across a spontaneous symmetry breaking in the 3D DGPE lattice . . . . .	69
4-6	System size scaling of post-quench relaxation in the 3D DGPE lattices . . . . .	71
4-7	Vorticity of a DGPE plaquette . . . . .	72
4-8	A non-contractible loop percolation as the reason for the symmetry breaking in the 3D DGPE lattice . . . . .	73
4-9	Mapping of the topological defects of the CDW and of the DGPE lattice . . . . .	75
4-10	Illustration of the role of topological defects in the slowing down of the order parameter's recovery in the 3D DGPE lattice . . . . .	75

---

4-11	Snapshots of vorticity for three individual quenches at the same post-quench time in the 3D DGPE lattice . . . . .	76
4-12	Snapshots of the time-evolution of vorticity for a strong quench in the 3D DGPE lattice . . . . .	79
4-13	Snapshots of the time-evolution of vorticity for a weak quench in the 3D DGPE lattice . . . . .	80
4-14	Estimating the ergodization time of the 3D DGPE lattice for the energy range containing a spontaneous symmetry breaking . . . . .	81

# List of Tables

2.1	Comparison of the largest Lyapunov exponents obtained from the direct calculation with those extracted from Loschmidt echoes . . . .	39
3.1	Summary of numerical tests for validation of the routine for extracting the ergodization time . . . . .	57

Never mind, the notion of trying to twirl time is a *trouvaille*; it resembles the neat formula a physicist finds to keep people happy until the next chap snatches the chalk.

—Vladimir Nabokov,  
Look at the Harlequins!

# Chapter 1

## Introduction

### 1.1 Foundations of Statistical Physics

The foundations of thermodynamics were laid in the 19th century by Carnot, Kelvin and Clausius [4–6]. Later, Maxwell and Boltzmann established the statistical foundations of the thermodynamic laws by applying Newtonian mechanics to, hypothetical at that time, molecules in gas [7, 8]. The daunting problem of solving the equations of motion for a colossal number of interacting particles (of the order of  $10^{23}$ ) was reduced to just a few variables by the introduction of several ingenious and intuitive assumptions about the microscopic dynamics in the thermodynamic equilibrium. Further cornerstones in the foundations of statistical physics were laid by Gibbs, Planck and Einstein [9–11], who extended the scope of statistical physics to radiation and condensed matter systems.

Given the relative simplicity of the basic assumptions of statistical physics, it is surprising that, for some of them, rigorous mathematical proofs or well-posed applicability limits have been actively debated for more than a century and still require further investigation.

Boltzmann and Gibbs used the “molecular chaos hypothesis” requiring the internal dynamics of a typical interacting many-body system to be chaotic and ergodic. Since the pioneering works of Poincare on the three-body problem [12], chaos theory has become a subject of active research. Lyapunov studied the stability of trajectories of dynamical systems to perturbations [13]. Now, a classical system is

called chaotic if its phase space trajectories are exponentially sensitive to infinitesimal perturbations. The exponents characterizing sensitivity are called Lyapunov exponents. The original assumption that the results of averaging over phase space and over time are equivalent for a physical observable—“the ergodic hypothesis”—has been actively disputed since the Poincaré recurrence theorem [12]. In 1930s, in the works by Birkhoff [14] and von Neumann [15], the mean and pointwise ergodic theorems were proven for special classes of dynamical systems.

Original debates over quantification of chaotic and ergodic properties of many-body systems had taken place before quantum mechanics was developed in 1920s. In many respects, quantum statistical physics relied on Gibbs’ classical statistical physics, which, at that moment, was already recognized as a well-developed theory. Classical statistical ensembles were straightforwardly generalized to quantum systems by replacing a classical Hamiltonian and observables with their quantum counterparts. Given that chaos and ergodicity require well-defined phase-space trajectories for their classical definition, it is more problematic to reintroduce these concepts for quantum systems for which the whole notion of phase space is poorly defined. The theories of quantum chaos [16] and quantum ergodicity [17] have been constantly advancing, but are mostly left out of scope of this Thesis.

While trying to derive the irreversibility of thermodynamic processes required by the second law of thermodynamics, Boltzmann introduced entropy as the H-function and proved that it would grow monotonically under the special assumption of molecular chaos and ergodicity. Yet, Loschmidt objected to the H-theorem by arguing that it is impossible to deduce irreversibility from fully time-reversible Newtonian mechanics. In Loschmidt’s *Gedankenexperiment* of reversing all velocities of molecules in a gas, a time-reversal of the system’s dynamics is achieved (Loschmidt echo), thus leading to a process with increasing H-function (decreasing entropy)—known as Loschmidt’s paradox. Experimentally, the Loschmidt echo was observed in NMR in the 1970s [18, 19]. Another debate over quantitative aspects of ergodicity dates back to the Poincaré recurrence theorem [12], stating that a dynamical system in a bounded phase space, after a sufficiently long time, is going to pass arbitrarily close to the initial point. The Zermelo paradox points at the H-function’s quasi-periodicity

stemming from the Poincaré recurrence theorem [20]—a direct contradiction to the Boltzmann H-theorem and the second law of thermodynamics.

However, as already noted by Boltzmann [21, 22] and since then became fairly obvious for the practitioners in the field [14, 23], the ergodization time of many-particle systems, defined via the Poincaré recurrence time, is impractically long to be observable on experimental timescales and, hence, to be relevant to measurable properties. Instead, a more practical, but less mathematically stringent criterion is usually used. Namely, a many-particle system is called “ergodic” as soon as it establishes the Boltzmann-Gibbs equilibrium on an experimentally observable timescale [24]. It still remains a challenge to define the corresponding ergodization time and to measure this time experimentally.

In the 1940s, Krylov studied relaxation processes in statistical systems [25, 26], and stressed that in real physical systems ergodicity *per se* is seldom present and the notion of chaotic mixing is more physically relevant. If one chooses a set of points in the phase space of a mixing system and tracks the evolution of this set over time, the set eventually spreads over the whole shell constrained by the energy and other integrals of motion. Its volume would be conserved due to the Liouville theorem.

The relation between mixing and ergodicity has been extensively studied in ergodic theory and produced the ergodic hierarchy classifying the properties of dynamic systems into five levels: ergodicity, weak mixing, strong mixing, Kolmogorov and Bernoulli, in the ascending order of randomness [24].

In the 1950s, Kolmogorov and Sinai introduced the concept of Kolmogorov-Sinai (KS) entropy, which is positive in a chaotic dynamical system. It is equal to the sum of all positive Lyapunov exponents of the system [27, 28]. The KS entropy is now used as a practical definition of a classical chaotic system: when a system has at least one positive Lyapunov exponent, it has a positive KS entropy. The KS entropy also gives an upper bound for the information entropy production rate (the Shannon entropy) of the process generated by a chaotic system [29–31]. The method of extracting the KS entropy from a time-series of an observable is laborious, but it was attempted with limited success for the Brownian motion [32–35] and for spin lattices [36]. In the 1960s, Sinai investigated dynamical billiards and proved that a

dynamical system can be both chaotic and ergodic [37, 38].

For more than half a century after the original works of Maxwell, Boltzmann and Gibbs, only analytical methods were available, which limited rigorously treatable model systems to few-body or special kinds of analytically solvable many-body systems. By the mid-20th century, the direct numerical simulations of nonlinear many-body systems became possible. In 1953, the work of Fermi, Pasta, Ulam and Tsingou was the first attempt to numerically investigate ergodicity and thermalization in chains of nonlinear classical oscillators [39]. Since then, numerical simulations serve as an indispensable tool for testing the foundations of statistical physics.

In this Thesis, we investigate the ergodicity and the dynamic thermalization of the discrete Gross-Pitaevskii equation (DGPE) on one-, two- and three-dimensional lattices. The DGPE describes the quasi-classical regime of Bose-Einstein condensates on optical lattices and can be also applicable to the dynamics of superconductors, superfluids and charge-density-wave materials.

In the rest of this Chapter, we define the largest Lyapunov exponent of a chaotic dynamical system, discuss the Loschmidt echo and its quantum extension in the form of out-of-time-order correlators (OTOCs). Next, we will formally define the DGPE lattice and review the state-of-the-art knowledge about its dynamic and thermodynamic properties. This Chapter ends with the outline of the rest of the Thesis.

## 1.2 Classical chaos and Lyapunov exponents

In general, a conservative system with  $2V$ -dimensional phase space is characterized by a spectrum of  $V$  pairs of Lyapunov exponents of the same absolute value and opposite signs. The largest Lyapunov exponent,  $\lambda_{\max}$ , describes the average expansion rate along the direction of the corresponding eigenvector in tangential space.

A classical system is called chaotic if it has at least one positive Lyapunov exponent, hence it is exponentially sensitive to perturbations of initial conditions. In quantitative terms, this means that when two phase space trajectories  $\mathbf{R}_1(t)$  and  $\mathbf{R}_2(t)$  are initially infinitesimally close to each other, their separation from each

other,  $\delta\mathbf{R}(t) = \mathbf{R}_2(t) - \mathbf{R}_1(t)$ , after sufficiently long time is controlled by the largest positive Lyapunov exponent,  $\lambda_{\max}$ . The definition of the largest Lyapunov exponent reads

$$\lambda_{\max} \equiv \frac{1}{t} \lim_{t \rightarrow \infty, |\delta\mathbf{R}(0)| \rightarrow 0} \left( \log \frac{|\delta\mathbf{R}(t)|}{|\delta\mathbf{R}(0)|} \right). \quad (1.1)$$

If a chaotic dynamic system is ergodic, the largest Lyapunov exponent defined by Eq. (1.1) must not depend on the choice of the initial conditions on a shell of fixed integrals of motion and thus must be characteristic of the whole shell.

The definition (1.1) is not practical for numerical simulations because it, in general, requires unachievable computational precision. Instead, the standard numerical algorithm [40, 41] is usually used. This algorithm tracks two trajectories: the reference trajectory  $\mathbf{R}_1(t)$  and the slightly perturbed trajectory  $\mathbf{R}_2(t) = \mathbf{R}_1(t) + \delta\mathbf{R}(t)$ . The ratio  $\log \frac{|\delta\mathbf{R}(t)|}{|\delta\mathbf{R}(0)|}$  fluctuates in time as the reference trajectory  $\mathbf{R}_1(t)$  explores the energy shell. The algorithm uses the instantaneous stretching rates defined as  $\lambda(t) = \frac{d}{dt} \log \frac{|\delta\mathbf{R}(t)|}{|\delta\mathbf{R}(0)|}$ , and the largest Lyapunov exponent is then obtained as the average of instantaneous stretching rates over a sufficiently long time:  $\lambda_{\max} = \overline{\lambda(t)}$ .

In numerical simulations,  $\lambda_{\max}$  can be obtained from the direct calculations of the phase space trajectories  $\mathbf{R}_1(t)$  and  $\mathbf{R}_2(t)$ . However, such an approach is impractical experimentally, because it requires tracking all phase-space coordinates of the system. An alternative, more practical approach was proposed in Refs. [42]. That approach is based on monitoring the effect of Loschmidt echo on the equilibrium noise of almost any observable.

### 1.3 Loschmidt echoes and out-of-time-order correlators (OTOCs)

The Loschmidt echo is a time reversal of a system's dynamics, which can be realized in practice by reversing the sign of the system's Hamiltonian. In recent years, there has been a renaissance of theoretical and experimental interest in the Loschmidt echoes in the form of out-of-time-order correlators (OTOCs). Originally, the OTOCs

first appeared in the late 1960s in the work of Larkin and Ovchinnikov [43], yet not in the context of chaos. The pioneering works on the relation of OTOCs (in the form of Loschmidt echoes) and the Lyapunov exponents in classical and quantum spin lattices were done in the early 2010s [42, 44, 45]. In these works, the presence of exponential sensitivity of an OTOC for classical spin lattices, and quantum large-spin lattices was demonstrated in numerical simulations. At the same time, the study of quantum lattices of spin-1/2 [42] showed the absence of the exponential regime of the OTOC. However, the original works had drawn less attention than the subsequent works on the application of OTOCs to the problem of a bound on chaos in quantum systems by Kitaev [46] and Maldacena, Shenker and Stanford [47]. Those works conjectured that the largest Lyapunov exponent is limited by temperature,  $\lambda_{\max} \leq 2\pi k_B T/\hbar$ . After that, experimental probes of OTOCs in quantum many-body systems were implemented, for example, in nuclear spins [48] and trapped-ion quantum magnets [49, 50]. Also, OTOCs have drawn much theoretical attention and have been studied for different model systems: the quantum kicked rotator [51, 52], the quantum stadium billiard [53], the non-linear sigma model [54], the Dicke model [55], the Bose-Hubbard model [56] and many others [57–73].

In this Thesis, a version of the Loschmidt echo involving measuring equilibrium noise of an observable is considered, its quantum counterpart in the form of OTOC is also discussed. In Fig. 1-1, we outline the Loschmidt echo routine. It consists of the following steps.

(i) Measuring and recording the equilibrium noise of an observable  $\mathbf{X}$  as a function of time  $t$  for a system governed by Hamiltonian  $\mathcal{H}$ . At time  $\tau$ , reversing the sign of the Hamiltonian with a slight perturbation of the system at the moment of the Hamiltonian reversal, and measuring and recording the equilibrium noise after the reversal. The noise is to be denoted as  $\mathbf{X}(\tau - \Delta t)$  and  $\mathbf{X}(\tau + \Delta t)$ , where  $\Delta t = |t - \tau|$ .

(ii) Calculating the difference of the equilibrium noise of observable  $\mathbf{X}$  before and after slightly imperfect time reversal:

$$\Delta\mathbf{X}(\Delta t) \equiv \mathbf{X}(\tau + \Delta t) - \mathbf{X}(\tau - \Delta t). \quad (1.2)$$

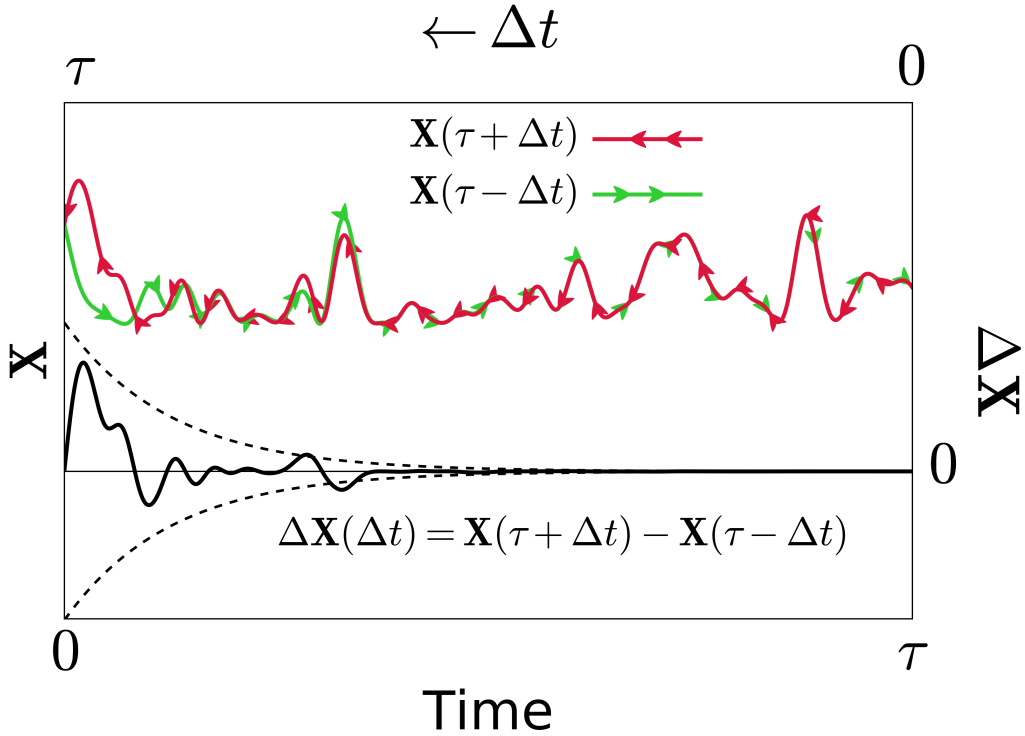


Figure 1-1: Sketch of a slightly imperfect noise reversal. Equilibrium noise of an observable  $\mathbf{X}$  before and after an imperfect time reversal of a system’s dynamics at time  $\tau$  is denoted, respectively, as  $\mathbf{X}(\tau - \Delta t)$  (green line) and  $\mathbf{X}(\tau + \Delta t)$  (red line), where  $\Delta t = |t - \tau|$ . In order to facilitate visual comparison, “Time” on the horizontal axis represents  $t$  before the time reversal and  $2\tau - t$  after the time reversal. The difference between the direct and the reversed noise  $\Delta\mathbf{X}(\Delta t) \equiv \mathbf{X}(\tau + \Delta t) - \mathbf{X}(\tau - \Delta t)$  (thick black line) fluctuates around 0. For a chaotic system, the envelope of  $\Delta\mathbf{X}(\Delta t)$  grows exponentially (dashed lines).

If the perturbation is infinitesimally small, the quantity  $\mathbf{X}(\tau + \Delta t)$  will be tracking the quantity  $\mathbf{X}(\tau - \Delta t)$ , while gradually departing from it as  $\Delta t$  increases.

(iii) Repeating the procedure of measuring  $\Delta\mathbf{X}(\Delta t)$  for an ensemble of randomly chosen initial conditions on an energy shell.

Defined by Eq. (1.2),  $\Delta\mathbf{X}(\Delta t)$  is the basic observable that will allow us to extract the chaotic and ergodic properties of a many-particle system. In Chapters 2 and 3, we will consider the Loschmidt echo for the equilibrium noise generated by the DGPE system, and show how to extract the largest Lyapunov exponent and estimate the ergodization time from it.

The quantum-mechanical description of Loschmidt echoes involves out-of-time-

order correlators (OTOCs) [42, 45, 49–52, 57, 58, 64, 65, 74, 75] having the form

$$\langle \hat{A}(0)\hat{B}(t)\hat{A}(0)\hat{B}(t) \rangle, \quad (1.3)$$

where  $\hat{A}(0)$  and  $\hat{B}(t)$  are two quantum operators taken at different times.

To illustrate the quantum-classical correspondence between the quantity of interest (1.2) in the Loschmidt echo routine and a quantum OTOC, let us consider

$$|\Delta \mathbf{X}(\Delta t)|^2 = 2\mathbf{X}^2 - \mathbf{X}(\tau + \Delta t)\mathbf{X}(\tau - \Delta t) - \mathbf{X}(\tau - \Delta t)\mathbf{X}(\tau + \Delta t). \quad (1.4)$$

We focus here on the last two terms. They are equal classically, but can become different in the quantum case, if  $\mathbf{X}(\tau - \Delta t)$  does not commute with  $\mathbf{X}(\tau + \Delta t)$ . Both of the terms become OTOCs in the quantum limit after calculating their quantum equilibrium averages. Below, we show this for  $\langle \mathbf{X}(\tau + \Delta t)\mathbf{X}(\tau - \Delta t) \rangle$ .

Let us consider a quantum system in equilibrium described at  $t = 0$  by Hamiltonian  $\hat{\mathcal{H}}$ . The thermal density matrix of the system is  $\hat{\rho}_0 \cong \exp\left(-\frac{\hat{\mathcal{H}}}{T}\right)$ . We are interested in the fluctuations of an observable quantity represented by quantum operator  $\hat{\mathbf{X}}$ . Let us further assume that the Hamiltonian changes sign at  $t = \tau$ , and, at the same moment of time, the system components experience an infinitesimally small random perturbation describable by quantum operator  $\hat{R}$  (see Ref. [42] for a concrete example). As a result, operator  $\hat{\mathbf{X}}$  evolves as

$$\hat{\mathbf{X}}(t) = \begin{cases} e^{i\hat{\mathcal{H}}t}\hat{\mathbf{X}}(0)e^{-i\hat{\mathcal{H}}t}, & t < \tau \\ e^{i\hat{\mathcal{H}}\tau}\hat{R}^+e^{-i\hat{\mathcal{H}}(t-\tau)}\hat{\mathbf{X}}(0)e^{i\hat{\mathcal{H}}(t-\tau)}\hat{R}e^{-i\hat{\mathcal{H}}t}, & t > \tau \end{cases}. \quad (1.5)$$

We now consider the quantum average

$$\langle \hat{\mathbf{X}}(\tau + \Delta t)\hat{\mathbf{X}}(\tau - \Delta t) \rangle \equiv \text{Tr} \left\{ \hat{\mathbf{X}}(\tau + \Delta t)\hat{\mathbf{X}}(\tau - \Delta t)\hat{\rho}_0 \right\},$$

which, with the help of Eq. (1.5) and a simple manipulation, can be transformed into

$$\langle \hat{\mathbf{X}}(\tau + \Delta t)\hat{\mathbf{X}}(\tau - \Delta t) \rangle = \text{Tr} \left\{ \hat{R}^+\hat{\mathbf{X}}(-\Delta t)\hat{R}\hat{\mathbf{X}}(-\Delta t)\hat{\rho}_0 \right\}. \quad (1.6)$$

Noting that  $\hat{\mathbf{X}}$ , as a physical observable, must be describable by a Hermitian operator, i.e.  $\hat{\mathbf{X}}^+(t) = \hat{\mathbf{X}}(t)$ , we rewrite Eq. (1.6) as  $\langle \hat{\mathbf{X}}(\tau + \Delta t)\hat{\mathbf{X}}(\tau - \Delta t) \rangle = \langle \hat{R}^+(0)\hat{\mathbf{X}}^+(-\Delta t)\hat{R}(0)\hat{\mathbf{X}}(-\Delta t) \rangle$ , which is the standard form of OTOC.

## 1.4 Microcanonical thermodynamics

The microcanonical ensemble is the ensemble of all points on the energy shell in the phase space of a dynamical system. The microcanonical temperature is defined as:

$$\beta \equiv \frac{1}{T} \equiv \frac{\partial S}{\partial E}, \quad (1.7)$$

where  $S$  is the microcanonical entropy proportional to the logarithm of the volume of the energy shell  $w(E)$ ,  $S \equiv \log \frac{w(E)}{(2\pi\hbar)^{V-\frac{1}{2}}}$ . In this Thesis, the Boltzmann's constant is set to be equal to unity,  $k_B \equiv 1$  (except for Chapter 4, where a mapping of the 3D DGPE lattice's properties to those of a real material is discussed). A recipe for calculating the microcanonical temperature from conservative dynamics was introduced in the pioneering works of Rugh [76, 77] and den Otter [78, 79]. The original definition of the dynamical temperature for an ergodic system reads:

$$\frac{1}{T(E)} \equiv \lim_{t \rightarrow \infty} \frac{1}{t} \int_0^t d\tau \Phi(\mathbf{R}(\tau)), \quad (1.8)$$

where  $\mathbf{R}(\tau)$  is a phase space trajectory and the observable

$$\Phi = \nabla \left( \frac{\nabla \mathcal{H}}{\|\nabla \mathcal{H}\|^2} \right), \quad (1.9)$$

is representative of the geometric properties of the Hamiltonian on the energy shell in the phase space.

Approaches similar to that of Rugh have been extensively used for Bose-Einstein condensates (BECs), which are often well isolated from the environment [80–83].

We adapt a numerical recipe, developed for classical spin lattices with one integral of motion [84] and consistent with Rugh's analytical approach [76, 77], to the calculation of the microcanonical temperature of the DGPE lattices with two integrals of motion. The original idea is to replace the functional in Eq. (1.9) with

its approximate numerical value by sampling the vicinity of the point in phase space  $\mathbf{R}(\tau)$ , and generating an ensemble of energy realizations, corresponding to each sample point. Then, by calculating the variance of energy fluctuations  $\langle \Delta E^2 \rangle$  and the mean fluctuation  $\langle \Delta E \rangle$ , one can extract the local approximation to  $\Phi(\mathbf{R})$  as

$$\Phi \equiv \frac{2\langle \Delta E \rangle}{\langle \Delta E^2 \rangle}. \quad (1.10)$$

We note that  $\langle \Delta E \rangle \neq 0$  due to the fact that, in general, there are exponentially more states above the energy shell than below it, which in turn reflects the fact that the entropy in Eq. (1.7) is proportional to the logarithm of the energy shell volume, and the temperature is positive. The temperature is then calculated as the time average of Eq. (1.10),  $1/T = \bar{\Phi}$ .

We use Eq. (1.10) with an additional constraint due to the fixed second integral of motion, the number of particles, hence, when sampling the vicinity of a phase space point, we sample only the vicinity on the shell of a fixed number of particles,  $\langle \dots \rangle_N$ , which gives

$$T = \frac{\langle \Delta E^2 \rangle_N}{2\langle \Delta E \rangle_N}. \quad (1.11)$$

From the same sampling, we can also obtain the chemical potential as

$$\mu = -T \frac{2\langle \Delta N \rangle_E}{\langle \Delta N^2 \rangle_E}. \quad (1.12)$$

## 1.5 Discrete Gross-Pitaevskii equation (DGPE)

The DGPE is a classical mean-field approximation for the single-orbital Bose-Hubbard model, which is defined by the Hamiltonian

$$\hat{\mathcal{H}}_{BH} = -J \sum_{\langle i,j \rangle} \hat{a}_i^+ \hat{a}_j + \frac{U}{2} \sum_i \hat{n}_i \hat{n}_i, \quad (1.13)$$

where  $\hat{a}_i^+$  and  $\hat{a}_i$  are the quantum creation and annihilation operators for site  $i$  respectively,  $\hat{n}_i \equiv \hat{a}_i^+ \hat{a}_i$  is the number of particles at site  $i$ ,  $J$  is the hopping parameter,  $U$  is the on-site interaction parameter, and the notation  $\langle i, j \rangle$  stands for the nearest-neighbor sites. For the single-orbital Bose-Hubbard model to be valid, the hopping

term  $J$  must be relatively small, so that the lattice potential is deep enough and, as a result, the gap  $\Delta_0$  between the lowest and the second lowest bands is sufficiently large [85, 86].

When the number of bosons in each potential well is sufficiently large, the following substitution:  $\hat{a}_i \rightarrow \psi_i$ ,  $\hat{a}_i^\dagger \rightarrow \psi_i^*$ ,  $\hat{n}_i \rightarrow n_i \equiv |\psi_i|^2$ , allows one to approximate the quantum Bose-Hubbard Hamiltonian (1.13) with the classical mean-field DGPE Hamiltonian:

$$\mathcal{H} = -J \sum_{\langle i,j \rangle} \psi_i^* \psi_j + \frac{U}{2} \sum_i |\psi_i|^4, \quad (1.14)$$

where  $\psi_j$  is a complex number, describing the order-parameter of a condensate at site  $j$ .  $J$  and  $U$  are two parameters, controlling the hopping and the nonlinear on-site interactions, respectively. The total number of sites, i.e. the lattice volume, is denoted by  $V$ , hence  $i = 1 \dots V$ .

The DGPE is the corresponding Hamilton's equations of motion for Hamiltonian (1.14):

$$i \frac{d\psi_j}{dt} = -J \sum_{k \in \text{NN}(j)} \psi_k + U |\psi_j|^2 \psi_j, \quad (1.15)$$

where the summation over  $j$  extends over the nearest-neighbors  $\text{NN}(i)$  of site  $i$ , the number of which for a  $d$ -dimensional cubic-like lattice is  $2d$ . The DGPE conserves the total energy  $E$  (the r.h.s. of Eq. (1.14)), as well as the total number of particles:

$$N \equiv \sum_{j=1}^V n_j = \sum_{j=1}^V |\psi_j|^2. \quad (1.16)$$

The microcanonical state of the DGPE system is naturally defined by the three parameters  $(E, N, V)$ . All of them are extensive. It is useful to introduce the corresponding intensive parameters: the energy density,

$$\varepsilon = E/V, \quad (1.17)$$

i.e. the energy per lattice site, and the particle density, i.e. the number of bosons

per lattice site,

$$n = N/V. \quad (1.18)$$

In the chaotic regime, the DGPE adequately approximates the quantum dynamics of the Bose-Hubbard model at the timescales of order of the Ehrenfest time:

$$\tau_E \sim \frac{1}{\lambda_{\max}} \log n, \quad (1.19)$$

which represents the typical timescale of washing out the classical chaotic dynamics due to quantum interference. In order to observe the exponential growth regime of the initial perturbation in a quantum system, the typical  $n$  should be, at least, of the order of  $10 \dots 100$ . In such a case, the Ehrenfest time would span several Lyapunov times, which is sufficient for the objectives of this Thesis.

To reduce the number of free parameters in simulations, it is further convenient to rescale  $\psi_j$ , such that the particle density is equal to unity,  $\tilde{\psi}_j = \psi_j/\sqrt{n}$ . Then Hamiltonian (1.14) reads:

$$\mathcal{H} = nJ \left( - \sum_{\langle i,j \rangle} \tilde{\psi}_i^* \tilde{\psi}_j + \frac{g}{2} \sum_i |\tilde{\psi}_i|^4 \right), \quad (1.20)$$

where  $g = Un/J$ . After the rescaling of time  $\tilde{t} = tJ$ , the corresponding dimensionless equations of motions can be written as

$$i \frac{d\tilde{\psi}_j}{d\tilde{t}} = - \sum_{k \in \text{NN}(j)} \tilde{\psi}_k + g |\tilde{\psi}_j|^2 \tilde{\psi}_j. \quad (1.21)$$

The phase space of a conservative dynamical system defined by Eqs. (1.21) is  $2V$ -dimensional.

## 1.6 Dynamic and thermodynamic properties of the DGPE

The DGPE has been studied in various contexts. It is usually called “DGPE”, when applied to Bose-Einstein condensates [87, 88]. In laser physics and nonlinear optics, it is rather known as the discrete nonlinear Schrödinger equation (DNLSE) [89, 90]. When the universality classes of the XY-model are studied, an analog of the DGPE is called the “soft-spin”  $O(2)$ , the “soft spin” XY, or the “soft spin”  $\varphi^4$  model [91–95]. The DGPE is a special case of a more general discrete self-trapping equation [96, 97].

Many results were obtained for 1D DGPE chains with nearest-neighbor interactions. Those include the absence of one-to-one correspondence between the microcanonical state variables,  $(\epsilon, n)$ , and the grand-canonical variables  $(\beta, \mu)$  in the thermodynamic limit [98]. There exist microcanonical states above the infinite grand-canonical temperature, which are accessible in microcanonical simulations. The important feature of those states is the presence of localized breather-like excitations that are almost decoupled from the rest of the system. The existence of breathers is proven to be a general property spanning beyond the DGPE to the time-reversible or Hamiltonian networks of weakly coupled oscillators [99]. They were observed in Bose-Einstein condensates in a one-dimensional optical lattice [100].

In the last two decades, the non-Gibbs states at energies higher than those corresponding to  $\beta = 0$  have been extensively studied. The idea of separating the system into two subsystems, a condensate and hot localized breathers above it, proved to be useful. In a series of papers, Rumpf analytically studied the microcanonical entropy of the 1D DGPE chain, linked the localization of energy to having two conserved quantities, and investigated a transition from a low-energy regime without breathers to a high-energy regime with breathers, and examined the metastability of breathers [101–103]. There is a non-zero activation energy for the excitation of breathers if the lattice dimension is larger than critical, which is the case for 3D lattices [104, 105]. A microcanonical study of the phase containing localized breathers showed that such states can have negative temperatures and, for 1D DGPE chains,

may equilibrate at times inaccessible in numerical simulations [106, 107]. Later, the slow relaxation times were linked to the second integral of motion, the norm conservation, and to a coarsening process where a higher breather gets less coupled to its background, thus its relaxation effectively becomes frozen [108–113]. However, later it was shown that the non-Gibbs states cannot be simply described by the Gibbs states with negative temperatures [114]. More complicated settings based on the DGPE have been also investigated, for example the DGPE with disorder [115], and the DGPE with dissipation or in contact with a thermal bath [109], but they are out of scope of this Thesis.

## 1.7 Topological defects in lattice systems

Topological defects in condensed matter physics have been studied since the prediction of existence of quantum vortices in superfluid helium by Onsager in 1949 [116]. More thoroughly, these vortices were described by Feynman in 1955 [117]. In 1957, Abrikosov [118] used the notion of vortices to explain type-II superconductivity. For this and related works, he received the Nobel Prize in 2003. The existence of vortices is a generic topological property caused by the fact that the superfluid order parameter has phase that can vary in space. The superfluid velocity is proportional to the gradient of phase, hence the velocity field is normally irrotational and its circulation within a closed loop in superfluid is zero. However, if the loop encircles a non-superfluid region, the circulation can be non-zero, which is equivalent to the presence of a vortex.

Vortices are topological objects. Their appearance in 2D XY-model leads to the Berezinskii-Kosterlitz-Thouless (BKT) transition [119–121], for which Kosterlitz and Thouless received the Nobel Prize in 2016. The BKT transition is of the infinite order. Recently, it was shown that the classical XY-models can be effectively simulated and controlled experimentally in the coupled arrays of exciton-polariton condensates [122, 123].

In 3D systems, vortices are linear rather than point-like objects. Therefore, the amount of energy much larger than  $T$  is required for them to appear. In the con-

text of the 3D DGPE lattices, the dimensionality of the lattice is 3, whereas the dimensionality of the order parameter of each condensate is 2, hence the topological defects in this systems have to be one-dimensional [124]. In practice, the topological defects in such systems either form closed-loop vortices, for example in systems with periodic boundary conditions, or form linear vortices terminating at open boundaries. The 3D DGPE model is in this respect similar to the three-dimensional  $O(2)$ ,  $U(1)$  and XY-models.

Vortex loops in 3D systems can possibly emerge when a temperature associated with a spontaneous symmetry breaking is crossed by non-adiabatic cooling. This is the so-called Kibble-Zurek mechanism originally introduced in the cosmological context [125–128]. When a system is driven across the temperature of spontaneous symmetry breaking at a finite rate, then, due to the critical fluctuations, it cannot fully equilibrate. Hence, space-separated uncorrelated domains of the ordered phase emerge. The topological defects are then formed once the domains become smoothly connected.

Once the topological defects appear in the system, they may lead to glassy dynamics associated with the extreme slowing down of relaxation [129–132]. This occurs due to high activation barriers for the annihilation of topological defects [133]. Such a glassy system has long dynamical memory and can experience aging phenomena [134].

In the 3D XY-model and the 3D  $O(2)$  model in equilibrium, the percolation of vortex loops is responsible for a phase transition and a symmetry breaking [135–137]. In the context of high- $T_c$  superconductors, the role of vortex-loop interactions was studied in Refs. [138, 139].

The non-equilibrium properties of vortex loops and the phase-ordering kinetics have been also studied for the  $O(n)$  and the XY-models in continuous space [140–145]. For the continuous 3D Gross-Pitaveskii equation, vortex tangles can emerge, after non-equilibrium quenches, which leads to a significant slowing down of the condensate formation [146–149]. Various versions of Gross-Pitaevskii equations were used for simulating turbulence and vortex rings [150–159]. Long-lived vortices were also observed in the simulations of a trapped quantum gas with the help

of a stochastic version of the Gross-Pitaevskii equation [160]. The experiments with Bose-Einstein condensates showed evidence of the spontaneous formation of vortices and topological defects [161–164].

## 1.8 Thesis structure

The outline of the rest of this Thesis is the following.

**Chapter 2 - Extracting Lyapunov exponents** A method for extracting the largest Lyapunov exponent from monitoring the equilibrium noise of the DGPE lattices after an imperfect time-reversal of the dynamics (Loschmidt echo) is proposed and validated numerically.

**Chapter 3 - Estimating ergodization time** A method for estimating the ergodization time of a many-particle system from Loschmidt echoes is proposed and validated numerically for the DGPE lattices. The relation of this method to OTOCs is established.

**Chapter 4 - Non-equilibrium quenches** Non-equilibrium quenches across the ordering phase transition of 3D DGPE lattices are simulated. The role of closed-loop vortices in slowing down the recovery of the order parameter is analyzed. The scaling of the order-parameter recovery time with the lattice size is obtained.

**Chapter 5 - Conclusions and outlook**

Nobody can imagine in physical terms the act of reversing the order of time. Time is not reversible. Reverse motion is used in films only for comic effects—the resurrection of a smashed bottle of beer.

—Vladimir Nabokov,  
Look at the Harlequins!

## Chapter 2

# Experimentally realizable method for extracting Lyapunov exponents in an interacting many-particle system

One of the outstanding issues of the foundations of modern statistical physics is how to produce experimental evidence that a typical many-particle system is indeed chaotic. The practical challenge here is that it is impossible: first, to monitor all phase space coordinates of a many-body system and, second, to prepare initial conditions with very high accuracy required for extracting Lyapunov exponents. A method of extracting the largest Lyapunov exponent of a many-particle classical system without using full phase space trajectories was proposed in Ref. [42]. The method is based on the Loschmidt echo for the equilibrium noise of an observable (see Section 1.3). In Ref. [42], the possibility to extract the largest Lyapunov exponent was demonstrated for a lattice of classical spins, whereas, in the present Chapter, we generalize the same analysis to a system of coupled Bose-Einstein condensates (BEC) on a lattice in the classical regime describable by the DGPE. In other words, we consider the classical dynamics of this system, despite the fact that the system is of quantum origin. The advantage of coupled Bose-Einstein condensates over classical spins is that the former were already realized experimentally. In particular, Struck et al. [165] have recently performed an experimental simulation of frustrated classical magnetism using Bose-Einstein condensates of ultracold

atoms. However, Ref. [165] concentrated on simulating the low-temperature equilibrium properties of the system, while the present Chapter concentrates on the finite-temperature dynamics and its time-reversal. Time-reversal of the DGPE was previously considered in Refs. [166, 167], but not in the context of extracting the largest Lyapunov exponent. An alternative time-reversal procedure analogous to the sign change of all particle velocities in classical mechanics was already experimentally realized for the propagation of a wave-packet of intense light in a nonlinear crystal, which is describable by the continuous nonlinear Schrödinger equation, an analog of the continuous Gross-Pitaevskii equation [168]. We further note that, for Bose gases in optical lattices, the extraction of Lyapunov exponents from OTOCs was considered in Ref. [169] in intermediate and high-temperature regimes not describable by the DGPE.

In this Chapter, we propose theoretically an experimentally realizable method to demonstrate the Lyapunov instability and to extract the value of the largest Lyapunov exponent for a chaotic many-particle interacting system. We support the theoretical analysis by direct numerical simulations demonstrating that the largest Lyapunov exponent can indeed be extracted from the Loschmidt echo routine. We also discuss possible values of experimental parameters required for implementing this proposal.

## 2.1 Lyapunov exponent from Loschmidt echo: general idea

For extracting the largest Lyapunov exponent (1.1) defined in Section 1.2, it is necessary to track two phase space trajectories  $\mathbf{R}_1(t)$  and  $\mathbf{R}_2(t)$  that are initially infinitesimally close to each other. Their separation from each other after sufficiently long time is controlled by  $\lambda_{\max}$ . In practice,  $\lambda_{\max}$  describes the average expansion rate along the direction of the corresponding eigenvector in tangential space, which typically has fluctuating projections on all phase space axes. Let us choose one of the axes of the phase space to correspond to the observable quantity of interest  $\mathbf{X}$ . In such a case, it is expected that the projection of the difference between the

two separating phase trajectories  $\mathbf{R}_1(t)$  and  $\mathbf{R}_2(t)$  on this axis will exhibit erratic behavior, but the envelope of that behavior will grow exponentially and will be controlled by  $\lambda_{\max}$ .

If the system is ergodic the value of  $\lambda_{\max}$  does not depend on where the two phase space trajectories start, but the corresponding eigenvector and the resulting fluctuating projection on the chosen axis do. It is therefore expected that if one averages over an ensemble of initial conditions on the same energy shell, then the fluctuating component of the difference between the trajectories would average into a constant multiplied by a factor  $\exp(\lambda_{\max}t)$  (for more detailed discussion see Section 3.1.3).

As suggested in Ref. [42], the above considerations can be converted into the following scheme of extracting  $\lambda_{\max}$ . We apply the Loschmidt echo routine described in Section 1.3 to a chaotic classical system and produce the quantity of interest defined by Eq. (1.2):  $|\Delta\mathbf{X}(\Delta t)| = |\mathbf{X}(\tau + \Delta t) - \mathbf{X}(\tau - \Delta t)|$ . It fluctuates as a function of time, but its envelope is modulated by  $\exp(\lambda_{\max}\Delta t)$ . The preceding consideration then suggests that  $\lambda_{\max}$  can be extracted from the following average over the initial conditions

$$\lambda_{\max} = \frac{1}{\Delta t} \langle \log |\mathbf{X}(\tau + \Delta t) - \mathbf{X}(\tau - \Delta t)| \rangle, \quad (2.1)$$

where  $\tau$  should be larger than  $\Delta t$ <sup>1</sup>.

The typical behavior of  $\langle \log |\mathbf{X}(\tau + \Delta t) - \mathbf{X}(\tau - \Delta t)| \rangle$  as a function of  $\Delta t$  for almost any reasonable quantity  $\mathbf{X}$  is qualitatively depicted in Fig. 2-1. It starts growing from a tiny value at  $\Delta t = 0$  and then evolves through a transient regime, where all Lyapunov exponents contribute to the growth, and the largest one is not dominant yet. After the transient regime, the system enters the exponential growth regime, where the largest Lyapunov exponent controls the growth. For any finite initial difference between the two departing phase space trajectories, the exponential growth regime is eventually followed by the saturation regime, where  $|\mathbf{X}(\tau + \Delta t) - \mathbf{X}(\tau - \Delta t)|$  is no longer small enough to be describable by linearized

<sup>1</sup>In Chapter 3, we will also consider the logarithm of the ensemble average of the quantity of interest defined by Eq. (3.3) as opposed to the ensemble average of the logarithm of the quantity of interest defined by Eq. (2.1). A systematic correction in the value of  $\lambda_{\max}$  will be related to the ergodization time of the system.

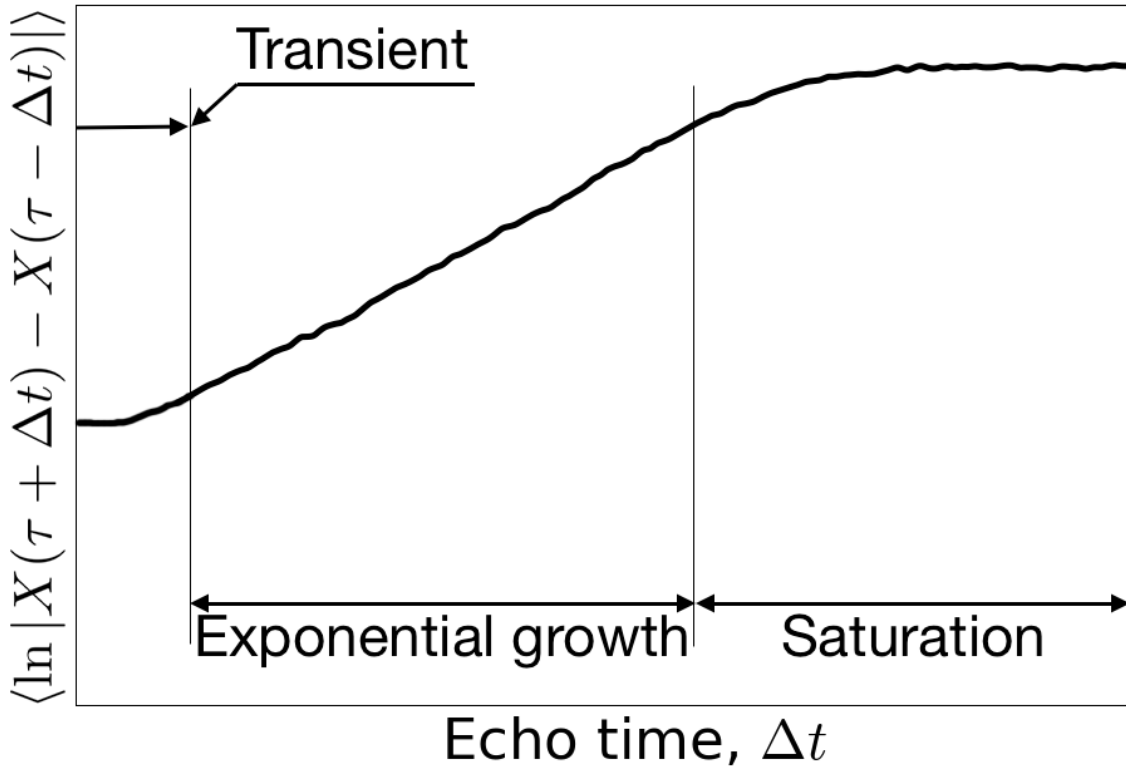


Figure 2-1: Sketch of a typical Loschmidt echo response  $\langle \log |X(\tau + \Delta t) - X(\tau - \Delta t)| \rangle$  (thick black line). Three characteristic regimes described in the text are indicated: transient, exponential growth and saturation.

dynamics. This means that, experimentally or numerically, the perturbation of a perfect time-reversal should be small enough, so that the time  $\Delta t$  for which  $|X(\tau + \Delta t) - X(\tau - \Delta t)|$  remains small is sufficiently long to extract  $\lambda_{\max}$ , i.e. the exponential growth regime must span at least a decade of the perturbation growth.

In chaotic systems, no matter how small the above perturbation is, the separation between the direct and the reversed phase space trajectories is bound to grow and reach large values characteristic of the saturation regime. This is the quintessential “butterfly effect” of chaotic dynamics. It means that, in an experiment, one does not need to specially create a perturbation — any imperfection of the time-reversal procedure will initialize the butterfly effect. Practically in computer simulations, we introduce an additional small perturbation. The strength of the initial perturbation controls the time span of the exponential growth regime before its transition to the saturation regime.

As follows from the above analysis, the method does not use any specific prop-

erties of quantity  $\mathbf{X}$ , thus it can be either scalar or vector. If one chooses a  $K$ -dimensional vector observable  $\mathbf{X} = \{X_i\}$ , then the perturbation of interest  $|\mathbf{X}(\tau + \Delta t) - \mathbf{X}(\tau - \Delta t)|$  can be defined as  $\sqrt{\sum_{i=1}^K (X_i(\tau + \Delta t) - X_i(\tau - \Delta t))^2}$ .

We, finally, remark, that, as demonstrated in Ref. [42], the qualitative picture of the three regimes, that are sketched in Fig. 2-1, remains valid also when the perturbation making the time-reversal imperfect comes not only from a small shaking of the system at time  $\tau$ , but also from an imperfect reversal of system's Hamiltonian.

## 2.2 Formulation of the problem

For all DGPE calculations (see Section 1.5) in this Chapter, we have chosen  $J = 1$ ,  $U = 1$  and the initial conditions  $|\psi_i|^2 = n_i(0) = 1$  with almost random phases of  $\psi_i$ , fixed such that the energy per one site  $\varepsilon = 1$  (corresponding to the microcanonical temperature  $T \sim 2 \dots 6$  dependent on the dimensionality of the lattice), see Eq. (1.17), by the procedure described in Section 2.3. With the above choice, the energy is nearly equally distributed among different sites and between the hopping and the interaction terms in Eq. (1.14). This allows the system to stay in the ergodic regime without long-lived solitonic or breather-like solutions. (The experience with classical spin lattices [170, 171] indicates that many-body classical systems are generically ergodic and chaotic at energies corresponding to sufficiently high temperatures.)

We mark all the variables corresponding to the time interval preceding the time-reversal at time  $\tau$  with a subscript “-” and succeeding the time-reversal with a subscript “+”.

Loschmidt echo is implemented as follows. The time evolution of the system during time interval  $[0, \tau]$  is governed by the Hamiltonian  $\mathcal{H}_-$  (1.14) and, after time  $\tau$ , by the sign-reversed Hamiltonian  $\mathcal{H}_+ = -\mathcal{H}_-$ , i.e. we change the sign of the Hamiltonian parameters at time  $\tau$ :  $J_+ = -J_-$ ,  $U_+ = -U_-$ . How to realize such a time-reversal experimentally will be discussed in Section 2.5.3. At the moment of time reversal, we also introduce a tiny perturbation to the state vector:  $\psi_i(\tau + 0) = \psi_i(\tau - 0) + \delta\psi_i$ , where  $\{\delta\psi_i\}$  is a random vector, subject to the constraint

$$\sqrt{\sum_i |\delta\psi_i|^2} = 10^{-8}.$$

We have chosen a set of on-site occupations  $n_i \equiv |\psi_i^2|$  as the quantity of interest  $\mathbf{X}(t) \equiv \{n_1, n_2, \dots, n_V\}$ . Thus, we characterize the Loschmidt echo by the function  $G(\Delta t) \equiv \langle \log |\mathbf{X}(\tau + \Delta t) - \mathbf{X}(\tau - \Delta t)| \rangle$ , which, for the chosen quantity of interest, can be written as

$$G(\Delta t) \equiv \left\langle \log \sqrt{\sum_{i=1}^V [\Delta n_i(\Delta t)]^2} \right\rangle \xrightarrow{\Delta t \rightarrow \infty} \lambda_{\max} \Delta t, \quad (2.2)$$

where  $\Delta n_i(\Delta t) \equiv n_i(\tau + \Delta t) - n_i(\tau - \Delta t)$ , and  $\langle \dots \rangle$  denotes the ensemble averaging over initial conditions; the asymptotic relation for the regime of the exponential growth of perturbation, from which the value of the largest Lyapunov exponent can be extracted is explained in Section 2.1.

In the following sections, we demonstrate the validity of the above proposition by, first, directly calculating  $\lambda_{\max}$  according to the algorithm from Section 1.2, and then comparing it with the value extracted from Eq. (2.2) on the basis of direct simulations of Loschmidt echoes.

We will do this for a one-dimensional lattice with 10 sites, a two-dimensional square lattice of size  $10 \times 10$  and a three-dimensional cubic lattice of size  $4 \times 4 \times 4$  with nearest-neighbor interactions and periodic boundary conditions.

## 2.3 Numerical algorithm

To simulate the solutions of the DGPE, we employ the 4th order Runge-Kutta algorithm with discretization step  $\delta t = 0.001$ . This limits the algorithmic error to  $O(\delta t^5)$  or roughly  $10^{-15}$ , whereas, by using the quadruple-precision numbers, we fix the machine precision to roughly  $10^{-33}$ . The choice of a relatively simple integrator (Runge-Kutta) is justified by the fact that the energy drift of the DGPE solutions due to the non-symplectic nature of the algorithm is negligible for the purposes of this Thesis. See Ref. [172] for more advanced integration schemes.

The value of  $\lambda_{\max}$ , in general, depends on the two conserved quantities of the system  $E$  and  $N$ .

We generate an ensemble of initial conditions corresponding to  $\varepsilon = 1$  and  $n = 1$ . We do this by choosing initially all  $|\psi_i| = 1$ , with random phases. Then, we minimize  $(\varepsilon - 1)^2 + (n - 1)^2$  by the steepest descent optimization procedure.

As mentioned in Section 2.2, we introduce a small perturbation at the moment of time-reversal by adding a random perturbation  $\{\delta\psi_i\}$  to the state vector  $\{\psi_i\}$ . The length of the perturbation vector is  $10^{-8}$ . This procedure slightly changes  $E$  and  $N$ , but the resulting difference in the value of the largest Lyapunov exponent is several orders of magnitude smaller than the chosen precision of 3 significant digits. Therefore, we can neglect it.

For further details one can refer to the source code published in a GitHub repository<sup>2</sup>.

### 2.3.1 Direct calculation of the largest Lyapunov exponent

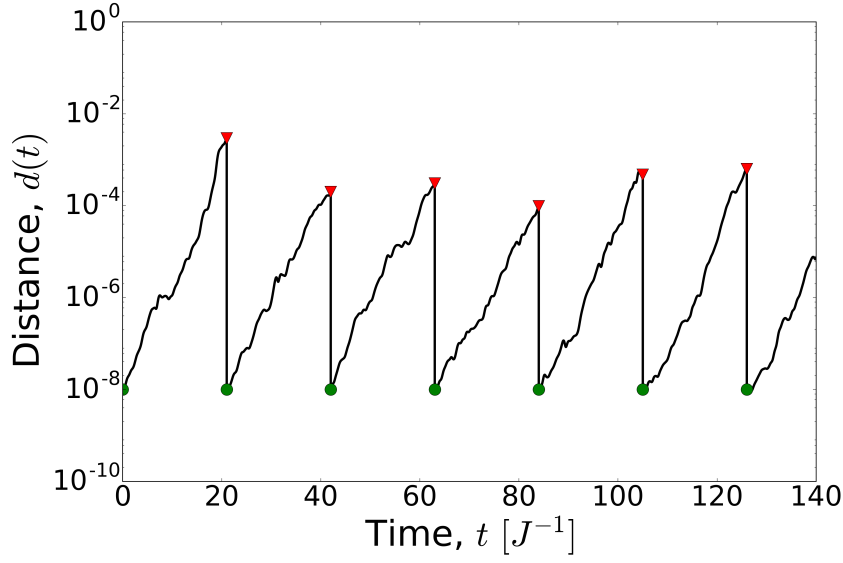
The definition of the largest Lyapunov exponent from Eq. (1.1) is not practical. Instead, we perform the direct calculation of the largest Lyapunov exponent  $\lambda_{\max}$  following the standard numerical algorithm described in Section 1.2. Hence, we track two trajectories: the reference trajectory  $\mathbf{R}_1(t)$  and the slightly perturbed trajectory  $\mathbf{R}_2(t) = \mathbf{R}_1(t) + \delta\mathbf{R}(t)$ ,  $d(t) = |\delta\mathbf{R}(t)|$ . The algorithm starts with  $|\delta\mathbf{R}(0)| = d_0$  and then lets  $\delta\mathbf{R}(t)$  grow during time interval  $T_0$ , then it shifts  $\mathbf{R}_2(t)$  closer to  $\mathbf{R}_1(t)$  by resetting the length of  $\delta\mathbf{R}$  back to  $d_0$ . This procedure is repeated as many times as necessary, until the average of instantaneous stretching rates  $\log \left| \frac{d(t_m)}{d_0} \right|$  converges:

$$\lambda_{\max} = \frac{1}{MT_0} \sum_m^M \log \left| \frac{d(t_m)}{d_0} \right|, \quad (2.3)$$

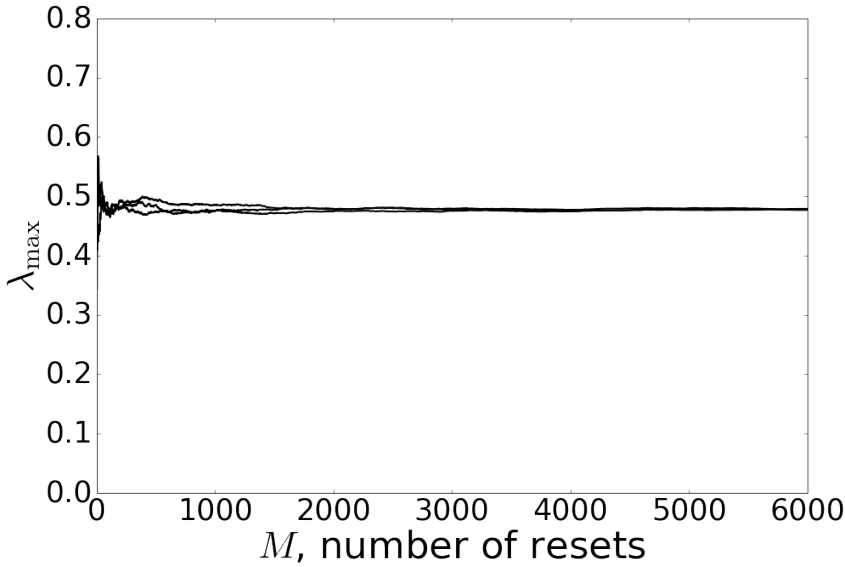
where  $M$  is the number of resets,  $m$  is the reset index,  $t_m$  is the time just before the  $m$ -th reset. The time evolution of the distance  $d(t)$  in the course of such simulation is presented in Fig. 2-2(a).

In all simulations, we test the ergodicity of system's dynamics numerically by checking that the values of  $\lambda_{\max}$  obtained for several randomly chosen initial conditions on a shell with the given values of  $\varepsilon$  and  $n$  are the same. In all cases reported

<sup>2</sup>The code used for the analysis in the present Thesis is published in a GitHub repository at <https://github.com/TarkhovAndrei/DGPE>



(a)



(b)

Figure 2-2: Illustrations of the numerical routine for computing  $\lambda_{\max}$  directly. (a) Black line: distance  $d(t) = \|\mathbf{R}_1(t) - \mathbf{R}_2(t)\|_2$  between two phase space trajectories  $\mathbf{R}_1(t)$  and  $\mathbf{R}_2(t)$  used for computing  $\lambda_{\max}$  for the DGPE on a one-dimensional lattice with  $N = 10$  sites. Time is divided into intervals of duration  $T_0 \approx 20$ , each starts at the reset time  $t_m$  (green dots), for which  $d(t_m) = d_0 = 10^{-8}$ , and finishes at time  $t_m + T_0$  (red triangles). According to Eq. (2.3), the contribution to  $\lambda_{\max}$  from each such an interval (instantaneous stretching rate) is  $\frac{1}{T_0} \log \left| \frac{d(t_m)}{d_0} \right|$ . (b) Ergodicity test: lines represent  $\lambda_{\max}$  obtained from Eq. (2.3) as a function of the number of resets  $M$ . Each line is obtained for different randomly-chosen initial conditions for  $\mathbf{R}_1(t)$  on the same shell of constant  $\varepsilon$  and  $n$ . Convergence to a single value of  $\lambda_{\max}$  with time indicates that the system is ergodic.

below, this test confirmed ergodicity. One example of such a test is illustrated in Fig. 2-2(b).

### 2.3.2 Loschmidt echo simulations

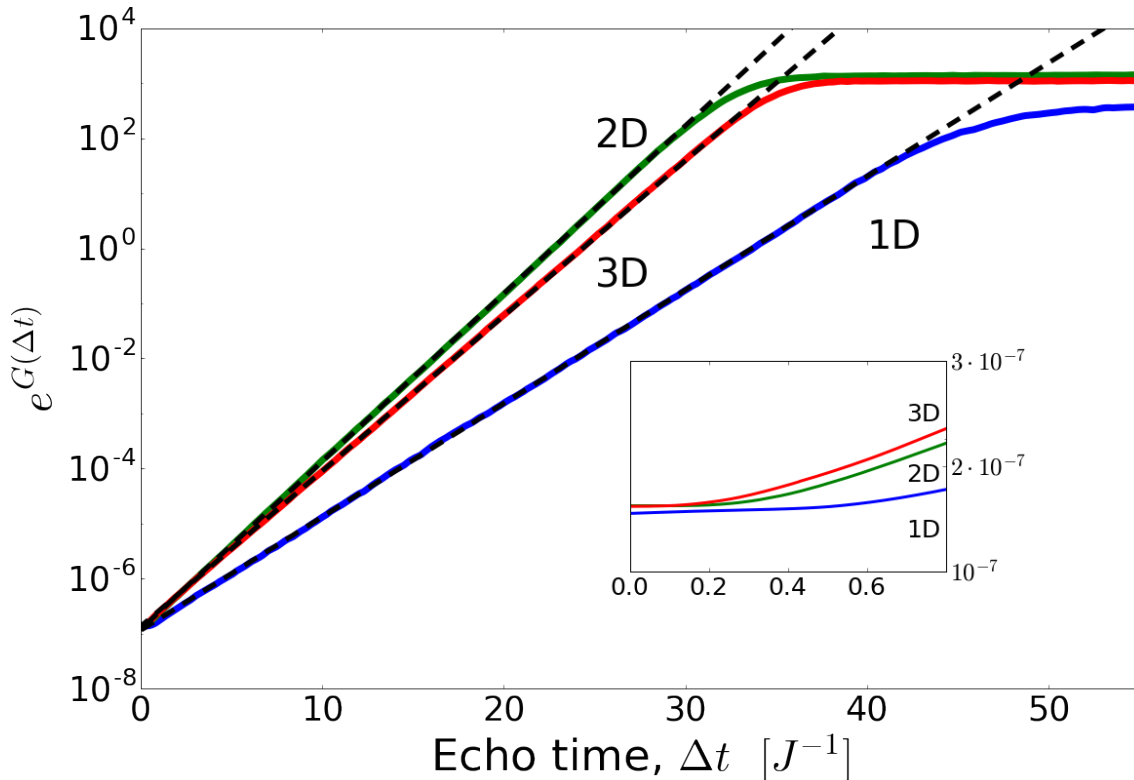


Figure 2-3: Loschmidt echo response  $\exp(G(\Delta t))$  obtained from Eq. (2.2) for a one-dimensional chain of 10 sites (1D, blue line), a two-dimensional  $10 \times 10$  square lattice (2D, green line) and a three-dimensional  $4 \times 4 \times 4$  cubic lattice (3D, red line). The inset shows the behavior of  $\exp(G(\Delta t))$  in the transient regime at small echo times, where all Lyapunov exponents contribute to the growth. The transient regime takes longer time for lower dimensions. In Table 2.1, the values of  $\lambda_{\max}$  obtained by fitting the exponential growth regime according to Eq. (2.2) are compared to the results of averaging of instantaneous stretching rates from Eq. (2.3).

We have computed the Loschmidt echo response function  $G(\Delta t)$  given by Eq. (2.2) for one-, two- and three-dimensional lattice geometries with the parameters defined in Section 2.2. The results of these simulations are presented in Fig. 2-3.

As clearly seen in Fig. 2-3, the expected exponential growth regime of  $G(\Delta t)$  is present in all three cases. The values of  $\lambda_{\max}$  characterizing this regime are summarized in Table. 2.1, where they are also compared with the values of  $\lambda_{\max}$

obtained from the direct calculation described in Section 2.3.1. The agreement between the two sets of values is within the numerical accuracy of the calculations. Similar agreement was demonstrated previously in Ref. [42] for classical spins. We finally note here that the fact that the largest Lyapunov exponent for the 3D cubic lattice is slightly smaller than that for the 2D square lattice is presumably a finite size effect related to the small size of the 3D lattice, which is consistent with the previous observations for classical spin lattices [170].

	$\lambda_{\max}$ from direct calculation, Eq. (2.3)	$\lambda_{\max}$ from Loschmidt echo, Eq. (2.2)
1D	$0.481 \pm 0.002$	$0.475 \pm 0.004$
2D	$0.703 \pm 0.003$	$0.702 \pm 0.004$
3D	$0.648 \pm 0.002$	$0.650 \pm 0.003$

Table 2.1: Comparison of the largest Lyapunov exponents  $\lambda_{\max}$  obtained from the direct averaging of instantaneous stretching rates, Eq. (2.3), with those extracted from the Loschmidt echoes according to Eq. (2.2) and shown in Fig. 2-3 for one-, two- and three-dimensional lattices.

## 2.4 Applicability of DGPE as a constraint on experimental implementation

Throughout this Chapter, we used the DGPE to model the dynamics of Bose-Einstein condensates on a lattice. In order to observe experimentally the regime of exponential growth  $G(\Delta t)$  and to extract from this regime the value of  $\lambda_{\max}$ , the measured system should be such that the DGPE approximates its dynamics with a very high accuracy. The question then arises whether such an accuracy is feasible for realistic experimental settings. To address this question, we have to define the experimental regime, where both conditions would be satisfied simultaneously: the Bose-Hubbard model from Eq. (1.13) would be applicable and the classical mean-field approximation to it would be sufficiently accurate.

For the single-orbital Bose-Hubbard model to be valid, the hopping term  $J$  must be relatively small, so that the lattice potential is deep enough and, as a result, the gap  $\Delta_0$  between the lowest and the second lowest bands is sufficiently large [85, 86]. In addition, in order for a Lyapunov instability to be observable, not only

the order-parameters  $\psi_i$  but also small deviations  $\delta\psi_i$  should be well defined in the mean-field approximation, which implies sufficiently large values of  $n_i$ . The implementation of the proposal then requires the following conditions to be satisfied: (i)  $J \ll \Delta_0$  — the condition for not involving the second band, (ii)  $Un_j \lesssim J$  — the condition preventing the system from exhibiting self-trapping [173–178], (iii) ideally, the number of particles per well  $n_i$  should be of the order of 500 or larger [85, 86, 179]. In such a case, the Ehrenfest time of the system defined in Eq. (1.19) would span several Lyapunov times sufficient for detecting the Lyapunov instability. (Although in the simulations we used the numbers of particles per well  $|\psi_i(0)|^2 = 1$ , the simulation results also represent any case with  $U|\psi_i(0)|^2 = 1$ , i.e. for  $|\psi_i(0)|^2 = 500$  they correspond to  $U = 0.002$ .) We note here that (ii) together with (iii) imply that the condition for the validity of the mean-field approximation in the Bose-Hubbard model,  $U/J \ll 1$ , is automatically fulfilled. It should be possible to satisfy all the above conditions with an optical lattice having potential depth of the order of  $5 \div 10$  recoil energies and not too strong interactions between atoms [180]. We also note that the numerical experience with large quantum spins [45] indicates that even  $n_i \sim 15$  might be already sufficient to extract the largest Lyapunov exponent.

## 2.5 Experimental Proposal

An experiment implementing the proposal should satisfy the following requirements: (i) high accuracy of the measurements of the number of particles  $n_i$  for individual sites leading to the high accuracy of  $G(\Delta t)$  extracted from these measurements, (ii) high accuracy of the experimental realization of the time-reversed Hamiltonian and (iii) high accuracy of the DGPE approximation for the given experimental setting. The relative accuracy in each case should be at least  $10^{-2}$  and, preferably, better. Let us now consider the above requirements one by one.

### 2.5.1 Measurement of the quantity of interest

In order to extract  $G(\Delta t)$  from experiment, the initial and the final values of  $n_i$  should be measured with high accuracy. In principle, there exist techniques, such

as the absorption imaging [181] or the resonant fluorescence detection [182] that allow one to achieve the required accuracy. In particular, the current state-of-the-art record for the resonant fluorescence detection [182] is to measure the number of atoms of the order of one thousand with accuracy better than one percent. However, the proposal implies an additional requirement, namely, that the initial measurement should not significantly perturb  $n_i$ , so that the measured values represent the initial conditions for the actual experimental run. This implies that destructive techniques, such as absorption imaging, would not be suitable for the initial measurement, because they would destroy the condensate. Therefore, it is preferable that at least the initial measurement is performed by a non-destructive technique, such as, e.g., dispersive (off-resonance) imaging [183, 184] or the techniques used in Refs. [185, 186]. The alternative approach would be to controllably prepare the initial state with an accurate *a priori* knowledge of the initial number of particles on each site. The final measurement can then be done by either a destructive or a non-destructive imaging technique.

## 2.5.2 Initial and final conditions

We propose to create the optical lattice initially with sufficiently high potential barriers between adjacent sites, which would suppress hopping between them while the initial occupations are measured. Then, the barriers should be lowered to the heights corresponding to the desired value of the hopping parameter  $J$ . The barriers should be lowered sufficiently fast, so that the initial occupations of individual wells remain the same. At the same time, after the barriers are lowered the initial phases of individual order-parameters  $\psi_i$  are expected to be random. Thereby an ensemble of random initial conditions is to be implemented. After this, both the direct and the reversed time evolution should last for a time  $\tau$  each. Then, the barriers should be raised again, so that the final occupations of individual wells can be measured slowly and accurately.

### 2.5.3 Time-reversal of dynamics

In order to reverse the sign of the Hamiltonian  $\mathcal{H}$  (1.14) at time  $\tau$ , one can change the sign of the hopping parameter  $J$  and the interaction parameter  $U$ .

The sign-reversal of  $J$  can be implemented using fast periodic shaking of the optical lattice. As shown in Refs. [165, 187, 188], the effective hopping parameter  $J$  depends on the periodic forcing amplitude  $F$  and the modulation frequency  $\omega$  as follows:

$$J(F, \omega) = \mathcal{J}_0 \left( \frac{d|F|}{\hbar\omega} \right) \tilde{J}, \quad (2.4)$$

where  $\mathcal{J}_0$  is the zeroth order Bessel function,  $\tilde{J}$  is the bare hopping parameter and  $d$  is the lattice spacing. Since  $\mathcal{J}_0$  is a sign-alternating function, one can find pairs of parameters  $F_1, \omega_1$  and  $F_2, \omega_2$ , such that  $J(F_2, \omega_2) = -J(F_1, \omega_1)$ . Such a time-reversal can be implemented on the timescale of the order of the modulation frequency  $\omega$ , which is several kHz [165, 189, 190].

The sign-reversal of the interaction parameter  $U$  can be implemented with the help of Feshbach resonances [191, 192]. This parameter is proportional to the atomic  $s$ -wave scattering length  $a_{sc}$ , whose value and sign can be controlled by the value of external magnetic field  $B$ . Cesium or rubidium-85 could be good candidates for this kind of experiment, due to their broad Feshbach resonances [193–195]. In this case, the on-site interaction can be reversed on a timescale of fractions of ms.

According to the above proposal, the time-reversal of the effective Hamiltonian  $\mathcal{H}$  can be implemented within a fraction of ms, whereas the system dynamics controlled by the values of  $J$  and  $U$  can be at least one order of magnitude slower.

Bose-Einstein condensates with attractive interaction (which will be required either for the forward or the backward time-evolution) are in general unstable to collapse. However, if they are constrained to a finite volume, the collapse happens only for numbers of atoms above a certain critical value, which for realistic optical lattice parameters can be above 1000 per lattice site [196–201]. As mentioned earlier, the implementation of the proposal requires about 500 atoms per lattice site.

Another useful possibility that potentially improves the flexibility of experimen-

tal implementation is to achieve the time-reversal not by realizing the strict condition  $\mathcal{H}_+ = -\mathcal{H}_-$ , but, instead, borrowing the idea from the magic echo of nuclear magnetic resonance [202, 203], to change the sign of  $J$  and  $U$  in such a way that the Hamiltonian before the time-reversal  $J_-, U_-$  are related to the parameters after the time-reversal  $J_+, U_+$  as follows:  $J_+ = -cJ_-$ ,  $U_+ = -cU_-$ , where  $c$  is some positive constant. In such a case,  $\mathcal{H}_+ = -c\mathcal{H}_-$ , so that the time-reversal routine would consist of the direct time-evolution taking time  $\tau$  and the reversed time-evolution taking time  $\tau/c$ .

### 2.5.4 Lattice geometry

Experimentally realized optical lattices are, normally, not quite translationally invariant because of the presence of physical borders. This, in particular, leads to an effective position-dependent on-site potential and/or position-dependent hopping, whose values near the borders of the lattice are different from those in the bulk. In such a case, the time-reversal of the full Hamiltonian requires reversing the sign of the above position-dependent terms, which, in turn, poses an additional experimental complication. It is, therefore, preferable for implementing the proposal to use an optical lattice that actually has periodic boundary conditions, which, for all practical purposes, leaves us with a ring-shaped one-dimensional lattice. Such a lattice can be realized, for example, on the basis of an interference pattern of two Laguerre-Gauss modes with different orbital indices [204, 205].

## 2.6 Discussion

In this Chapter, we proposed a method to extract the largest Lyapunov exponent for a lattice of Bose-Einstein condensates on the basis of a Loschmidt echo routine. We have validated this method by numerical simulations and discussed its possible experimental implementation with ultracold bosonic atoms in optical lattices. A successful realization of this proposal may produce the long-sought direct experimental evidence that the dynamics of a typical many-particle system is chaotic. This, in turn, would put the theory of dynamic thermalization on a firmer foundation.

Because her memory is too short. As with so many phenomena of time, recurrent combinations are perceptible as such only when they cannot affect us any more—when they are imprisoned so to speak in the past, which *is* the past just because it is disinfected.

—Vladimir Nabokov,  
Bend Sinister

## Chapter 3

# Extracting ergodization time from the Lyapunov process

In this Chapter, we define the ergodization time of a chaotic system as the characteristic time one needs to monitor the system in order to extract its primary chaotic parameter, namely, the largest Lyapunov exponent. The advantage of this definition is that it is unbiased in the sense of not being coupled to any particular system's coordinate. The ergodization time can be also defined as a typical self-averaging time for a chosen observable [112], however, such a definition depends on the choice of the observable, which, in turn, make it difficult to compare ergodization times in systems with qualitatively different degrees of freedom. The goal is to theoretically propose and numerically test a method based on the Loschmidt echo, which can be used to experimentally determine whether the system ergodizes, and if yes, then to extract the ergodization time. We validate the method by the numerical simulation of an array of coupled Bose-Einstein condensates in the regime describable by the DGPE (1.15). Various aspects of this Chapter are relevant to the previous investigations of lattice gauge models [206–210] and spin lattice models [42, 45, 170, 171]. The relation between the present results to OTOCs in quantum systems is also to be discussed in the end of this Chapter.

For extracting the ergodization time, the standard Loschmidt echo routine, described in Section 1.3 and sketched in Fig. 1-1, is extended to include the following steps. The statistics of the quantity of interest from Eq. (1.2) is gathered for an en-

semble of random initial conditions on a shell of the chosen energy and the number of particles. The gathered statistics is used for calculating two kinds of ensemble averages  $\langle \log |\Delta \mathbf{X}(\Delta t)| \rangle$  and  $\log \langle |\Delta \mathbf{X}(\Delta t)| \rangle$ . For  $\Delta t \rightarrow \infty$ , the former average approaches  $\lambda_{\max} \Delta t$ , while the latter one approaches  $\Lambda \Delta t$ , where  $\lambda_{\max}$  is the largest Lyapunov exponent, and  $\Lambda$  is a parameter to be discussed later. As we show below, the ergodization time  $\tau_{erg}$  is proportional to the difference between  $\Lambda$  and  $\lambda_{\max}$ .

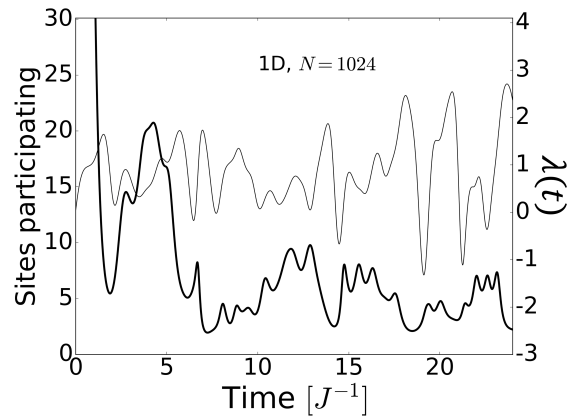
The method is generally applicable to systems where time-reversal of the dynamics can be practically implemented. As in Chapter 2, we illustrate the method for one-, two- and three-dimensional DGPE lattices, and choose a set of on-site occupations  $\mathbf{X}(t) = \{n_1, n_2, \dots, n_V\}$  as a measurable quantity of interest.

## 3.1 Ergodization time

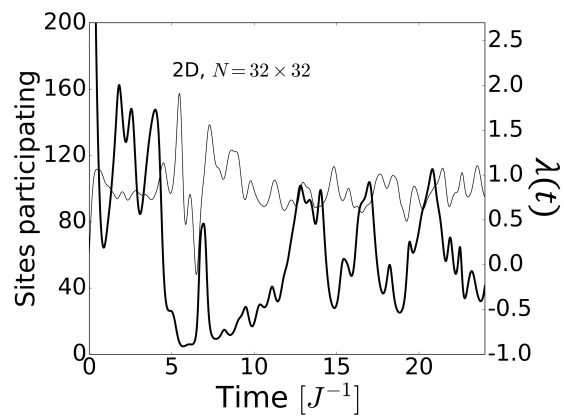
### 3.1.1 Definition of ergodization time based on the Lyapunov process

In Section 1.2, we defined the instantaneous stretching rates  $\lambda(t) = \frac{d}{dt} \log \left| \frac{D(t)}{D(0)} \right|$ , where  $D(t) = |\delta \mathbf{R}(t)|$  is the distance between the two phase-space trajectories. The largest Lyapunov exponent can be calculated as the average of instantaneous stretching rates over time:  $\lambda_{\max} = \overline{\lambda(t)}$ . In Fig. 3-1, we plot  $\lambda(t)$  for one-, two- and three-dimensional lattices along with the number of lattice sites actively participating in the Lyapunov eigenvector corresponding to the largest Lyapunov exponent. The Lyapunov eigenvectors are normally localized in the sense that the projections on the axes representing individual sites are large only for a small subset of sites, which itself depends on time  $t$ . The number of sites participating in the Lyapunov eigenvector is defined as the reciprocal of the inverse participation ratio for the perturbation  $\delta \psi_j(t)$  corresponding to  $\delta \mathbf{R}(t)$ :  $\left( \sum_j |\delta \psi_j(t)|^2 \right)^2 / \sum_j |\delta \psi_j(t)|^4$ . The fluctuations of  $\lambda(t)$  and the number of participating lattice sites are anti-correlated.

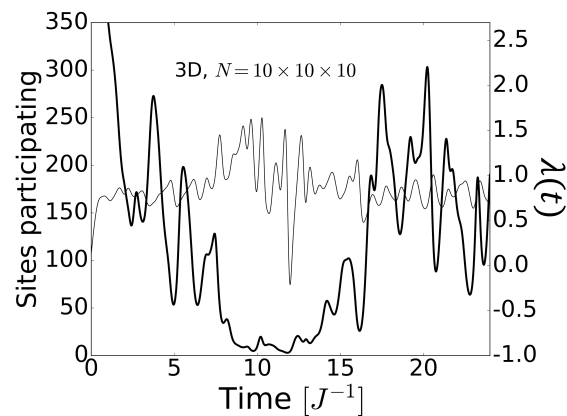
Let us consider the fluctuations of the instantaneous stretching rates  $\delta \lambda(t) \equiv \lambda(t) - \lambda_{\max}$ , and introduce their autocorrelator



(a)



(b)



(c)

Figure 3-1: Fluctuations of instantaneous stretching rates  $\lambda(t)$  (thin black lines) and the number of sites participating in the Lyapunov eigenvector (thick black lines) for: (a) a 1D chain of 1024 sites, (b) a 2D square lattice  $32 \times 32$ , (c) a 3D cubic lattice  $10 \times 10 \times 10$ .

$$\varphi(t) \equiv \langle \delta\lambda(t)\delta\lambda(0) \rangle. \quad (3.1)$$

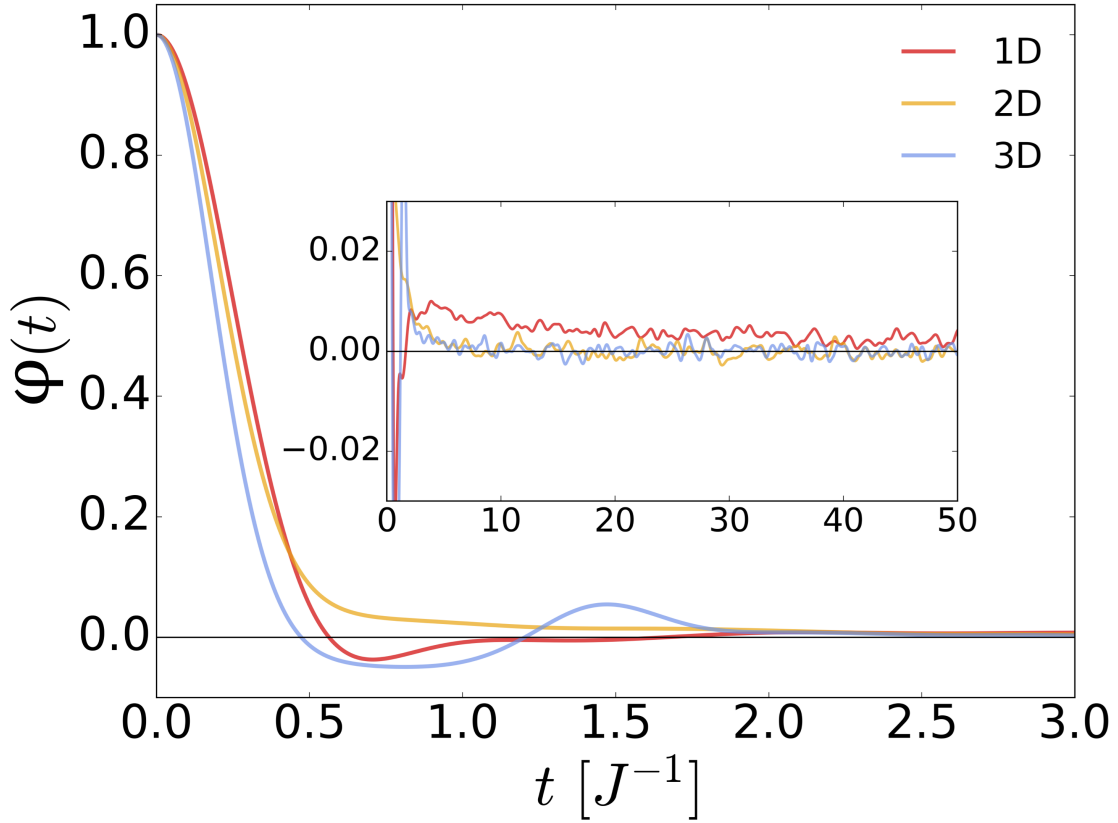


Figure 3-2: Autocorrelation function  $\varphi(t)$  for instantaneous stretching rates  $\lambda(t)$  for a 1D chain of 100 sites (red), a 2D square lattice  $10 \times 10$  (orange), a 3D cubic lattice  $4 \times 4 \times 4$  (light blue). In the inset, the tails of  $\varphi(t)$  are plotted for longer times.

In Fig. 3-2, we plot the autocorrelation function  $\varphi(t)$  for three chosen lattices. We propose to use the convergence of  $\overline{\lambda(t)}$  as an indicator of ergodization, and define the ergodization time as

$$\tau_{erg} \equiv \frac{1}{\langle \delta \lambda^2 \rangle} \int_0^\infty \varphi(t) dt. \quad (3.2)$$

As shown in Fig. 3-1, the Lyapunov process is controlled by dynamically localized Lyapunov eigenvectors. Hence, the ergodization time (3.2) defined from such a process would be also a *local measure* of ergodization.

In contrast to the typical diffusion time across the system (the Thouless time), which is a more global measure of ergodization, the ergodization time defined in terms of the Lyapunov process is sensitive to the variations in the local environment of different lattice sites. Glass is an example, where such a local ergodization breaks down.

### 3.1.2 Ergodization time from Loschmidt echoes

The Loschmidt echo is implemented as in Chapter 2. However, in addition to the function  $G(\Delta t)$  from Eq. (2.2), we introduce a new kind of ensemble averaging of  $\Delta n_i(\Delta t)$ :

$$W(\Delta t) \equiv \log \left\langle \sqrt{\sum_{i=1}^V [\Delta n_i(\Delta t)]^2} \right\rangle \xrightarrow{\Delta t \rightarrow \infty} \Lambda \Delta t, \quad (3.3)$$

where

$$\Lambda \equiv \frac{1}{t} \log \left\langle \exp \int_0^t \lambda(t') dt' \right\rangle. \quad (3.4)$$

The function  $G(\Delta t)$  and the relation (2.2) were used in Chapter 2 for extracting  $\lambda_{\max}$ . Now, we concentrate on the relation (3.3). The reason for the difference between parameter  $\Lambda$  (sometimes referred to as the generalized maximum Lyapunov exponent [211–214]) and  $\lambda_{\max}$  is the different order of operations of taking logarithm and ensemble averaging. This difference is controlled by the amplitude and the correlation time of fluctuations  $\delta\lambda(t)$ . In order to demonstrate this, we first note that

$$\Lambda - \lambda_{\max} = \frac{1}{t} \log \left\langle e^{\int_0^t \delta\lambda(t') dt'} \right\rangle. \quad (3.5)$$

The average on the right-hand side can be calculated analytically on the basis of the assumption that variable  $\int_0^t \delta\lambda(t') dt'$  is Gaussian, by a stochastic-noise method analogous to the one developed by Anderson and Weiss [215] in a different context, namely, for the calculation of exchange-narrowed magnetic resonance linewidths.

We represent the average on the right-hand side of Eq. (3.5) as

$$\left\langle e^{\int_0^t \delta\lambda(t') dt'} \right\rangle = \int dY P_t(Y) e^Y, \quad (3.6)$$

where

$$Y(t) = \int_0^t \delta\lambda(t') dt' = \lim_{\delta t \rightarrow 0} \delta t \sum_{t_i} \delta\lambda(t_i), \quad (3.7)$$

and  $P_t(Y)$  is the probability distribution of  $Y(t)$ . We assume that the system fluctuates near equilibrium, and, therefore, the process  $\delta\lambda(t)$  is stationary, i.e. its probability distribution  $p(\delta\lambda(t_i))$  is independent of  $t_i$ .

If  $\delta\lambda(t)$  is a Gaussian random variable, then  $Y$  is also a Gaussian random variable for all times, i.e.  $P_t(Y)$  is Gaussian. If  $p(\delta\lambda)$  is not Gaussian, but the variable  $\delta\lambda(t)$  has a finite memory time  $\tau_{erg}$ , then  $P_t(Y)$  still becomes Gaussian for  $t \gg \tau_{erg}$  (consequence of the central limit theorem).

Assuming Gaussianity of  $P_t(Y) \equiv (2\pi \langle Y(t)^2 \rangle)^{-\frac{1}{2}} \exp\left(-\frac{Y^2}{2\langle Y(t)^2 \rangle}\right)$ , we can rewrite Eq. (3.6) as:

$$\left\langle e^{\int_0^t \delta\lambda(t') dt'} \right\rangle = (2\pi \langle Y^2 \rangle)^{-\frac{1}{2}} \int dY e^{-\frac{Y^2}{2\langle Y^2 \rangle} + Y} = e^{\frac{\langle Y^2 \rangle}{2}}. \quad (3.8)$$

We calculate the variance of  $Y$  as

$$\langle Y^2 \rangle = \left\langle \left[ \int_0^t \delta\lambda(t') dt' \right]^2 \right\rangle = \int_0^t dt' \int_0^t dt'' \langle \delta\lambda(t') \delta\lambda(t'') \rangle. \quad (3.9)$$

Since  $\delta\lambda(t)$  is assumed to be stationary:  $\langle \delta\lambda(t') \delta\lambda(t'') \rangle = \langle \delta\lambda(0) \delta\lambda(t'' - t') \rangle \equiv \varphi(t'' - t')$ , and Eq. (3.9) becomes

$$\langle Y^2(t) \rangle = \int_0^t dt' \int_{-t'}^{t-t'} \varphi(t'') dt'' = \int_0^t dt' g(t'), \quad (3.10)$$

where  $g(t') = \int_{-t'}^{t-t'} \varphi(t'') dt''$ . The dynamics is time-reversible, thus  $\varphi(-t') = \varphi(t')$ , and  $\dot{g}(t') = -\varphi(t - t') + \varphi(-t') = -\varphi(t - t') + \varphi(t')$ . The integration of Eq. (3.10) by parts leads to

$$\begin{aligned} \langle Y^2(t) \rangle &= t \cdot g(t) - \int_0^t dt' \cdot t' \dot{g}(t') = \\ &= t \int_{-t}^0 \varphi(t'') dt'' - \int_0^t dt' \cdot t' \varphi(t') + \int_0^t dt' \cdot t' \varphi(t - t') = \\ &= t \int_0^t \varphi(t') dt' - \int_0^t dt' \cdot t' \varphi(t') + \int_0^t dt' \cdot (t - t') \varphi(t') = \\ &= 2 \int_0^t dt' (t - t') \varphi(t'). \end{aligned} \quad (3.11)$$

We substitute Eq. (3.11) into Eq. (3.8), and finally obtain

$$\left\langle e^{\int_0^t \delta\lambda(t') dt'} \right\rangle = e^{\int_0^t dt' (t-t') \varphi(t')}. \quad (3.12)$$

This integral converges if  $\varphi(t)$  decays faster than  $\frac{1}{t^2}$ . In such a case, for  $t \rightarrow \infty$

$$\left\langle e^{\int_0^t \delta\lambda(t) dt} \right\rangle = C e^{\int_0^t dt' \varphi(t')}, \quad (3.13)$$

where  $C = \exp\left(-\int_0^\infty dt' \cdot t' \varphi(t')\right)$ .

Using this relation together with Eq. (3.2), we obtain  $\Lambda - \lambda_{\max} = \int_0^\infty \varphi(t') dt' \equiv \langle \delta\lambda^2 \rangle \tau_{erg}$ . Therefore, the ergodization time can be expressed as

$$\tau_{erg} = \frac{\Lambda - \lambda_{\max}}{\langle \delta\lambda^2 \rangle}. \quad (3.14)$$

### 3.1.3 Independence of the choice of an observable

If it were experimentally possible to track all phase-space coordinates of a system, then one could have obtained the largest Lyapunov exponent by identifying the phase-space direction  $\delta\mathbf{R}$  along which the growth of a perturbation is the quickest—the Lyapunov eigenvector corresponding to the largest Lyapunov exponent. However, a realistic experiment is limited to an observable  $\mathbf{X}$ . It is overwhelmingly likely for the eigenvector to have a non-zero projection onto  $\mathbf{X}$ . This means that

$$\Delta\mathbf{X}(\Delta t) = \Delta\mathbf{X}(0) \cos \alpha(\Delta t) e^{\int_0^{\Delta t} \lambda(t') dt'}, \quad (3.15)$$

where  $\alpha(\Delta t)$  is the angle between the eigenvector and the direction corresponding to  $\Delta\mathbf{X}(\Delta t)$  in the many-dimensional phase space.

Here, we consider the growth of the initial difference  $\Delta\mathbf{X}(0)$  introduced by an imperfect time reversal, and justify the relations (2.2) and (3.3) for  $\Delta t \rightarrow \infty$  (cf. Ref. [42]) for an arbitrary observable  $\mathbf{X}$ :  $G(\Delta t) \equiv \langle \log |\Delta\mathbf{X}(\Delta t)| \rangle \xrightarrow{\Delta t \rightarrow \infty} \lambda_{\max} \Delta t$  and  $W(\Delta t) \equiv \log \langle |\Delta\mathbf{X}(\Delta t)| \rangle \xrightarrow{\Delta t \rightarrow \infty} \Lambda \Delta t$ . We use Eq. (3.15) to express  $G(\Delta t)$  as

$$G(\Delta t) = \left\langle \log |\Delta\mathbf{X}(0)| + \log |\cos \alpha(\Delta t)| + \log e^{\int_0^{\Delta t} \lambda(t') dt'} \right\rangle, \quad (3.16)$$

where the first term is constant, the second term remains limited from above after

ensemble averaging over initial conditions, and the third term is the only one growing linearly with  $\Delta t$ . The second term  $\log |\cos \alpha(\Delta t)|$  may appear problematic for  $\Delta t$  corresponding to  $|\cos \alpha(\Delta t)| = 0$ . However, this singularity is integrable: it vanishes after ensemble averaging. Given the definition of  $\lambda_{\max}$  from Section 3.1.1, Eq. (3.16) implies Eq. (2.2).

To prove the relation (3.3) for  $W(\Delta t)$ , we assume that  $|\cos \alpha(\Delta t)|$  is uncorrelated with  $e^{\int_0^{\Delta t} \lambda(t') dt'}$  and hence factorize the average  $\left\langle |\Delta \mathbf{X}(0) \cos \alpha(\Delta t)| e^{\int_0^{\Delta t} \lambda(t') dt'} \right\rangle \xrightarrow{\Delta t \rightarrow \infty} \langle |\Delta \mathbf{X}(0) \cos \alpha(\Delta t)| \rangle \cdot \left\langle e^{\int_0^{\Delta t} \lambda(t') dt'} \right\rangle$ . This assumption is, presumably, appropriate for almost any non-local observable. It is supported by the extensive numerical experience, e.g. Refs. [42, 45, 170, 171], showing that the eigenvectors corresponding to  $\lambda_{\max}$  exhibit rather erratic behavior. The above factorization leads to

$$W(\Delta t) = \log \langle |\Delta \mathbf{X}(0) \cos \alpha(\Delta t)| \rangle + \log \left\langle e^{\int_0^{\Delta t} \lambda(t') dt'} \right\rangle, \quad (3.17)$$

which, given the definition of  $\Lambda$  from Eq. (3.4), implies Eq. (3.3).

### 3.1.4 Relation to OTOCs in quantum systems

As shown in Section 1.3, the quantum-mechanical description of Loschmidt echoes involves OTOCs. We now illustrate that the parameter  $\Lambda$  introduced in Eq. (3.3) for characterization of the exponential growth of  $W(\Delta t)$  in the classical case, such that

$$\langle |\Delta \mathbf{X}(\Delta t)| \rangle \sim \exp(\Lambda \Delta t), \quad (3.18)$$

also characterizes the growth of an OTOC in a quantum system, when the system's constituents are describable quasi-classically. Following Ref. [42], we observe that relation (3.18) implies  $\langle |\Delta \mathbf{X}(\Delta t)|^2 \rangle \sim \exp(2\Lambda \Delta t)$ . In other words,

$$\Lambda = \frac{1}{2} \frac{d}{d(\Delta t)} \left[ \lim_{\Delta t \rightarrow \infty; |\Delta \mathbf{X}(0)| \rightarrow 0} \log \langle |\Delta \mathbf{X}(\Delta t)|^2 \rangle \right], \quad (3.19)$$

where  $|\Delta \mathbf{X}(\Delta t)|^2$  is defined by Eq. (1.4), and in the quantum case transforms to an OTOC (1.6). Finally, we note that the quantum counterpart of the maximum classical Lyapunov exponent can be defined as

$$\lambda_{\max}^Q = \frac{1}{2} \frac{d}{d(\Delta t)} \lim_{\Delta t \rightarrow \infty; \hat{R} \rightarrow \hat{1}} \text{Tr} \left\{ \hat{\rho}_0 \log \left( \hat{\mathbf{X}}^2(\tau + \Delta t) + \hat{\mathbf{X}}^2(\tau - \Delta t) - \hat{\mathbf{X}}(\tau + \Delta t)\hat{\mathbf{X}}(\tau - \Delta t) - \hat{\mathbf{X}}(\tau - \Delta t)\hat{\mathbf{X}}(\tau + \Delta t) \right) \right\}. \quad (3.20)$$

The temperature-dependent constraint on the exponential growth rate  $\Lambda$  of OTOCs (when the exponential growth regime exists, which is not always the case [42]) discussed in Section 1.3, in turn, imposes a constraint on the largest Lyapunov exponent  $\lambda_{\max}$  for a quantum system. As follows from the present Chapter, as well as from Refs. [45, 51, 216], the value of  $\Lambda$  is, in general, larger than  $\lambda_{\max}$ . The interesting question then arises whether the difference between  $\Lambda$  and  $\lambda_{\max}$  approaches zero as the number of degrees of freedom in a system increases. The findings indicate that, for a lattice of a given dimension (1D, 2D and 3D),  $\Lambda - \lambda_{\max}$  remains finite for rather large systems. Yet, this difference decreases with the increase of the lattice dimension from 1D to 2D to 3D. It is particularly small for the 3D lattice considered in this Chapter, which is consistent with the classical spin simulations for 3D lattices done in Ref. [42], where the difference between  $\Lambda$  and  $\lambda_{\max}$  was within the computational uncertainty of the simulation and, hence, was overlooked.

We further remark that the difference  $\Lambda - \lambda_{\max}$  originates from the fluctuations of Loschmidt echo amplitude, which is, as shown in the present Chapter, sensitive to ergodicity breakdown in classical systems. The counterpart of this breakdown in quantum systems is the transition from an ergodic to a many-body localized phase. It was proposed in a related study [58], that the fluctuations of a Loschmidt echo in quantum systems are sensitive to the many-body localization transition.

Finally, even though the primary agenda of the present Chapter is to characterize ergodicity in large systems close to the thermodynamic limit, the method based on Loschmidt echoes should also be applicable to a-few-body systems. When classical a-few-body systems exhibit the breakdown of ergodicity, the ergodicity criterion proposed in Section 3.3 should be sensitive to this. As far as a-few-body quantum systems are concerned [217–219], it is an interesting question how their energy level

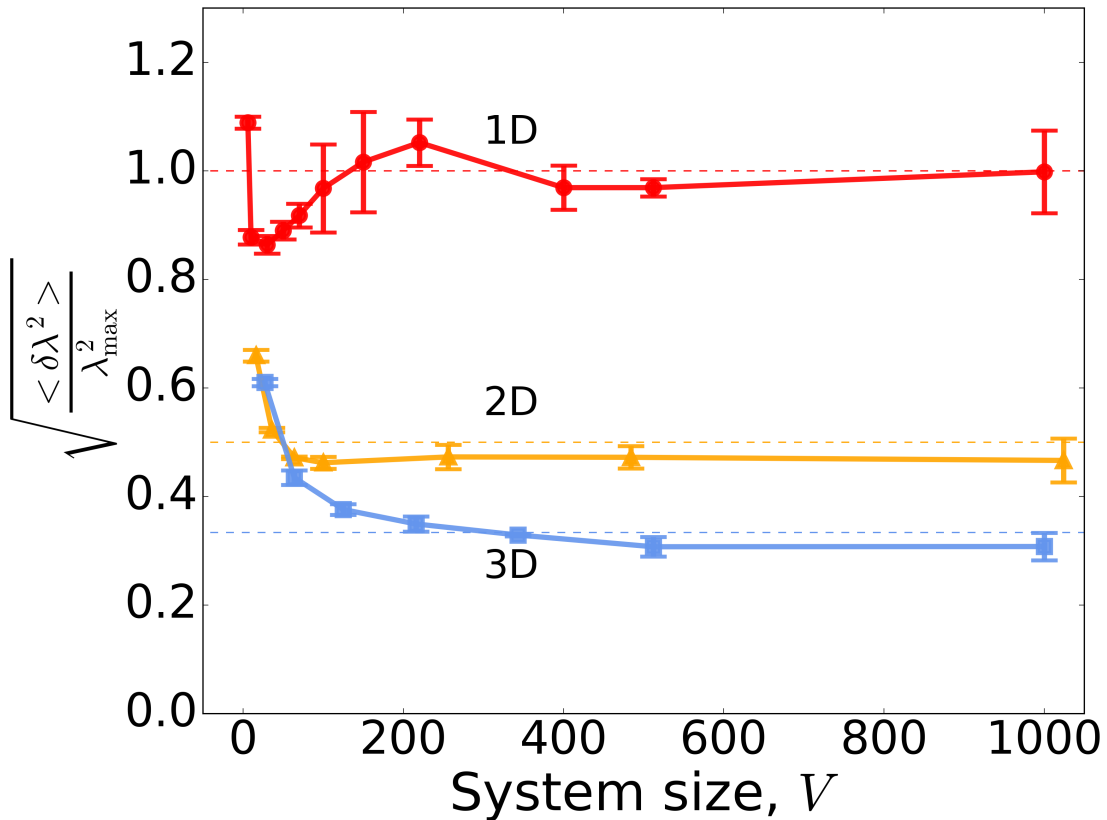


Figure 3-3: Numerical test of empirical estimate (3.21) for  $\langle \delta \lambda^2 \rangle$ . The dependence of  $\sqrt{\langle \delta \lambda^2 \rangle / \lambda_{\max}^2}$  on the number of lattice sites  $V$  for one- (red circles), two- (orange triangles) and three-dimensional (light blue squares) lattices. The dashed lines are plotted at the levels of  $1/d$ , where  $d$  is the lattice dimension.

spacing statistics is related to the ergodicity criterion in the classical limit. If a quantum system exhibits the Wigner-Dyson statistics of energy-level spacings in one energy range and does not exhibit it in the other one, then the respective energy shells in the classical limit likely change from ergodic to nonergodic. In such a case, the ergodicity criterion of Section 3.3 can be used to predict the level spacing statistics.

## 3.2 Extracting the ergodization time of DGPE lattices

The experimental use of Eq. (3.14) requires determining  $\lambda_{\max}$  and  $\Lambda$  from Eqs. (2.2) and (3.3) and, in addition, the knowledge of  $\langle \delta \lambda^2 \rangle$ . While there might be ways

of extracting  $\langle \delta\lambda^2 \rangle$  from experimental time-series, here we resort to an empirical estimate

$$\langle \delta\lambda^2 \rangle \approx \frac{\lambda_{\max}^2}{d^2}, \quad (3.21)$$

where  $d$  is the lattice dimension. In Fig. 3-3, we substantiate the estimate (3.21) on the basis of the direct numerical simulations. Why this approximation works so well for the DGPE on large lattices and whether it works for a more general class of systems needs further investigation. A possible explanation of Eq. (3.21) is that, in the simulations, the Lyapunov eigenvector corresponding to  $\lambda_{\max}$  tends to localize at only a handful of sites, which is consistent with other observations of wandering localization of Lyapunov eigenvectors [220–227].

The estimate (3.21) leads to the following approximation for the ergodization time

$$\tau_{erg} \approx \frac{\Lambda - \lambda_{\max}}{\lambda_{\max}^2} d^2. \quad (3.22)$$

### 3.3 Criterion of ergodicity

When the ergodicity of a system is about to break down, one obvious indicator of this is an anomalously large value of the ergodization time given by Eq. (3.14). One may wonder, however, whether the Loschmidt echo response contains other signatures of broken ergodicity. Below, we show that, indeed, it does. In an ergodic regime, the distribution of  $\log |\Delta \mathbf{X}(\Delta t)|$  should be Gaussian, and its variance  $\sigma_G^2(\Delta t) \equiv \langle \log^2 |\Delta \mathbf{X}(\Delta t)| \rangle - G^2(\Delta t)$  is supposed to grow linearly in time:

$$\sigma_G^2(\Delta t) \xrightarrow{\Delta t \rightarrow \infty} 2(\Lambda - \lambda_{\max})\Delta t. \quad (3.23)$$

In the opposite case of a non-ergodic regime, the averages in  $G(\Delta t)$  and  $W(\Delta t)$  converge poorly, which in turn leads to a non-Gaussian distribution for individual realizations of  $\log |\Delta \mathbf{X}(\Delta t)|$  [228], accompanied by a deviation from the linear growth of  $\sigma_G^2(\Delta t)$  given by Eq. (3.23). Thus, relation (3.23) can be used for an experimentally feasible test of ergodization.

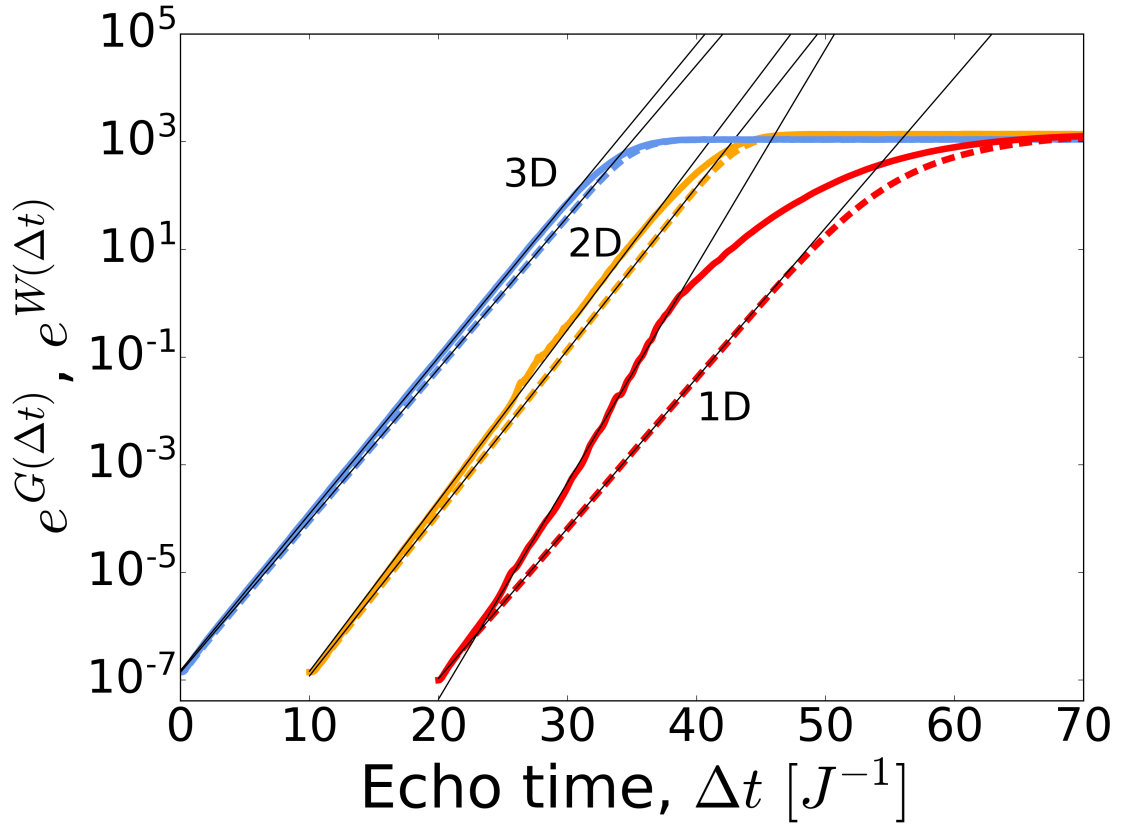


Figure 3-4: Loschmidt echo responses  $G(\Delta t)$  defined according to Eq. (2.2) (dashed lines), and  $W(\Delta t)$  defined by Eq. (3.3) (solid lines) for: a three-dimensional  $4 \times 4 \times 4$  cubic lattice (3D, light blue); a two-dimensional  $10 \times 10$  square lattice (2D, orange, shifted to the right by 10); a one-dimensional chain with 100 sites (1D, red, shifted to the right by 20). Thin black lines are linear fits from which  $\lambda_{\max}$  and  $\Lambda$ , listed in Table 3.1, were extracted.

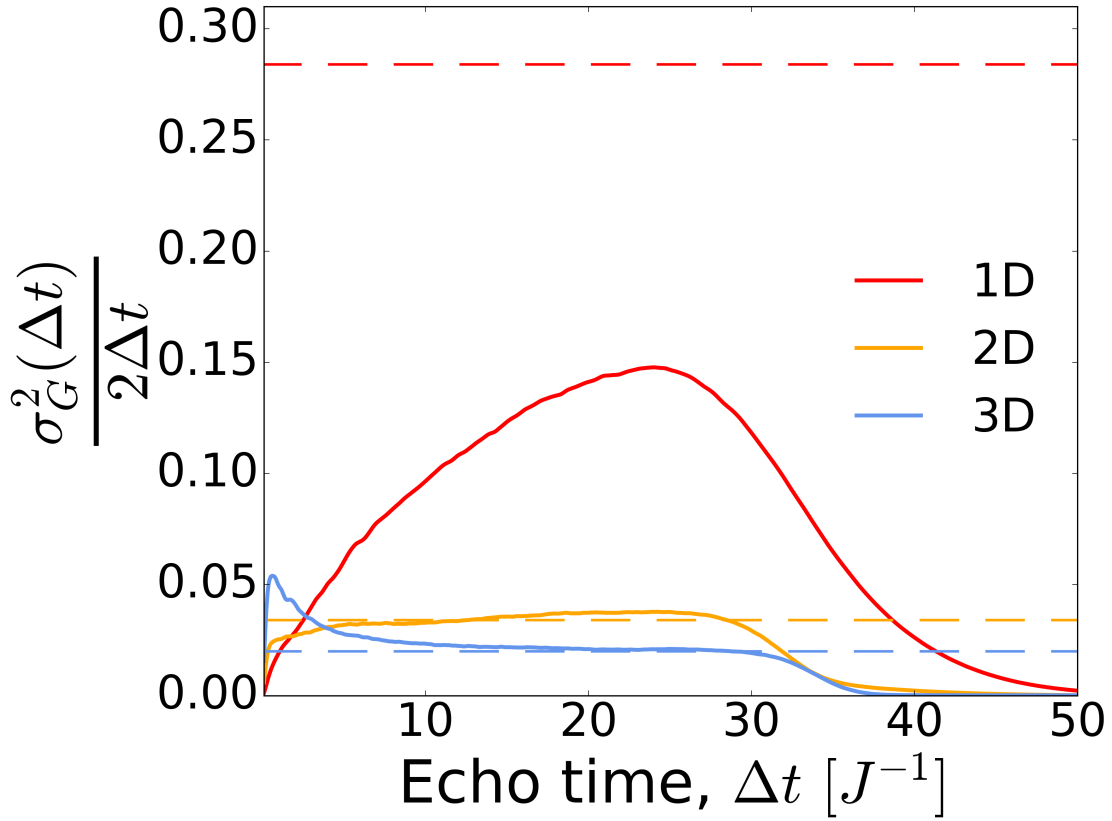


Figure 3-5: Ergodicity tests. The dependence of the ratio  $\frac{\sigma_G^2(\Delta t)}{2\Delta t}$  on the echo time  $\Delta t$  for a 1D chain of 100 sites (red), a 2D square lattice  $10 \times 10$  (orange), a 3D cubic lattice  $4 \times 4 \times 4$  (light blue). The dashed lines are plotted at the levels  $\Lambda - \lambda_{\max}$  corresponding to the plateaux expected for ergodizing systems. These plots imply that the 2D and 3D lattices are ergodized on the timescale of the simulations, while the 1D lattice is not.

### 3.4 Numerical experiments

For illustration, we chose the same three model systems as in Chapter 2 with the same DGPE parameters: a 1D chain  $V = 100$ , a 2D square lattice  $V = 10 \times 10$  and a 3D cubic lattice  $V = 4 \times 4 \times 4$ . The DGPE parameters are fixed such that  $J = 1$ ,  $U = 1$ ,  $\varepsilon = 1$ ,  $n = 1$ ,  $n_i(0) \equiv |\psi_i(0)|^2 = 1$  with almost random phases of  $\psi_i(0)$ . At the moment of time reversal  $\psi_i(\tau + 0) = \psi_i(\tau - 0) + \delta\psi_i$ , where  $\delta\psi_i$  is a random vector subject to  $\sqrt{\sum_i |\delta\psi_i|^2} = 10^{-8}$ . For further details one can refer to a GitHub repository<sup>1</sup>.

In order to test the relation (3.14), we calculated the two averages of Loschmidt

<sup>1</sup>The code used for the analysis in the present Thesis is published in a GitHub repository at <https://github.com/TarkhovAndrei/DGPE>

$V$	$d$	$\lambda_{\max}$	$\Lambda$	$\langle \delta\lambda^2 \rangle$		$\tau_{erg}$		
				Eq. (3.2)	Eq. (3.21)	Eq. (3.2)	Eq.(3.14)	Eq. (3.22)
100	1	$0.643 \pm 0.001$	$0.927 \pm 0.009$	$0.362 \pm 0.001$	$0.413 \pm 0.001$	$0.66 \pm 0.05$	$0.78 \pm 0.03$	$0.69 \pm 0.02$
$10^2$	2	$0.698 \pm 0.001$	$0.731 \pm 0.004$	$0.104 \pm 0.001$	$0.122 \pm 0.001$	$0.32 \pm 0.02$	$0.32 \pm 0.04$	$0.27 \pm 0.03$
$4^3$	3	$0.650 \pm 0.001$	$0.670 \pm 0.001$	$0.080 \pm 0.001$	$0.047 \pm 0.001$	$0.26 \pm 0.02$	$0.25 \pm 0.02$	$0.43 \pm 0.03$

Table 3.1: Summary of numerical tests of relations (3.14) and (3.22):  $V$  is the number of lattice sites,  $d$  is the lattice dimensionality,  $\lambda_{\max}$  and  $\Lambda$  are extracted from Fig. 3-4;  $\langle \delta\lambda^2 \rangle$  is extracted either directly from a time-series of local stretching rates according to Eq. (3.2) or from empirical estimate (3.21); the three values of  $\tau_{erg}$  are obtained on the basis of the definition (3.2), from the Loschmidt echo relation (3.14), and from the approximate relation (3.22).

echoes  $G(\Delta t)$  and  $W(\Delta t)$  for one-, two- and three-dimensional DGPE lattices. The results are presented in Fig. 3-4. The values of the characteristic exponents  $\lambda_{\max}$  and  $\Lambda$  extracted in each case are listed in Table 3.1. We also collected long enough time-series of instantaneous stretching rates  $\lambda(t)$ , then calculated the autocorrelation function  $\varphi(t)$  and extracted  $\langle \delta\lambda^2 \rangle$  and  $\tau_{erg}$ . It is worth noting that the above simulations are laborious. In order to obtain a sufficiently smooth function  $W(\Delta t)$ , one has to gather the ensemble of at least several hundreds Loschmidt echo realizations. Each Loschmidt echo realization requires simulation of the DGPE dynamics for double the echo time. The calculation of the autocorrelation function  $\varphi(t)$  also requires long-time simulations of the Lyapunov process. Overall, the procedures for large DGPE lattices become computationally expensive and require extensive CPU and GPU parallelization.

Table 3.1 compares three values of the ergodization time: the one calculated on the basis of the definition (3.2), the one given by Eq.(3.14) and the one given by the approximation (3.22). In Eq.(3.14), we used the directly calculated value of  $\langle \delta\lambda^2 \rangle$ .

For two- and three-dimensional lattices, the values of the ergodization time obtained from Eqs. (3.2) and (3.14) agree very well. At the same time, we observe clear discrepancy between Eqs. (3.2) and (3.14) for the one-dimensional lattice, which indicates that the system has not ergodized on the timescale covered by the Loschmidt echo. Non-ergodized fast growing samples in  $W(\Delta t)$  from Eq. (3.3) reach saturation significantly earlier than others: an indication of this in Fig. 3-4 is an early departure of  $W(\Delta t)$  from the linear growth regime.

Overall, the ergodization time decreases with the increasing lattice dimension,

being the longest in the one-dimensional case. The ergodization time is a *local measure* of ergodization because the Lyapunov eigenvectors are dynamically localized. Slow ergodization of one-dimensional chains (for Fermi-Pasta-Ulam, Klein-Gordon chains and DGPE) has also been noticed and investigated in Refs. [229, 230].

In all three cases, we further observe that the values obtained from Eq. (3.22) give a satisfactory approximation to Eq. (3.2).

We also performed the ergodicity test associated with relation (3.23). The results are presented in Fig. 3-5, where the ratio  $\frac{\sigma_G^2(\Delta t)}{2\Delta t}$  is plotted as a function of the echo time  $\Delta t$ . For the quickly ergodizing two- and three-dimensional systems, the above ratio levels off rather quickly around the expected value  $\Lambda - \lambda_{\max}$ , whereas for the slow-ergodizing one-dimensional case it never reaches the expected plateau.

### 3.5 Discussion

In this Chapter, we proposed a method of estimating ergodization time of a chaotic many-particle system by monitoring equilibrium noise before and after time reversal of dynamics, and validated it numerically by simulations of the discrete Gross-Pitaevskii equation. We showed that the difference between the largest Lyapunov exponent and the growth rate of the classical counterpart of OTOCs is proportional to the ergodization time of a system. We also introduced a related test for the breakdown of ergodicity. The ergodization time is a *local measure* of ergodization because the Lyapunov eigenvectors are dynamically localized. Hence, the ergodization time is particularly sensitive to the presence of localized highly energetic solitons or breathers weakly coupled to the rest of the system. The ergodization time is thus neither connected to the typical diffusion time (Thouless time) across the system, nor to the typical hydrodynamic timescales.

But if I do not cheat, some kind of atrocious obstacle, which would drive me mad if I persevered, prevents me from imagining the twist which transforms one direction into another, directly opposite. I am crushed, I am carrying the whole world on my back in the process of trying to visualize my turning around and making myself see in terms of ‘right’ what I saw in terms of ‘left’ and vice versa.

—Vladimir Nabokov,  
Look at the Harlequins!

## Chapter 4

# Investigation of non-equilibrium quenches across a second-order phase transition

The investigations presented in this Chapter were initially motivated by the experiment on the light-induced melting of a charge-density wave in  $\text{LaTe}_3$  [231] and then extended to cover related general questions. The Chapter described our simulations of non-equilibrium quenches across a spontaneous symmetry breaking in the 3D DGPE lattice, with a particular focus on the role of topological defects in establishing phase coherence after a quench.

### 4.1 Experimental motivation

Laser-induced melting of a unidirectional charge-density wave (CDW) in  $\text{LaTe}_3$  was investigated experimentally in Refs. [231]. The critical temperature of the CDW transition is about 700 K. By applying laser excitation, one can melt the CDW and temporarily destroy its order-parameter. In a time-resolved pump-probe experiment, the recovery dynamics of the CDW order was tracked. The experiment observed that the amplitude and the phase of the CDW after photo-excitation behave qualitatively differently: the amplitude recovers quickly, whereas, for sufficiently high pump pulse intensity, the recovery of phase coherence takes much longer times [232].

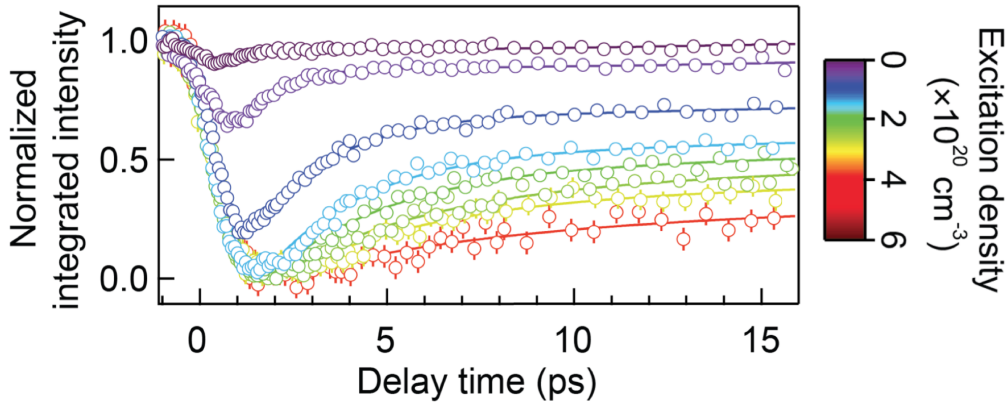


Figure 4-1: Time evolution of integrated intensity of the CDW electron diffraction peak after photo-excitation at varying laser pulse intensities (photo-excitation densities). The figure reproduced from Ref. [231] in adapted form.

In Fig. 4-1, we reproduce the experimental results on ultra-fast electron diffraction of the CDW: the normalized integrated intensity of the CDW diffraction peak is plotted as a function of delay time for various laser pulse intensities. The CDW diffraction peak intensity is proportional to the square of the CDW order-parameter. For smaller laser intensities, the CDW order-parameter never vanishes entirely. Rather it initially becomes smaller and later almost recovers to the initial value. For higher laser intensities, when the CDW becomes totally melted [232], the recovery takes much longer times, and, in fact, does not reach the equilibrium value on the timescale accessible in the experiment. The qualitative trend is that the higher the laser intensity, the slower the CDW order recovery. The authors provided indirect evidence that the slow recovery is caused by the emergence of topological defects of the CDW order, followed by their subsequent slow annihilation. Even though, such a scenario is rather natural, no direct evidence in its favor was presented. Ref. [232] has further found that the slow recovery in the experiment cannot be explained by the amplitude dynamics of the CDW order. Therefore, this slow relaxation was attributed to the phase of the order parameter likely associated with the topological defects.

The findings of Ref. [232] indicate that the initial response of  $\text{LaTe}_3$  following a strong photoexcitation is not describable by a single order parameter because the energy of the laser pulse is mainly absorbed by the electronic subsystem and then

it takes a time about 2 ps for the electronic subsystem to dissipate its energy into the lattice. Only after that, the local behavior of the system can be described by a single CDW order parameter. It is the relaxation in this later-time regime that we would like to describe with the help of the DGPE. The question can still arise whether the calculations based on the purely Hamiltonian DGPE dynamics would miss the dissipative contribution due to the coupling to the electronic excitations. Such a contribution certainly exists in the real material. However, we assume that, due to the smallness of the electronic specific heat relative to that of the lattice, the dissipation caused by the electronic excitations is sufficiently small to justify the applicability of the DGPE-based quench simulations for times longer than 2 ps.

## 4.2 Mapping charge-density wave dynamics to DGPE

In this Chapter, we use the 3D DGPE lattice as a simplified model for simulating the phase dynamics of CDW after a laser pulse. The mapping of the spatially inhomogeneous CDW order onto the DGPE is inspired by the mapping of the superconducting order in large enough domains onto the XY-model for studying classical phase fluctuations [233, 234].

In Fig. 4-2, a sketch of a typical dispersion relation for low-frequency excitations in a CDW material is presented. The process of the CDW formation is associated with softening of a phonon at the CDW wavevector  $\mathbf{q}_{CDW}$ . At the CDW critical temperature, the frequency of the soft phonon reaches zero and the CDW is formed.

The CDW is represented as a modulation of electron charge density in the form

$$\rho(\mathbf{r}) = \rho_0 + \rho_1 \cos(\mathbf{q}_{CDW}\mathbf{r} + \phi) \quad (4.1)$$

accompanied with a lattice displacement

$$\mathbf{r}_n \rightarrow \mathbf{r}_n + \mathbf{u} \cos(\mathbf{q}_{CDW}\mathbf{r}_n + \phi), \quad (4.2)$$

where  $u = |\mathbf{u}|$  and  $\phi$  are the amplitude and phase of the lattice distortion,  $\mathbf{q}_{CDW}$  is the CDW wave vector [232]. Far from equilibrium, the lattice distortion can be

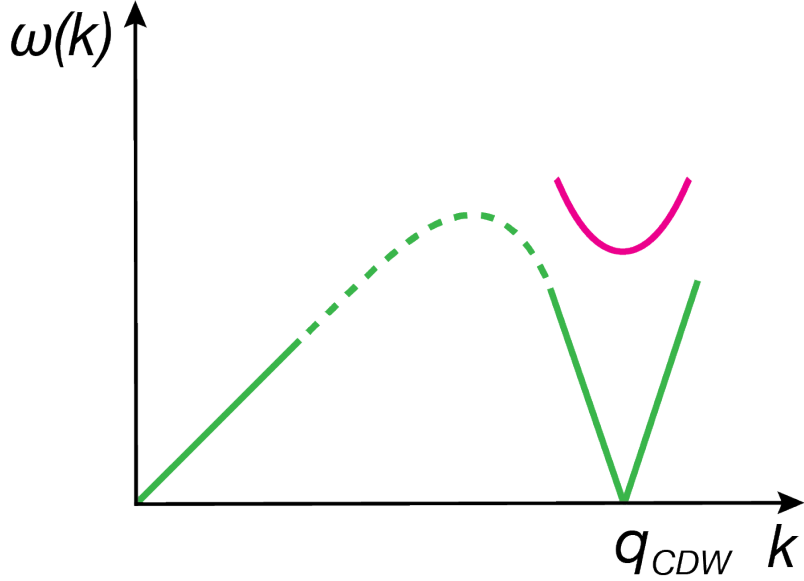


Figure 4-2: A typical acoustic phonon dispersion relation  $\omega(k)$  — green line. The acoustic phonon softening associated with the emergence of the CDW is shown as a sharp dip at the CDW wavevector  $\mathbf{q}_{CDW}$ . The red line represents the dispersion relation for temperatures higher than the critical temperature. The green dashed line represents the region, where the acoustic phonon modes are ill-defined.

out of phase with the electronic density modulation. Here, we are interested in the regime when the lattice and the electronic subsystem are correlated and evolve in phase. Hence, we can choose the complex number  $u \exp(i\phi)$  as the CDW order parameter. By allowing the CDW order parameter to slowly change in space and time,  $u(\mathbf{r}) \exp(i\phi(\mathbf{r}))$ , we can describe the elementary excitations of the CDW—phasons, phase excitations associated with  $\phi(\mathbf{r})$ , and amplitudons, amplitude excitations associated with  $u(\mathbf{r})$ .

To map the continuous CDW order  $u(\mathbf{r}) \exp(i\phi(\mathbf{r}))$  to the DGPE lattice  $\psi_j$ , we assume that each elementary volume of the CDW with a characteristic coherence length  $l$  represents a single site of the 3D DGPE lattice. The reasoning behind the classical modelling is that, for large enough domains, the quantum fluctuations can be neglected. Therefore, the mapping is achieved by averaging the CDW order parameter over a coherence volume around the 3D DGPE lattice site at  $\mathbf{r}_j$ :

$$\psi_j \sim \langle u(\mathbf{r}) e^{i\phi(\mathbf{r})} \rangle_{|\mathbf{r}-\mathbf{r}_j| \leq l}. \quad (4.3)$$

We use the 3D DGPE equation for the simulations because it possesses an excitation spectrum qualitatively similar to that of the CDW. The non-interacting DGPE has a frequency band with a quadratic dispersion relation at the bottom, which is similar to that of the CDW precursor mode at high temperatures (pink branch in Fig 4-2). Below  $T_c$ , this mode turns into the CDW phason with a linear spectrum (green line touching zero at the CDW wavevector  $\mathbf{q}_{CDW}$  in Fig. 4-2). The 3D DGPE with interaction also has excitations with linear dispersion at long wavelengths.

To finalize the mapping, we estimate three parameters of the 3D DGPE lattice:

- the hopping term  $J$
- the typical value of the “particle density” parameter  $n \equiv \langle |\psi_j|^2 \rangle$
- the nonlinearity parameter  $U$

Since the CDW coherent domains are typically larger than the crystal lattice period  $a$ , the CDW dynamics would occur at frequencies smaller than the Debye frequency  $\Omega_D \sim 4$  THz (in LaTe<sub>3</sub>). Hence, the hopping term  $J$  can be roughly estimated as

$$J = \Omega_D \frac{a}{l}. \quad (4.4)$$

The CDW coherence length [235] reads

$$l = \frac{\hbar v_F}{\pi \varepsilon_g}, \quad (4.5)$$

where  $v_F = \frac{2\varepsilon_F}{p_F}$  is the Fermi velocity,  $\varepsilon_g$  is the CDW energy gap. For LaTe<sub>3</sub>,  $\varepsilon_F \approx 1.5$  eV and  $p_F \approx \frac{3\pi \hbar}{8a}$  [236],  $\varepsilon_g \approx 0.35$  eV [237]. Hence, the direct application of that formula would give very short  $l \sim 2a$ . If, however, we take into account that the critical temperature  $60\text{meV} \approx 700$  K is smaller than the CDW energy gap, and replace the energy gap with the temperature in Eq. (4.5):

$$l \approx \frac{2\hbar}{\pi p_F} \frac{\varepsilon_F}{k_B T_c} \sim 10a, \quad (4.6)$$

hence, the present estimate for the hopping term gives  $J \sim 1$  ps<sup>-1</sup>.

A bit more involved analysis giving essentially the same estimate would start from the observation that both the DGPE and the real CDW materials [238, 239] exhibit strongly overdamped excitations in the vicinity of the phase transition temperature  $T_c$ . The experiment in Ref. [240] shows that at large temperatures the frequency width of the phase fluctuations is of the order of the amplitudon's frequency at the CDW wavevector  $\mathbf{q}_{CDW}$ ,  $\omega_{Am}(\mathbf{q}_{CDW})$ . We use that observation to estimate the parameter  $J$  by matching the amplitudon's frequency known from experiment and the first-principle calculations with the high-temperature frequency width of equilibrium fluctuations in the DGPE model:

$$\sqrt{2d}J \sim \omega_{Am}(\mathbf{q}_{CDW}), \quad (4.7)$$

where  $d = 3$  is the dimension of the lattice. The direct measurement of the amplitudon's frequency is challenging experimentally at  $k \neq 0$ . However, in the first-principles simulations of Ref. [241], it is shown that the amplitudon's frequency decreases for larger wavevectors, and, at the CDW wavevector  $\mathbf{q}_{CDW}$ , it reaches approximately 1/5 of its value at  $k = 0$ . We assume that such an estimate is also relevant for the CDW in LaTe<sub>3</sub>, hence  $\omega_{Am}(\mathbf{q}_{CDW}) \sim \omega_{Am}(0)/5$ . In LaTe<sub>3</sub>, the amplitudon's frequency is  $\omega_{Am}(0) = 2.2$  THz [242]. Therefore, our hopping parameter estimate is:

$$J \sim \frac{\omega_{Am}(0)}{5\sqrt{2d}} \sim 1 \text{ ps}^{-1}, \quad (4.8)$$

which is consistent with the value obtained from Eq. (4.4).

The typical parameter  $n$  can be estimated from the fact that at the critical temperature the hopping energy is of order of the thermal energy  $Jn \sim k_B T_c$ . Thus:

$$n \sim \frac{k_B T_c}{J} \sim \hbar \frac{T_c}{T_D} \frac{l}{a}. \quad (4.9)$$

Here, we used Eq. (4.4) and replaced  $\hbar\Omega_D$  with  $k_B T_D$ , where  $T_D \sim 200K$  is the Debye temperature for LaTe<sub>3</sub> [243]. This relation shows that the typical value of  $n/\hbar$  is a reasonably large number 10...40, which, in turn, justifies the classical

character of our modelling.

In order to estimate the nonlinearity parameter  $U$ , we match the phason velocity in the DGPE and the real CDW system. Let us first derive the phason velocity for the 3D DGPE model. In the 3D DGPE (1.14), the excitation spectrum above the condensate can be extracted by dividing  $\psi_j$  at each lattice site into the contribution from the condensate and the perturbation  $\psi_j(t) = \Psi_0 + \xi_j(t)$ . This leads to

$$i\dot{\Psi}_0 + i\dot{\xi}_j = -2dJ\Psi_0 - J \sum_{m \in \text{NN}(j)} \xi_m + U |\Psi_0 + \xi_j|^2 (\Psi_0 + \xi_j). \quad (4.10)$$

The solution for the unperturbed condensate  $i\dot{\Psi}_0 = -2dJ\Psi_0 + U |\Psi_0|^2 \Psi_0$  has the form of  $\Psi_0(t) = \sqrt{n_0} \exp(-it\mu)$ , where we denote the ‘‘number of particles’’ in the condensate as  $n_0 = |\Psi_0|^2$  and the chemical potential  $\mu = -2Jd + Un_0$ . Next, we introduce the perturbation in the rotating frame of reference by substituting  $\xi_j = \zeta_j e^{-it\mu}$ , and rewrite Eq. (4.10):

$$i\dot{\zeta}_j = -J \sum_{m \in \text{NN}(j)} \zeta_m - \mu\zeta_j + U (2n_0\zeta_j + n_0\zeta_j^* + 2\sqrt{n_0} |\zeta_j|^2 + \sqrt{n_0}\zeta_j^2 + |\zeta_j|^2\zeta_j). \quad (4.11)$$

Taking into account that  $\zeta_j \ll \sqrt{n_0}$ , we neglect higher order terms in  $\zeta_j$  and obtain

$$i\dot{\zeta}_j = -J \sum_{m \in \text{NN}(j)} \zeta_m - \mu\zeta_j + U (2n_0\zeta_j + n_0\zeta_j^*). \quad (4.12)$$

The spatial Fourier transform  $\zeta_j(t) = \sum_{\mathbf{k}} \zeta_{\mathbf{k}}(t) \exp(i2\pi\mathbf{k}\mathbf{r}_j)$  then gives:

$$i\dot{\zeta}_{\mathbf{k}} = \tilde{\varepsilon}(\mathbf{k})\zeta_{\mathbf{k}} + Un_0\zeta_{\mathbf{k}}^*, \quad (4.13)$$

where  $\tilde{\varepsilon}(\mathbf{k}) = \varepsilon(\mathbf{k}) - \mu + 2Un_0$ , with  $\varepsilon(\mathbf{k}) = -2J \sum_{e \in x,y,z} \cos(k_e l)$ .

Let us look for the solutions of Eq. (4.13) of the form

$$\zeta_{\mathbf{k}}(t) = u_{\mathbf{k}} e^{-i\omega_{\mathbf{k}} t} + v_{\mathbf{k}}^* e^{i\omega_{\mathbf{k}} t} = \begin{pmatrix} e^{-i\omega_{\mathbf{k}} t} & e^{i\omega_{\mathbf{k}} t} \end{pmatrix} \begin{pmatrix} u_{\mathbf{k}} \\ v_{\mathbf{k}}^* \end{pmatrix}, \quad (4.14)$$

Eq. (4.13) then leads to

$$\begin{pmatrix} e^{-i\omega_{\mathbf{k}}t} & e^{i\omega_{\mathbf{k}}t} \end{pmatrix} \begin{pmatrix} \omega_{\mathbf{k}}u_{\mathbf{k}} \\ -\omega_{\mathbf{k}}v_{\mathbf{k}}^* \end{pmatrix} = \begin{pmatrix} e^{-i\omega_{\mathbf{k}}t} & e^{i\omega_{\mathbf{k}}t} \end{pmatrix} \begin{pmatrix} \tilde{\varepsilon}(\mathbf{k})u_{\mathbf{k}} + Un_0v_{\mathbf{k}} \\ \tilde{\varepsilon}(\mathbf{k})v_{\mathbf{k}}^* + Un_0u_{\mathbf{k}}^* \end{pmatrix} \quad (4.15)$$

To find the dispersion relation for the excitations above the condensate, we diagonalize the matrix

$$\begin{pmatrix} \omega_{\mathbf{k}} - \tilde{\varepsilon}(\mathbf{k}) & -Un_0 \\ -Un_0 & -\omega_{\mathbf{k}} - \tilde{\varepsilon}(\mathbf{k}) \end{pmatrix} = 0, \quad (4.16)$$

and thereby obtain the dispersion relation

$$\omega_{\mathbf{k}} = \sqrt{\tilde{\varepsilon}^2(\mathbf{k}) - (Un_0)^2}, \quad (4.17)$$

which, after substituting  $\tilde{\varepsilon}(\mathbf{k})$ , gives

$$\omega_{\mathbf{k}} = \sqrt{\left(2J \sum_{e \in x,y,z} (1 - \cos(k_e l)) + Un_0\right)^2 - (Un_0)^2}. \quad (4.18)$$

For the long wavelengths

$$\omega_{\mathbf{k}} \approx \sqrt{(Jl^2\mathbf{k}^2)^2 + 2l^2JU n_0\mathbf{k}^2}. \quad (4.19)$$

Hence, the speed of phasons that follows from the 3D DGPE model is

$$c_{ph} = l\sqrt{2JU n_0}. \quad (4.20)$$

Let us assume that  $c_{ph}$  for the real material is known. We then use Eq. (4.20) to estimate the DGPE nonlinearity term  $g = Un/J$  as follows:

$$g = \frac{Un}{J} = \frac{1}{2} \left(\frac{c_{ph}}{Jl}\right)^2 = \frac{1}{2} \left(\frac{c_{ph}}{\Omega_D a}\right)^2 = \frac{(6\pi^2)^{2/3}}{2} \left(\frac{c_{ph}}{c_s}\right)^2, \quad (4.21)$$

where  $c_s \sim (6\pi^2)^{-1/3}\Omega_D a$  is the speed of sound. As a crude estimate, one can use  $c_{ph} \sim c_s$ , thereby obtaining  $g \sim 10$ .

To summarize, our estimates for the 3D DGPE parameters for LaTe<sub>3</sub> are:  $J \sim$

$1 \text{ ps}^{-1}$ ,  $n \sim 10 \dots 40\hbar$  and  $g \sim 10$ .

### 4.3 Model system

For simulating the phase-ordering kinetics of the CDW, we use the dimensionless Hamiltonian (1.20) and the dimensionless DGPE (1.21) with the parameters consistent with the mapping to the real CDW material from Section 4.2:  $J = 1$ ,  $U = 10$ ,  $n = 1$ ,  $g = Un/J = 10$ . All  $\psi_j$  are normalized so that  $n = n_j = 1$ . Time is also rescaled as in Section 1.5.

Before simulating non-equilibrium quenches from the high-energy non-ordered phase to the low-energy ordered phase, we study the equilibrium statistical properties of the 3D DGPE lattice including the ordering transition. The 3D DGPE lattice exhibits a transition to the low-temperature ordered phase characterized by a non-zero order parameter:

$$\Psi \equiv \frac{1}{V} \sum_{j=1}^V \psi_j. \quad (4.22)$$

Below, for comparison with the CDW experiment, we also use the parameter

$$\Delta \equiv |\Psi|^2. \quad (4.23)$$

Using the recipe from Section 1.4 for calculating the microcanonical temperature, we identify the critical temperature of the ordering transition. The procedure is the following. First, we initialize the state with uniform particle density  $|\psi_j|^2 = 1$  for all  $j$  and assign random phases to each  $\psi_j$ . Such an initial condition corresponds to energy density  $\varepsilon \sim 1$ . Then, we bring our system to the microcanonical energy shell with a given value of  $\varepsilon$ . We do this by adding to the DGPE a special norm-conserving, non-energy-conserving term as follows:

$$i \frac{d\psi_j}{dt} = - \sum_{k \in \text{NN}(j)} \psi_k + g |\psi_j|^2 \psi_j - iK(t) \psi_j \sum_{k \in \text{NN}(j)} (\psi_k^* \psi_j - \psi_k \psi_j^*), \quad (4.24)$$

where  $K(t)$  is a time-dependent parameter. The last term is increasing the total energy for  $K(t) > 0$ , while lowering it for  $K(t) < 0$ . We run the non-conservative dynamics of Eq. (4.24) with relatively small  $K$  equal to 0.01 or  $-0.01$  in order to increase or decrease the energy of the system respectively. When we reach the required energy, we switch off the non-conservative term by putting  $K$  equal to 0, and allow the system to thermalize on the energy shell for a sufficiently long time. Once the system has thermalized, we determine the temperature for the energy shell using the procedure described in Section 1.4. Namely, we perform the averaging of  $\Phi$  defined by Eq. (1.10). By spanning the energy range of interest, we acquire the dependence  $T(\varepsilon)$ , from which we extract the specific heat:

$$c_v \equiv \frac{\partial \varepsilon}{\partial T} = \left( \frac{\partial T}{\partial \varepsilon} \right)^{-1}. \quad (4.25)$$

The phase transition is indicated by the peak of  $c_v(T)$ . Simultaneously, we follow the emergence of order by computing the value of the order parameter  $\Delta$  as a function of energy and temperature.

In Fig. 4-3, we plot  $\varepsilon(T)$ ,  $c_v(T)$  and  $\Delta(T)$ . Due to the singular dependence of  $T(\varepsilon)$ , the transition is rather sharp: both the symmetry breaking and the specific heat singularity occur close to  $T_c \approx 1.9$ . In Fig. 4-4, we also demonstrate the dependencies  $T(\varepsilon)$ ,  $c_v(\varepsilon)$  and  $\Delta(\varepsilon)$ .

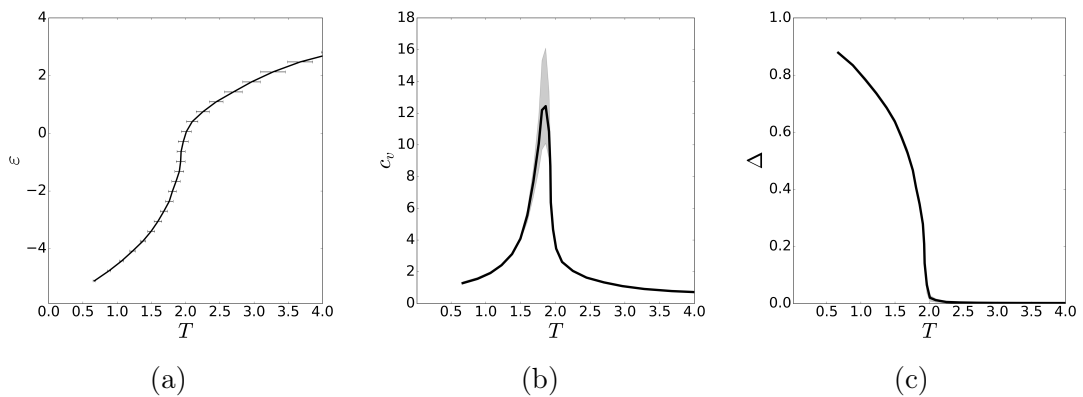


Figure 4-3: Signatures of the spontaneous symmetry breaking in the 3D DGPE lattice: (a) energy density,  $\varepsilon(T)$ , (b) specific heat  $c_v(T)$  and (c) the order parameter,  $\Delta(T)$  as functions of temperature  $T$ .

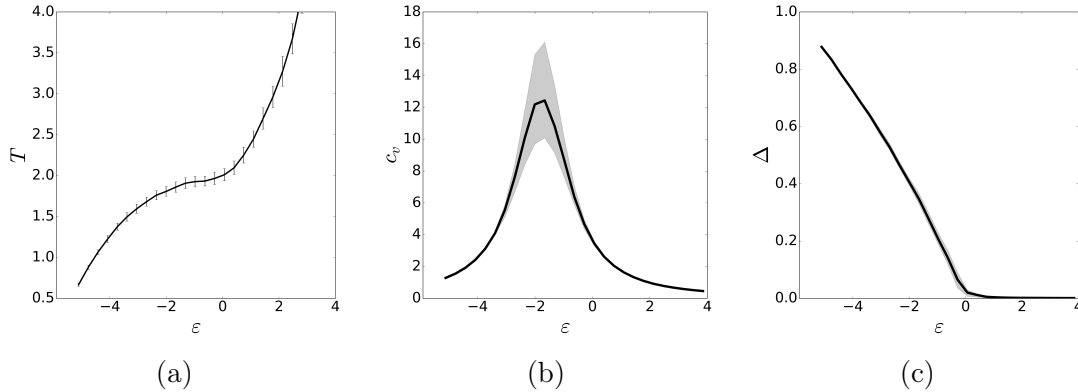


Figure 4-4: Signatures of the spontaneous symmetry breaking in the 3D DGPE lattice: (a) temperature,  $T(\varepsilon)$ , (b) specific heat  $c_v(\varepsilon)$  and (c) the order parameter,  $\Delta(\varepsilon)$  as functions of the energy density  $\varepsilon$ .

## 4.4 Quenching protocol

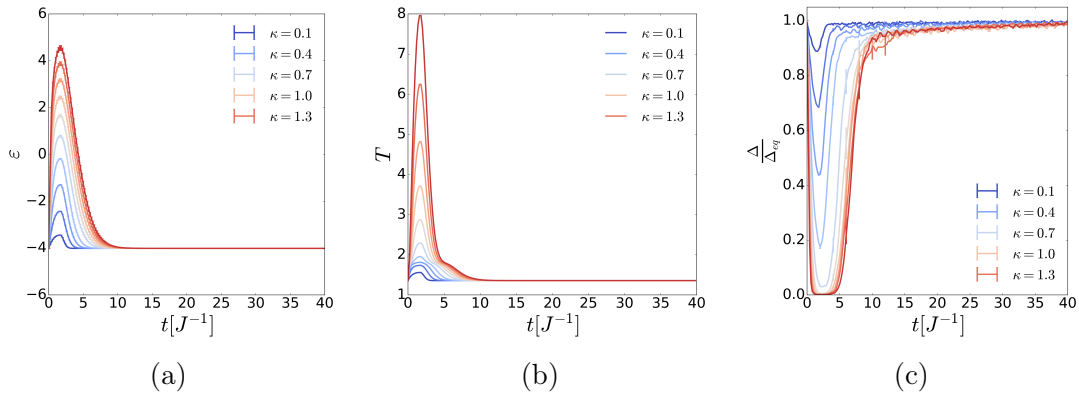


Figure 4-5: The non-equilibrium quench protocol. (a) energy density,  $\varepsilon(t)$ , (b) temperature,  $T(t)$ , (c) the order parameter normalized to its equilibrium value  $\Delta(t)/\Delta_{eq}$ — all as a function of time after the quench. Color represents the value of the quenching rate  $\kappa$ .

We choose a quenching protocol aimed at mimicking the experiment on laser-induced melting of the CDW order [231]. In the experiment, the system is initially at equilibrium at  $T \sim T_c/2$ . The laser pulse deposits the energy to the system and, as a result, the temperature of the electronic subsystem initially increases but then, once the laser pulse terminates, it starts decreasing because the energy is transferred from electrons to phonons, which have much higher specific heat [232]. Likewise, in our quenching protocol, we start with temperature  $T \sim T_c/2$ ; the DGPE lattice is initially heated and then cooled by using the time-dependent parameter  $K(t)$  in

Eq. (4.24). The time-dependence of  $K(t)$  is chosen as a bell-shaped function which initially increases and then decreases on the characteristic hopping timescale of the 3D DGPE. Our specific choice is:

$$K(t) = \kappa \frac{\gamma_2 e^{-\gamma_2 t} - \gamma_1 e^{-\gamma_1 t}}{\gamma_2 - \gamma_1} - \gamma (1 - e^{-\gamma_2(t-t^*)}) \frac{E(t) - E_0}{E^* - E_0}, \quad (4.26)$$

where  $\kappa$  is the parameter controlling the quench strength;  $\gamma = 0.01$ ,  $\gamma_1 = 1$  and  $\gamma_2 = 0.3$  are the parameters controlling the temporal profile of  $K(t)$ ,  $t^* = \log(\gamma_1/\gamma_2)/(\gamma_1 - \gamma_2)$  is the time of the maximum for the first term in Eq. (4.26),  $E_0$  is the initial energy of the system,  $E(t)$  is the energy at time  $t$ , and  $E^* = E(t^*)$ . The quenching procedure conserves  $\langle |\psi_j|^2 \rangle$  corresponding to  $n = 1$ . For further details one can refer to the source code published in a GitHub repository<sup>1</sup>.

In Fig. 4-5, we illustrate how the typical quenching protocol is implemented. By tuning the controlling parameter  $\kappa$ , we change the amount of energy pumped into the system during the quench. In Fig. 4-5a, the time-dependent energy density profile is shown. In Fig. 4-5b, we plot the temperature that would correspond to the monitored energy dependence if, at each moment of time, the system were at equilibrium. For this purpose we use the function  $T(\varepsilon)$  plotted in Fig. 4-4a. For  $\kappa > 0.5$ , there is a time range, where the energy and temperature of the system are above the critical values associated with the ordering phase transition. In Fig. 4-5c, it can be seen how the monitored order-parameter disappears and then reappears in the course of the quench.

We expect that the dynamics of the DGPE lattice in the quenching protocol described above corresponds to the dynamics of the real CDW material only in the regime where the DGPE is exiting the quench, i.e. at times  $t > 3$ .

## 4.5 Simulation of non-equilibrium quenches

In Fig. 4-6, we show the behavior of the order parameter relaxation back to equilibrium for the 3D DGPE cubic lattices of sizes  $V = 20 \times 20 \times 20$ ,  $V = 30 \times 30 \times 30$ ,

<sup>1</sup>The code used for the analysis in the present Thesis is published in a GitHub repository at <https://github.com/TarkhovAndrei/DGPE>

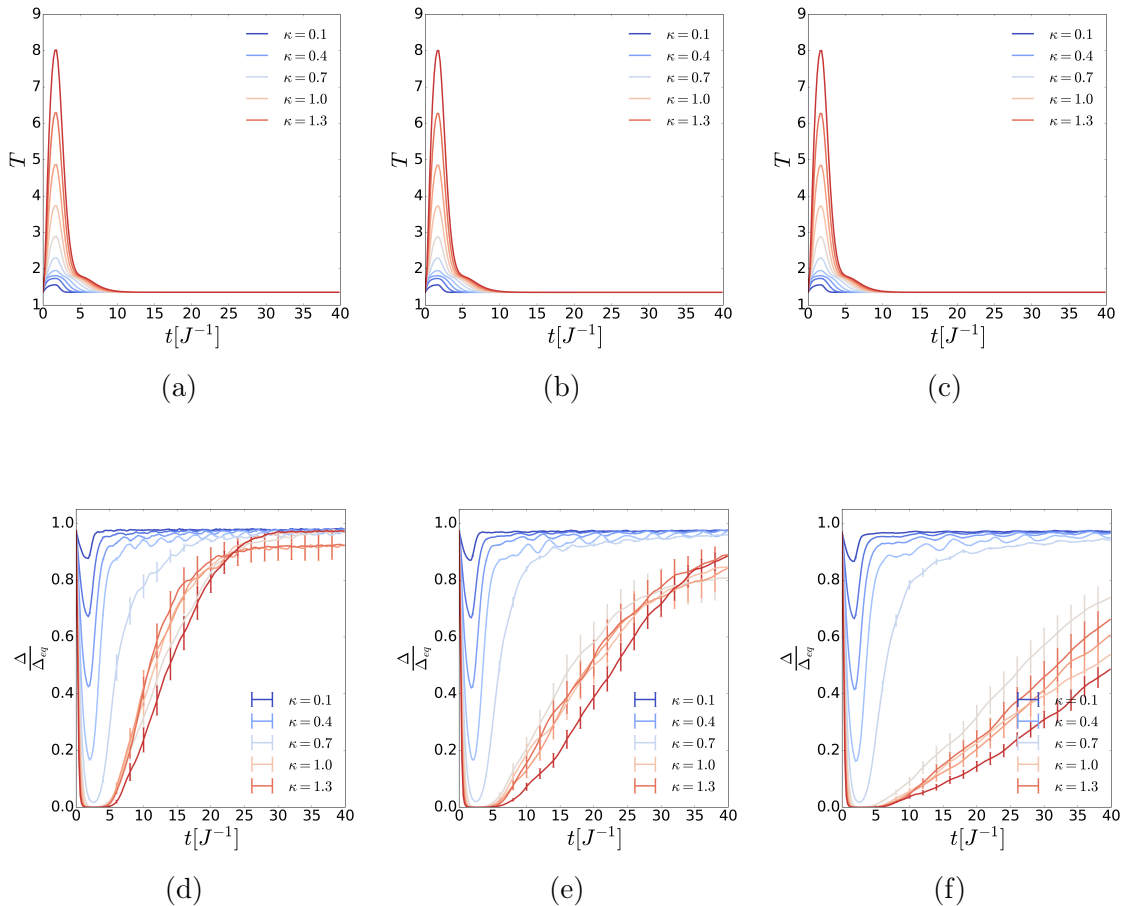


Figure 4-6: System size scaling of the order parameter recovery after the quench:  $\Delta(t)/\Delta_{eq}$  for almost identical quenching protocol  $T(t)$ . Upper panel:  $T(t)$ . Lower panel:  $\Delta(t)/\Delta_{eq}$ . The system sizes: (a,d)  $V = 20^3$ , (b,e)  $V = 30^3$ , (c,f)  $V = 40^3$ . Color represents the value of the quenching rate  $\kappa$ .

$V = 40 \times 40 \times 40$ .

Although, the quenching protocol is the same for all three lattices, the recovery time of the order parameter is strongly affected by the system size for the quenches crossing the phase transition. As argued in the next section, this is the result of the influence of topological defects on the recovery of the order parameter, in conceptual agreement with the Kibble-Zurek mechanism [125–128].

Overall, the quench response of the 3D DGPE lattice presented in Fig. 4-6 is strongly reminiscent of the experimental behavior shown in Fig. 4-1.

## 4.6 Topological defects induced by the quench

### 4.6.1 Definition of vorticity for the 3D DGPE lattice

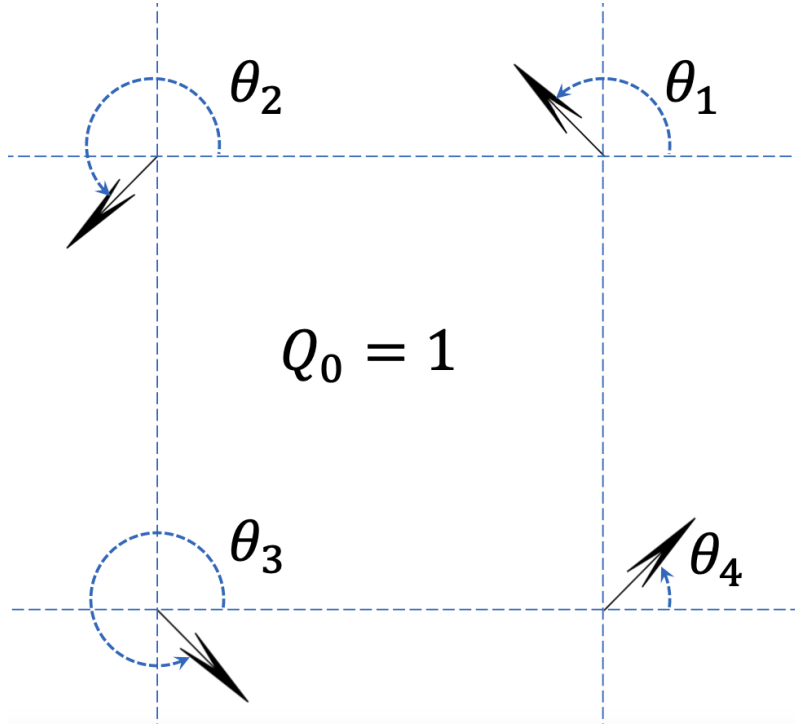


Figure 4-7: Example of a DGPE plaquette with vorticity  $Q_0 = 1$  according to Eq. (4.30).

The discrete Gross-Pitaevskii equation (1.21) can be considered as a finite-difference approximation to the continuous Gross-Pitaevskii equation:

$$i \frac{\partial \psi(\mathbf{r}, t)}{\partial t} = -\nabla^2 \psi(\mathbf{r}, t) + g |\psi(\mathbf{r}, t)|^2 \psi(\mathbf{r}, t), \quad (4.27)$$

where  $\psi(\mathbf{r}, t) = \sqrt{n(\mathbf{r}, t)} \exp(i\theta(\mathbf{r}, t))$ . One can introduce the current density:

$$\mathbf{j}(\mathbf{r}, t) \equiv -i(\psi^*(\mathbf{r}, t)\nabla\psi(\mathbf{r}, t) - \psi(\mathbf{r}, t)\nabla\psi^*(\mathbf{r}, t)) = 2n\nabla\theta(\mathbf{r}, t), \quad (4.28)$$

and the velocity of the condensate flow  $\mathbf{v}_s(\mathbf{r}, t) \equiv \nabla\theta(\mathbf{r}, t)$ . The system is irrotational in the absence of vortices, that is  $\nabla \times \mathbf{v}_s(\mathbf{r}, t) = 0$  [244]. When a vortex is present,  $\nabla \times \mathbf{v}_s(\mathbf{r}, t) \neq 0$  in the core of the vortex. The flux of  $\nabla \times \mathbf{v}_s(\mathbf{r}, t)$  through a chosen

surface is quantized:

$$\iint (\nabla \times \mathbf{v}_s, d\mathbf{S}) = \oint (\mathbf{v}_s, d\mathbf{l}) = \oint \nabla\theta d\mathbf{l} = 2\pi Q, \quad (4.29)$$

where  $Q$  is the topological charge.

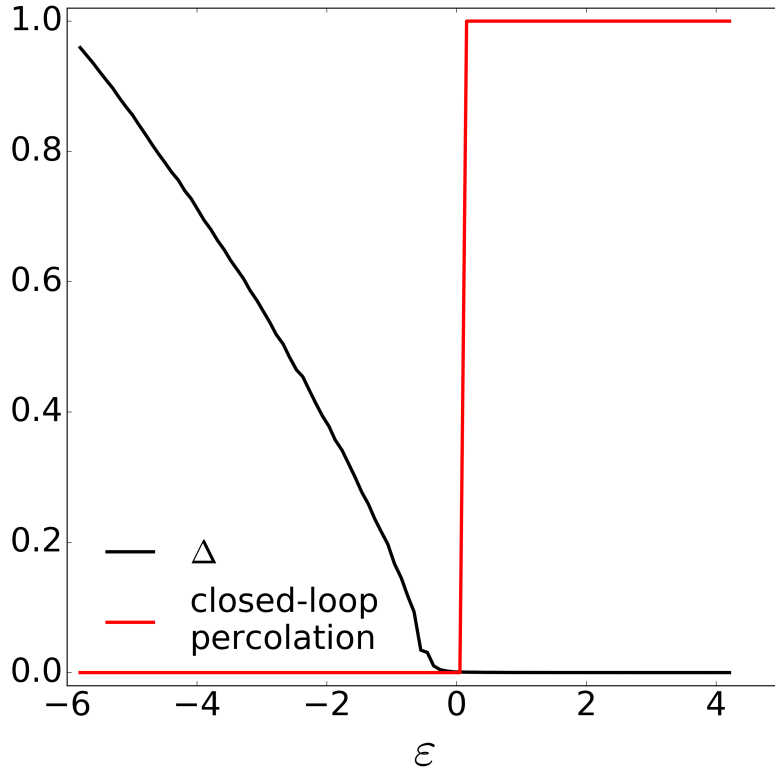


Figure 4-8: A non-contractible loop percolation as the reason for the symmetry breaking in the 3D DGPE lattice. Black line—the order parameter,  $\Delta(\varepsilon)$ , as functions of the energy density, red line—the presence of a non-contractible closed-loop vortex in the system (0—no such loop, 1—the loop has percolated). The system's volume  $V = 30^3$ .

In the discrete case, we define the vorticity using the topological charge of each square plaquette formed by 4 adjacent sites. As an example, a cubic unit cell with 8 lattice sites as its vertices contains 6 differently oriented plaquettes, which are the faces of this cube. Thus, each lattice site on a 3D cubic lattice contributes to 8 thus defined plaquettes.

We define the topological charge (vorticity) of a plaquette such that it can have values 0, 1,  $-1$ . This definition is implemented as follows. Recalling that for each lattice site  $\psi_j = \sqrt{n_j} \exp(i\theta_j)$ , we obtain the vorticity for a chosen plaquette by

enumerating its vertices as 1, 2, 3, 4, then defining the vorticity  $Q_0$  of the plaquette as:

$$Q_0 = \frac{1}{2\pi} [(\theta_2 - \theta_1)|_{\text{mod } \pi} + (\theta_3 - \theta_2)|_{\text{mod } \pi} + (\theta_4 - \theta_3)|_{\text{mod } \pi} + (\theta_1 - \theta_4)|_{\text{mod } \pi}]. \quad (4.30)$$

In Fig. 4-7, we demonstrate an example of a plaquette with vorticity  $Q_0 = 1$ .

In order to analyze the spatial configurations of vorticity, we define the dual lattice, which is obtained by translating the original lattice by vector  $(1/2, 1/2, 1/2)$ . Thus, each of the sites of the dual lattice finds itself surrounded by 8 sites of the original lattice, which form 6 plaquettes. We further introduce a binary measure of vorticity  $Q_j$  for the dual lattice defined such that  $Q_j = 0$  if all adjacent plaquettes have zero vorticity, and  $Q_j = 1$  otherwise. Finally, we introduce the average vorticity  $Q_{av}$  for the entire dual lattice as

$$Q_{av} = \frac{\sum_j^V Q_j}{V}. \quad (4.31)$$

In addition, in the pictorial representation, we use variable  $\mathbf{u}_j$ , which is the finite difference analog of the curl  $\nabla \times \mathbf{v}_s(\mathbf{r}, t)$  for each dual lattice site.

In Fig. 4-8, we demonstrate that the spontaneous symmetry breaking coincides with the percolation of a non-contractible closed-loop vortex through the whole system. The vortex is called non-contractible, when it crosses the whole system and closes via the periodic boundary conditions.

In Fig. 4-9, we illustrate how the mapping of Eq. (4.3) from the CDW order parameter to the DGPE lattice transforms the topological defects of the CDW, dislocations, to the DGPE topological defects, vortices.

## 4.6.2 Monitoring the vorticity in the course of the quench

In Fig. 4-10, we present the evidence that the emergence of vortices is responsible for the slowing down of the order parameter recovery after a strong quench for

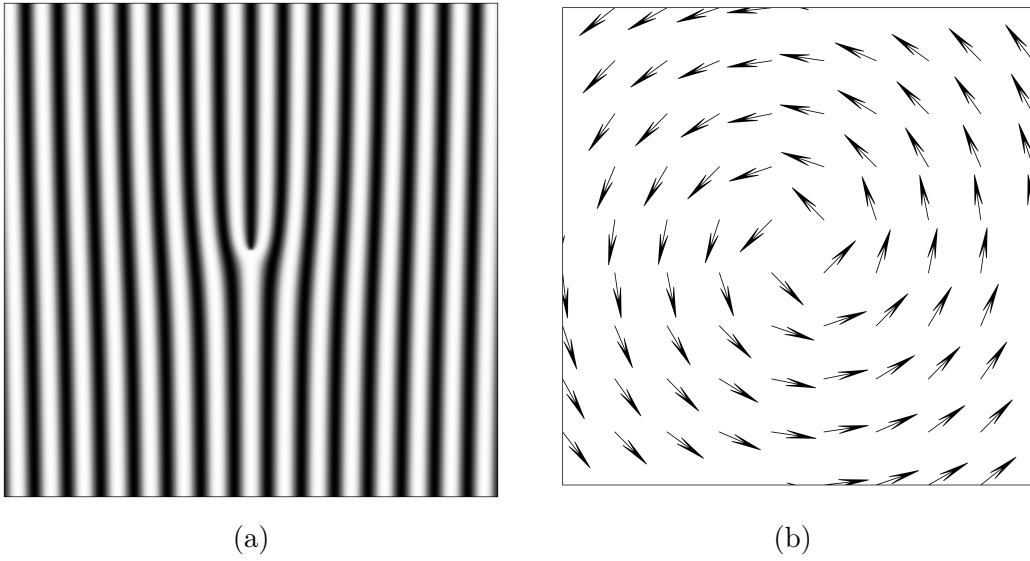


Figure 4-9: Mapping of the topological defects of the CDW to the DGPE lattice: (a) a dislocation of the CDW order,  $u(\mathbf{r}) \exp(i\phi(\mathbf{r}))$ , plotted as a 2D map of the electronic density modulation defined by Eq. (4.1)—white and black represent the CDW regions with the increased and decreased electronic density respectively, (b) a vortex of the DGPE lattice corresponding to the CDW dislocation after the mapping—each arrow represents  $\psi_j$ .

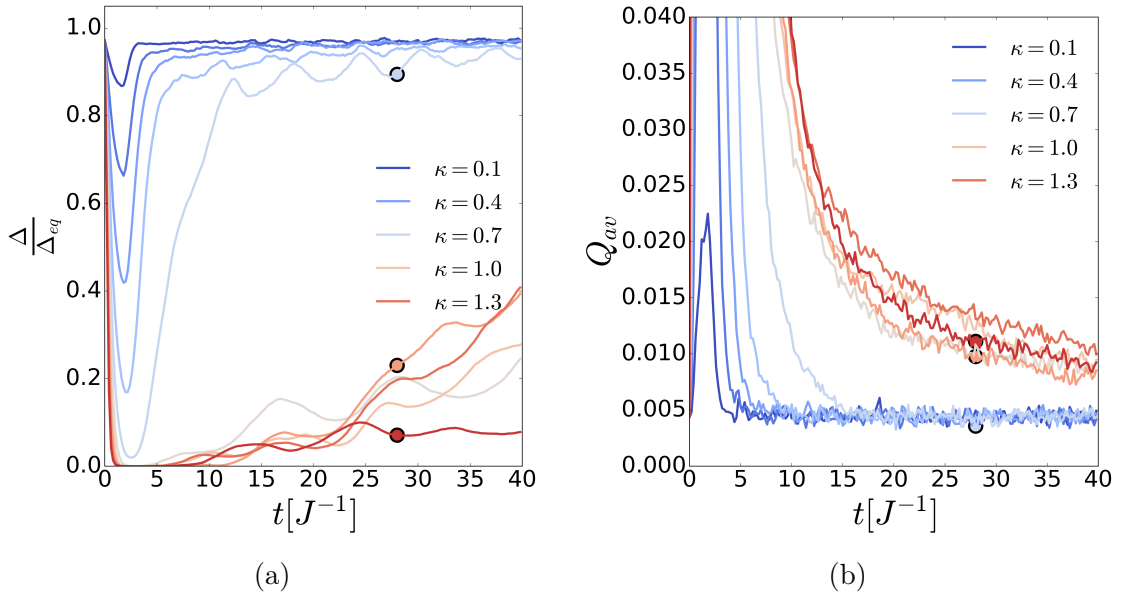
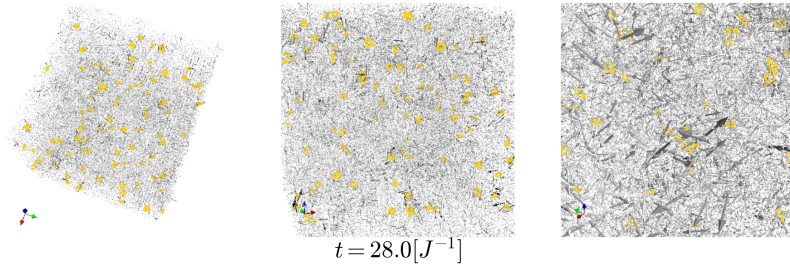
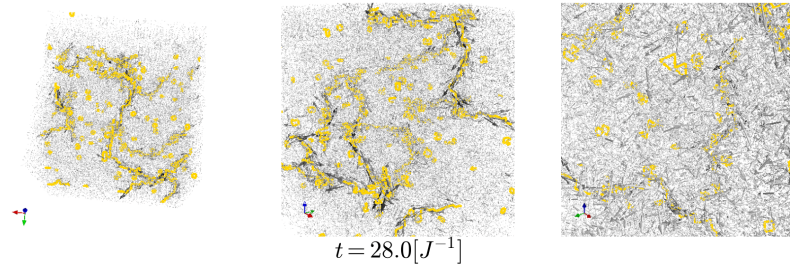


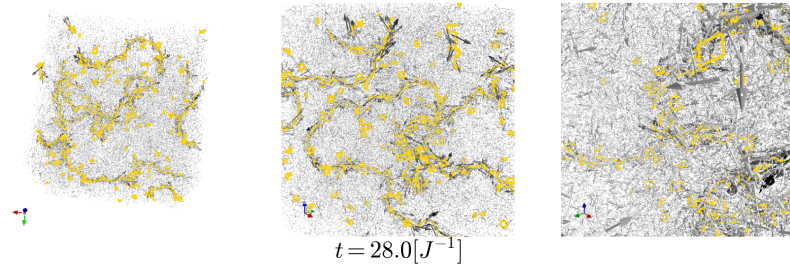
Figure 4-10: Illustration of the role of topological defects in the slowing down of the order parameter recovery for  $V = 50^3$ : (a) order parameter normalized to its equilibrium value  $\Delta(t)/\Delta_{eq}$  as a function of time; (b) the average vorticity  $Q_{av}(t)$  for the same system. Color represents the value of the quenching control parameter  $\kappa$  as indicated in the plot legend. The states corresponding to the three points (red, pink, blue) in each of the plots are to be analyzed below in more detail.



(a) Snapshot for the blue dot in Fig. 4-10



(b) Snapshot for the pink dot in Fig. 4-10



(c) Snapshot for the red dot in Fig. 4-10

Figure 4-11: Snapshots of vorticity for three individual quenches at time  $t = 28[J^{-1}]$  and  $V = 50^3$ , marked in Fig. 4-10 by (a) blue dot,  $\kappa = 0.7$ , (b) pink dot,  $\kappa = 1.14$ , (c) red dot,  $\kappa = 1.44$ . Each row contains three 2D projections of the same 3D lattice. Yellow color is used to depict the core of closed-loop vortices. As a guide-to-eye, we plot  $\mathbf{u}_j$ , the finite difference approximation of the vorticity, as black arrows. The full video for the pink dot is available by the link [https://youtu.be/OamCQ\\_QDqN0](https://youtu.be/OamCQ_QDqN0).

the DGPE lattice with size  $V = 50 \times 50 \times 50$ . The time-dependence of the order parameter for a range of quenching strengths is presented in Fig. 4-10a. In Fig. 4-10b, one can see that the quenches with the pronounced slowing down of the recovery are accompanied by the high value of the average vorticity  $Q_{av}(t)$ .

In Fig. 4-11, we provide a space-resolved view of the vorticity generated in the

course of the above quenches. Specifically, we present three 2D projections of the 3D snapshots of the vorticity for three different states marked in Fig. 4-10 by blue, pink and red dots. Fig. 4-11a illustrates a weak quench, for which the order parameter recovers quickly. One can see that the system does have regions of non-zero vorticity, but these regions are small and disconnected. On the contrary, Figs. 4-11b and 4-11c present snapshots for strong quenches, in which one can see much stronger vorticity percolating through large volumes of the system and forming clearly identifiable large vortex loops.

Fig. 4-12 illustrates the full time-evolution of the system presented in Fig. 4-11c and marked in Fig. 4-10 by the red dot. It shows that the vortex loops indeed evolve very slowly, which is consistent with the slow recovery of the order parameter. For comparison, in Fig. 4-13, we illustrate the time-evolution of the system of the small vorticity case pictured in Fig. 4-11a and marked in Fig. 4-10 by the blue dot. In this case, there are no large vortices, while all smaller vortices already disappeared by  $t = 18$ .

## 4.7 Ergodization time estimates

In this Section, we illustrate that the slowing down of the order parameter recovery is not related to an anomalously long local ergodization time in the underlying equilibrium states. For this purpose, we apply the results of Chapters 2 and 3. Namely, we implement the Loschmidt echoes for a 3D DGPE lattice with volume  $V = 10^3$ , from which we extract the largest Lyapunov exponent  $\lambda_{\max}$  from Eq. (2.2) and the OTOC parameter  $\Lambda$  from Eq. (3.3). In Fig. 4-14, we plot the values of  $\lambda_{\max}$  and  $\Lambda$  as functions of the energy density in the range  $\varepsilon \in (-6, 4)$ . We observe that the difference between them is insensitive to the phase transition, and, overall, does not indicate an anomalously long local ergodization time according to Eq. (3.22),  $\tau_{erg} = \frac{\Lambda - \lambda_{\max}}{\lambda_{\max}^2} d^2$ . The value of  $\tau_{erg}$  in all cases is smaller than  $0.4 [J^{-1}]$  for the whole energy range, thus it is much shorter than the typical post-quench order-parameter recovery times. This finding is consistent with the remark made in Section 3.1.1 that the ergodization time characterizes the dynamics of the system on the spatial

scale of a few lattice sites. Thus, it is not sensitive to the very slow relaxation of large-scale topological objects.

## 4.8 Discussion

In the preceding sections, a hypothesis that topological defects slow down the establishing of phase-coherence of CDW in the experiment on the laser-induced melting [231] was tested by direct simulations of the 3D DGPE lattice. Although, the DGPE is an over-simplified model for the CDW phase dynamics, our simulations have captured the important physics of the experiment.

Among the main limitations of applying the 3D DGPE lattices for studying the establishing CDW phase coherence is that the DGPE is isolated from the environment and there is no external environmental noise in the system. Moreover, the ionic lattice is incorporated into the simulations artificially by modulating the quenching rate  $K(t)$  so that the system after quench equilibrates back to its initial energy. The CDW amplitude relaxation is also missed in the DGPE model, hence, strictly speaking, the DGPE is applicable only after the CDW amplitude has recovered.

The simulations support the hypothesis that after photo-excitation of the CDW, topological defects are excited, and their slow annihilation dominates the process of establishing long-range phase coherence. The recovery rate of the 3D DGPE lattice is affected by the creation of topological defects in the form of closed-loop vortices, whose lifetime grows with increase of their length.

Finally, we would like to emphasize the conceptual difference between the present setting of strong photo-excitation quenches from the theoretical setting associated with the Kibble-Zurek mechanism. In the setting for the Kibble-Zurek mechanism, the system starts from a high-temperature equilibrium state. In contrast, in our setting the high-energy state reached in the course of the quench is strongly out-of-equilibrium. Whether this circumstance leads to the differences of the generated defects requires further investigation.

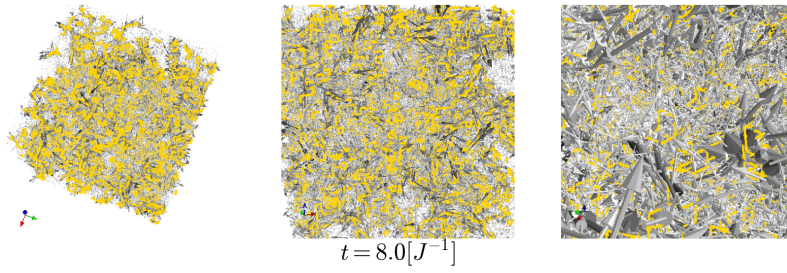
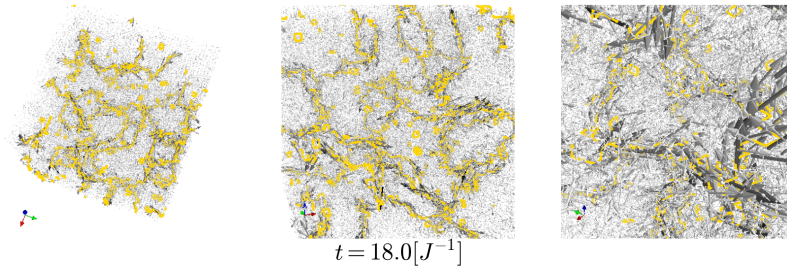
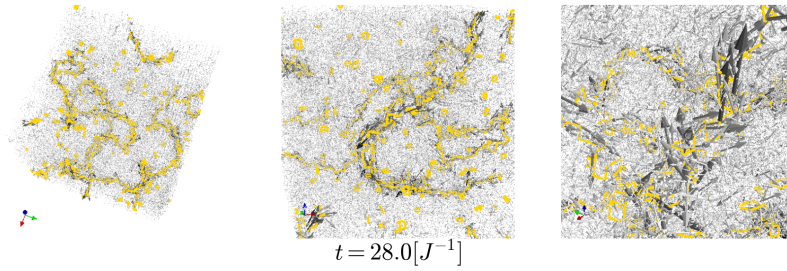
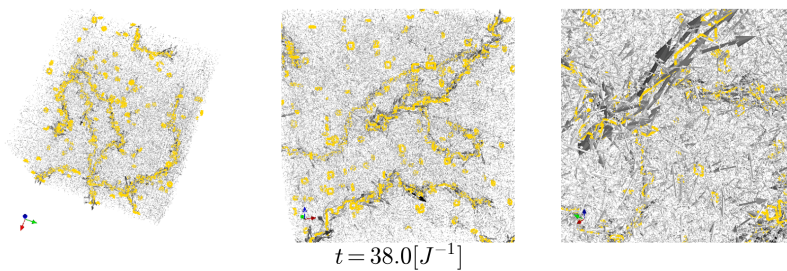
(a) Snapshot at time  $t = 8[J^{-1}]$ (b) Snapshot at time  $t = 18[J^{-1}]$ (c) Snapshot at time  $t = 28[J^{-1}]$ (d) Snapshot at time  $t = 38[J^{-1}]$ 

Figure 4-12: Snapshots for the post-quench time evolution of vortices in Fig. 4-10 for  $\kappa = 1.44$  (the red dot),  $V = 50^3$  for (a)  $t = 8[J^{-1}]$ , (b)  $18[J^{-1}]$ , (c)  $28[J^{-1}]$ , (d)  $38[J^{-1}]$ . Each row contains three 2D projections of the same 3D lattice. Yellow color depicts the core of closed-loop vortices. As a guide-to-eye, we plot  $\mathbf{u}_j$ , the finite difference approximation of the vorticity, as black arrows. The full video is available by the link <https://youtu.be/xCP1F8gYDtk>.

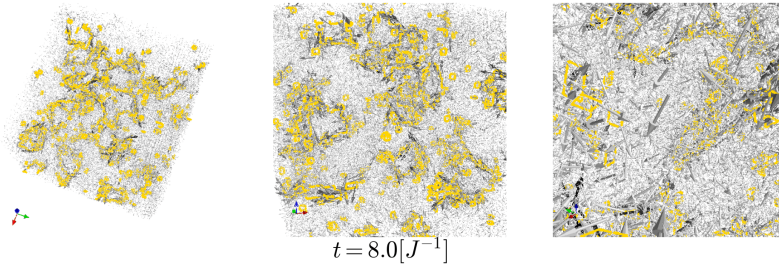
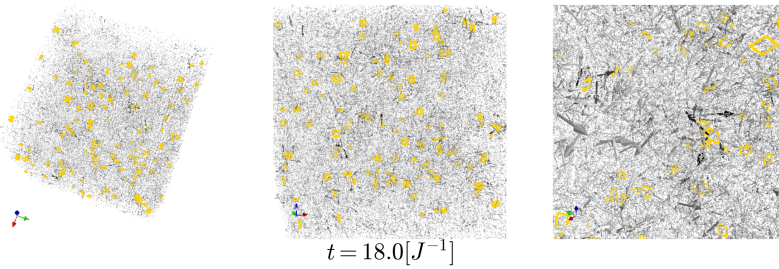
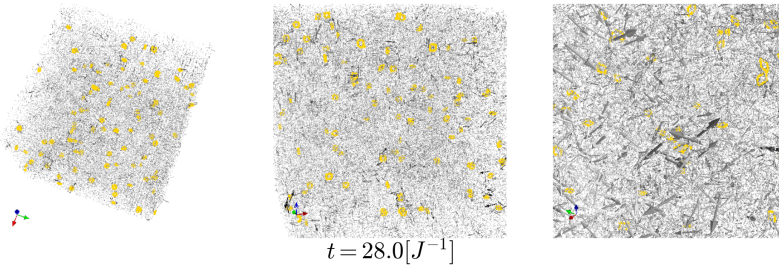
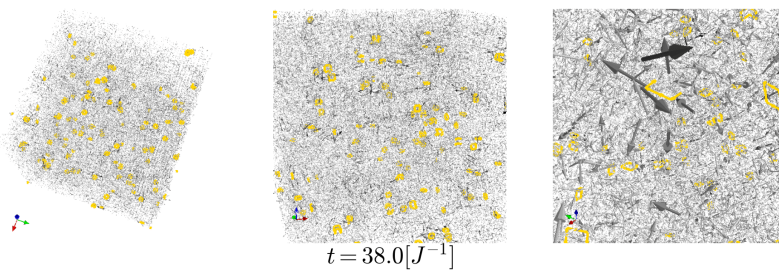
(a) Snapshot at time  $t = 8[J^{-1}]$ (b) Snapshot at time  $t = 18[J^{-1}]$ (c) Snapshot at time  $t = 28[J^{-1}]$ (d) Snapshot at time  $t = 38[J^{-1}]$ 

Figure 4-13: Snapshots for the post-quench time evolution of vortices in Fig. 4-10 for  $\kappa = 0.7$  (the blue dot),  $V = 50^3$  for (a)  $t = 8[J^{-1}]$ , (b)  $18[J^{-1}]$ , (c)  $28[J^{-1}]$ , (d)  $38[J^{-1}]$ . Each row contains three 2D projections of the same 3D lattice. Yellow color depicts the core of closed-loop vortices. As a guide-to-eye, we plot  $\mathbf{u}_j$ , the finite difference approximation of the vorticity, as black arrows. The full video is available by the link <https://youtu.be/YVyuQi2KCmw>.

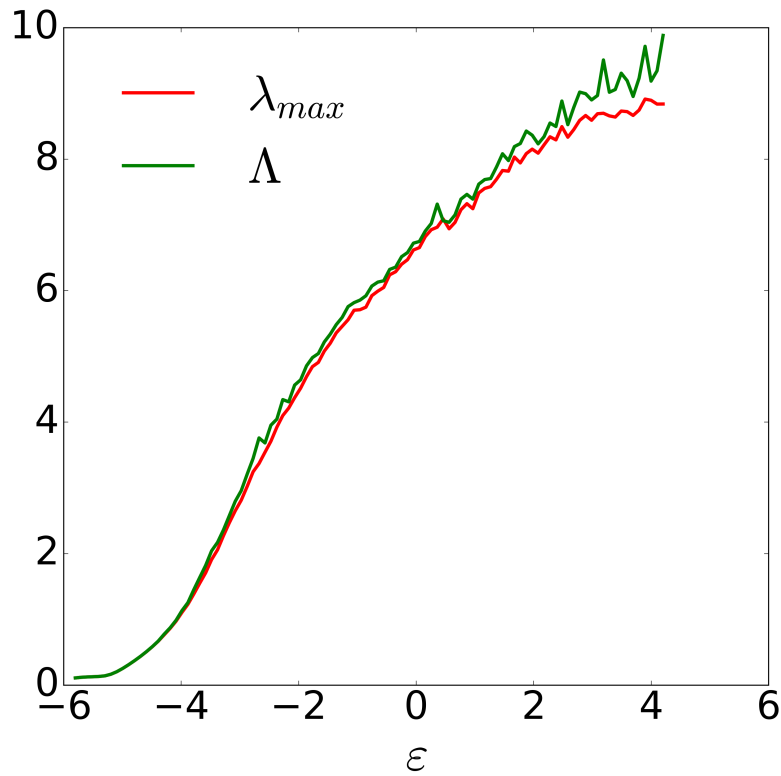


Figure 4-14: Estimating the ergodization time of the 3D DGPE lattice for the energy range containing a spontaneous symmetry breaking. The results of Loschmidt echoes simulations: (red line) the largest Lyapunov exponent  $\lambda_{max}$  from Eq. (2.2), and (green line)  $\Lambda$  from Eq. (3.3) as functions of the energy density,  $\varepsilon$ . The difference  $\Lambda - \lambda_{max}$  is proportional to the ergodization time according to Eq. (3.22).

A first draft, made in pencil, filled several blue *cahiers* of the kind used in schools, and upon reaching the saturation point of revision presented a chaos of smudges and scriggles. To this corresponded the disorder of the text which followed a regular sequence only for a few pages, being then interrupted by some chunky passage that belonged to a later, or earlier, part of the story.

—Vladimir Nabokov,  
Look at the Harlequins!

## Chapter 5

# Conclusions and outlook

In the present Thesis, we studied the ergodization dynamics of the discrete Gross-Pitaevskii equation on a lattice. The main results reported in the Thesis are:

1. We proposed an experimentally realizable method to demonstrate Lyapunov instability and extract the largest Lyapunov exponent by monitoring equilibrium noise of virtually any observable quantity before and after time reversal of dynamics (Loschmidt echo). The method was validated numerically for the one-, two- and three-dimensional DGPE lattices. We discussed its possible experimental implementation with ultracold bosonic atoms in optical lattices. A successful realization of our proposal may produce the long-sought direct experimental evidence that the dynamics of a typical many-particle system is chaotic. This would put the theory of dynamic thermalization on a firmer foundation.
2. We introduced a new characteristic time of ergodization as the time required to detect the largest Lyapunov exponent of the system. The quantity that needs to be monitored in order to extract the above ergodization time is the classical counterpart of the so-called quantum out-of-time-order correlators (OTOCs). We demonstrated that the exponential growth rate of an OTOC systematically exceeds the largest Lyapunov exponent of the system and showed that this difference becomes smaller with the increase of the dimensionality of the lattice. We put forward a practical criterion of whether the dynamics of the

system ergodizes over the times accessible by Loschmidt echoes.

3. We numerically investigated the dynamic thermalization of the 3D DGPE after fast thermal quenches across the second-order phase transition associated with a spontaneous symmetry breaking. We showed that topological defects emerge in this process and significantly slow down the phase relaxation of the system. At the same time, we showed that the dynamics of the system remains locally ergodic. The results of our simulations explain the recent experiment on laser-induced melting of a charge-density wave in  $\text{LaTe}_3$ . We thus demonstrate that the 3D DGPE can be used to simulate the dynamic thermalization in CDW materials.

Overall, the ergodization process in a many-particle system cannot be characterized by a single timescale. The findings of this Thesis support the view that the ergodization dynamics of many-particle systems is hierarchical in terms of timescales. At faster timescales, the Lyapunov process is dominant: it can be used to quantify the ergodization timescale relevant to establishing the local quasi-equilibrium. Our findings further indicate that on very long timescales, the appearance and disappearance of large topological objects are one of the factors determining the approach to the true equilibrium.

In the future, we plan a more detailed investigation of the microcanonical thermodynamics of the DGPE lattices. Specifically, we will study the thermodynamic regimes, where the assumptions of additivity and extensivity in the DGPE lattices are broken. Further investigations of non-equilibrium quenches in the presence of disorder are also planned.

# Bibliography

- [1] Andrei E Tarkhov, Sandro Wimberger, and Boris V Fine. “Extracting Lyapunov exponents from the echo dynamics of Bose-Einstein condensates on a lattice”. In: *Physical Review A* 96 (2017), p. 023624.
- [2] Andrei E Tarkhov and Boris V Fine. “Estimating ergodization time of a chaotic many-particle system from a time reversal of equilibrium noise”. In: *New Journal of Physics* 20.12 (2018), p. 123021.
- [3] Andrei E. Tarkhov et al. “The role of topological defects in the slowing down of recovery of a charge-density wave after laser-induced melting”. In: *in preparation* (2020).
- [4] Sadi Carnot. “Reflections on the motive power of fire, and on machines fitted to develop that power”. In: *Paris: Bachelier* (1824).
- [5] William Thomson Baron Kelvin. *Mathematical and physical papers*. Vol. 3. University Press, 1890.
- [6] Rudolf Clausius. *The mechanical theory of heat*. Macmillan, 1879.
- [7] James Clerk Maxwell. *Maxwell on molecules and gases*. MIT Press, 1986.
- [8] Ludwig Boltzmann. *Lectures on gas theory*. Courier Corporation, 2012.
- [9] Josiah Willard Gibbs. *Elementary principles in statistical mechanics: developed with especial reference to the rational foundation of thermodynamics*. C. Scribner’s sons, 1902.
- [10] Max Planck. *Treatise on thermodynamics*. Courier Corporation, 2013.
- [11] Albert Einstein. “On the motion required by the molecular kinetic theory of heat of small particles suspended in a stationary liquid”. In: *Annalen der Physik* 17.8 (1905), pp. 549–560.
- [12] Henri Poincaré. “On the three-body problem and the equations of dynamics”. In: *The Kinetic Theory Of Gases: An Anthology of Classic Papers with Historical Commentary*. World Scientific, 2003, pp. 368–376.
- [13] AM Lyapunov. “A general task about the stability of motion”. In: *PhD Thesis* (1892).
- [14] George D Birkhoff. “Proof of the ergodic theorem”. In: *Proceedings of the National Academy of Sciences* 17.12 (1931), pp. 656–660.
- [15] J v Neumann. “Proof of the quasi-ergodic hypothesis”. In: *Proceedings of the National Academy of Sciences* 18.1 (1932), pp. 70–82.

- [16] Fritz Haake. *Quantum signatures of chaos*. Vol. 54. Springer Science & Business Media, 2013.
- [17] EB Stechel and EJ Heller. “Quantum ergodicity and spectral chaos”. In: *Annual Review of Physical Chemistry* 35.1 (1984), pp. 563–589.
- [18] WK Rhim, A Pines, and JS Waugh. “Time-reversal experiments in dipolar-coupled spin systems”. In: *Physical Review B* 3.3 (1971), p. 684.
- [19] Horacio M Pastawski et al. “A nuclear magnetic resonance answer to the Boltzmann–Loschmidt controversy?” In: *Physica A: Statistical Mechanics and its Applications* 283.1-2 (2000), pp. 166–170.
- [20] Ernst Zermelo. “On a theorem of dynamics and the mechanical theory of heat”. In: *The Kinetic Theory Of Gases: An Anthology of Classic Papers with Historical Commentary*. World Scientific, 2003, pp. 382–391.
- [21] J.L. Lebowitz. “Boltzmann’s Entropy and Time’s Arrow”. In: *Physics Today* 46.9 (1993), pp. 32–38. DOI: [10.1063/1.881363](https://doi.org/10.1063/1.881363).
- [22] Ludwig Boltzmann. “Entgegnung auf die wärmetheoretischen Betrachtungen des Hrn. E. Zermelo”. In: *Annalen der Physik* 293.4 (1896), pp. 773–784.
- [23] A Ya Khinchin. *Mathematical foundations of statistical mechanics*. Dover, 1949.
- [24] Joseph Berkovitz, Roman Frigg, and F Kronz. “The ergodic hierarchy”. In: *The Stanford encyclopedia of philosophy*. Summer (2011).
- [25] N Krylov. “Relaxation processes in statistical systems”. In: *Nature* 153.3893 (1944), pp. 709–710.
- [26] Nikolai Sergeevich Krylov. *Works on the foundations of statistical physics*. Princeton University Press, 2014.
- [27] Andrei Nikolaevich Kolmogorov. “A new metric invariant of transitive dynamical systems and automorphisms of Lebesgue spaces”. In: *Trudy Matematicheskogo Instituta imeni VA Steklova* 169 (1985), pp. 94–98.
- [28] Yaha G Sinai. “On the notion of entropy of a dynamical system”. In: *Doklady of Russian Academy of Sciences*. Vol. 124. 3. 1959, pp. 768–771.
- [29] Gregory J Chaitin. “On the length of programs for computing finite binary sequences”. In: *Journal of the ACM (JACM)* 13.4 (1966), pp. 547–569.
- [30] Andrei N Kolmogorov. “Combinatorial foundations of information theory and the calculus of probabilities”. In: *Russian mathematical surveys* 38.4 (1983), p. 29.
- [31] Gregory J Chaitin. *Algorithmic Information Theory (Cambridge Tracts in Theoretical Computer Science)*. 1987.
- [32] Pierre Gaspard et al. “Experimental evidence for microscopic chaos”. In: *Nature* 394.6696 (1998), p. 865.
- [33] Carl Philip Dettmann, EGD Cohen, and H Van Beijeren. “Microscopic chaos from Brownian motion?” In: *Nature* 401.6756 (1999), pp. 875–875.

- [34] Peter Grassberger and Thomas Schreiber. “Microscopic chaos from brownian motion?” In: *Nature* 401.6756 (1999), pp. 875–876.
- [35] P Gaspard et al. “Microscopic chaos from brownian motion?” In: *Nature* 401.6756 (1999), pp. 876–876.
- [36] Tarek A Elsayed, Benjamin Hess, and Boris V Fine. “Signatures of chaos in time series generated by many-spin systems at high temperatures”. In: *Physical Review E* 90.2 (2014), p. 022910.
- [37] Yakov Grigor’evich Sinai. “On the foundations of the ergodic hypothesis for a dynamical system of statistical mechanics”. In: *Doklady Akademii Nauk*. Vol. 153. 6. Russian Academy of Sciences. 1963, pp. 1261–1264.
- [38] Yakov Grigor’evich Sinai. “Dynamical systems with elastic reflections. Ergodic properties of dispersing billiards”. In: *Uspekhi Matematicheskikh Nauk* 25.2 (1970), pp. 141–192.
- [39] Enrico Fermi et al. *Studies of the nonlinear problems*. Tech. rep. Los Alamos Scientific Lab., N. Mex., 1955.
- [40] Julien Clinton Sprott and Julien C Sprott. *Chaos and time-series analysis*. Vol. 69. Citeseer, 2003, pp. 116–117.
- [41] Sandro Wimberger. “Nonlinear dynamics and quantum chaos”. In: *Nonlinear Dynamics and Quantum Chaos. Series: Graduate Texts in Physics, ISBN: 978-3-319-06342-3. Springer International Publishing (Cham)* (2014).
- [42] Boris V Fine et al. “Absence of exponential sensitivity to small perturbations in nonintegrable systems of spins  $1/2$ ”. In: *Physical Review E* 89.1 (2014), p. 012923.
- [43] AI Larkin and Yu N Ovchinnikov. “Quasiclassical method in the theory of superconductivity”. In: *Sov. Phys. JETP* 28.6 (1969), pp. 1200–1205.
- [44] Tarek A Elsayed. “Chaos and Relaxation in Classical and Quantum Spin Systems”. PhD thesis. 2013.
- [45] Tarek A Elsayed and Boris V Fine. “Sensitivity to small perturbations in systems of large quantum spins”. In: *Physica Scripta* 2015.T165 (2015), p. 014011.
- [46] AY Kitaev. “Talks at KITP, University of California, Santa Barbara”. In: *Entanglement in Strongly-Correlated Quantum Matter* (2015).
- [47] Juan Maldacena, Stephen H Shenker, and Douglas Stanford. “A bound on chaos”. In: *Journal of High Energy Physics* 2016.8 (2016), p. 106.
- [48] Jun Li et al. “Measuring out-of-time-order correlators on a nuclear magnetic resonance quantum simulator”. In: *Physical Review X* 7.3 (2017), p. 031011.
- [49] Martin Gärttner et al. “Measuring out-of-time-order correlations and multiple quantum spectra in a trapped-ion quantum magnet”. In: *Nature Physics* 13.8 (2017), pp. 781–786.
- [50] Martin Gärttner, Philipp Hauke, and Ana Maria Rey. “Relating out-of-time-order correlations to entanglement via multiple-quantum coherences”. In: *Physical Review Letters* 120.4 (2018), p. 040402.

- [51] Efim B Rozenbaum, Sriram Ganeshan, and Victor Galitski. “Lyapunov exponent and out-of-time-ordered correlator’s growth rate in a chaotic system”. In: *Physical Review Letters* 118.8 (2017), p. 086801.
- [52] Ryusuke Hamazaki, Kazuya Fujimoto, and Masahito Ueda. “Operator Non-commutativity and Irreversibility in Quantum Chaos”. In: *arXiv preprint arXiv:1807.02360* (2018).
- [53] Efim B Rozenbaum, Sriram Ganeshan, and Victor Galitski. “Universal level statistics of the out-of-time-ordered operator”. In: *Physical Review B* 100.3 (2019), p. 035112.
- [54] Yunxiang Liao and Victor Galitski. “Nonlinear sigma model approach to many-body quantum chaos: Regularized and unregularized out-of-time-ordered correlators”. In: *Physical Review B* 98.20 (2018), p. 205124.
- [55] Jorge Chávez-Carlos et al. “Quantum and classical lyapunov exponents in atom-field interaction systems”. In: *Physical Review Letters* 122.2 (2019), p. 024101.
- [56] Annabelle Bohrdt et al. “Scrambling and thermalization in a diffusive quantum many-body system”. In: *New Journal of Physics* 19.6 (2017), p. 063001.
- [57] Koji Hashimoto, Keiju Murata, and Ryosuke Yoshii. “Out-of-time-order correlators in quantum mechanics”. In: *Journal of High Energy Physics* 2017.10 (2017), p. 138.
- [58] Maksym Serbyn and Dmitry A Abanin. “Loschmidt echo in many-body localized phases”. In: *Physical Review B* 96.1 (2017), p. 014202.
- [59] Rong-Qiang He and Zhong-Yi Lu. “Characterizing many-body localization by out-of-time-ordered correlation”. In: *Physical Review B* 95.5 (2017), p. 054201.
- [60] Brian Swingle and Debanjan Chowdhury. “Slow scrambling in disordered quantum systems”. In: *Physical Review B* 95.6 (2017), p. 060201.
- [61] Kevin Slagle et al. “Out-of-time-order correlation in marginal many-body localized systems”. In: *Physical Review B* 95.16 (2017), p. 165136.
- [62] Ruihua Fan et al. “Out-of-time-order correlation for many-body localization”. In: *Science bulletin* 62.10 (2017), pp. 707–711.
- [63] Yichen Huang, Yong-Liang Zhang, and Xie Chen. “Out-of-time-ordered correlators in many-body localized systems”. In: *Annalen der Physik* 529.7 (2017).
- [64] Naoto Tsuji, Tomohiro Shitara, and Masahito Ueda. “Out-of-time-order fluctuation-dissipation theorem”. In: *Physical Review E* 97.1 (2018), p. 012101.
- [65] Jordan S Cotler, Dawei Ding, and Geoffrey R Penington. “Out-of-time-order operators and the butterfly effect”. In: *Annals of Physics* 396 (2018), pp. 318–333.
- [66] Markus Schmitt and Stefan Kehrein. “Irreversible dynamics in quantum many-body systems”. In: *Physical Review B* 98.18 (2018), p. 180301.
- [67] Markus Schmitt et al. “Semiclassical echo dynamics in the Sachdev-Ye-Kitaev model”. In: *Physical Review B* 99.13 (2019), p. 134301.

- [68] Alexander Avdoshkin and Anatoly Dymarsky. “Euclidean operator growth and quantum chaos”. In: *arXiv preprint arXiv:1911.09672* (2019).
- [69] Alexander Schuckert and Michael Knap. “Many-body chaos near a thermal phase transition”. In: *SciPost Physics* 7.2 (2019), p. 022.
- [70] Silvia Pappalardi, Anatoli Polkovnikov, and Alessandro Silva. “Quantum echo dynamics in the Sherrington-Kirkpatrick model”. In: *arXiv preprint arXiv:1910.04769* (2019).
- [71] Yahya Alavirad and Ali Lavasani. “Scrambling in the Dicke model”. In: *Physical Review A* 99.4 (2019), p. 043602.
- [72] Oskar Schnaack et al. “Tripartite information, scrambling, and the role of Hilbert space partitioning in quantum lattice models”. In: *Physical Review B* 100.22 (2019), p. 224302.
- [73] Michael Rautenberg and Martin Gärttner. “Classical and quantum chaos in a three-mode bosonic system”. In: *Physical Review A* 101.5 (2020), p. 053604.
- [74] Markus Schmitt and Stefan Kehrein. “Irreversible dynamics in quantum many-body systems”. In: *Physical Review B* 98.18 (2018), p. 180301.
- [75] Markus Schmitt et al. “Semiclassical echo dynamics in the Sachdev-Ye-Kitaev model”. In: *Physical Review B* 99.13 (2019), p. 134301.
- [76] Hans Henrik Rugh. “Dynamical approach to temperature”. In: *Physical Review Letters* 78.5 (1997), p. 772.
- [77] Hans Henrik Rugh. “A geometric, dynamical approach to thermodynamics”. In: *Journal of Physics A: Mathematical and General* 31.38 (1998), p. 7761.
- [78] Wouter K den Otter and Willem J Briels. “The calculation of free-energy differences by constrained molecular-dynamics simulations”. In: *The Journal of Chemical Physics* 109.11 (1998), pp. 4139–4146.
- [79] Wouter K den Otter. “Thermodynamic integration of the free energy along a reaction coordinate in Cartesian coordinates”. In: *The Journal of Chemical Physics* 112.17 (2000), pp. 7283–7292.
- [80] MJ Davis, SA Morgan, and K Burnett. “Simulations of Bose fields at finite temperature”. In: *Physical Review Letters* 87.16 (2001), p. 160402.
- [81] P Blair Blakie and Matthew J Davis. “Projected Gross-Pitaevskii equation for harmonically confined Bose gases at finite temperature”. In: *Physical Review A* 72.6 (2005), p. 063608.
- [82] Matthew J Davis and P Blair Blakie. “Critical temperature of a trapped Bose gas: comparison of theory and experiment”. In: *Physical Review Letters* 96.6 (2006), p. 060404.
- [83] P Blair Blakie and Matthew J Davis. “Classical region of a trapped Bose gas”. In: *Journal of Physics B: Atomic, Molecular and Optical Physics* 40.11 (2007), p. 2043.
- [84] Astrid S de Wijn, B Hess, and Boris V Fine. “Chaotic properties of spin lattices near second-order phase transitions”. In: *Physical Review E* 92.6 (2015), p. 062929.

- [85] Oliver Morsch and Markus Oberthaler. “Dynamics of Bose-Einstein condensates in optical lattices”. In: *Reviews of Modern Physics* 78.1 (2006), p. 179.
- [86] Immanuel Bloch, Jean Dalibard, and Wilhelm Zwerger. “Many-body physics with ultracold gases”. In: *Reviews of Modern Physics* 80.3 (2008), p. 885.
- [87] Eugene P Gross. “Structure of a quantized vortex in boson systems”. In: *Il Nuovo Cimento (1955-1965)* 20.3 (1961), pp. 454–477.
- [88] LP Pitaevskii. “Vortex lines in an imperfect Bose gas”. In: *Sov. Phys. JETP* 13 (1961), p. 451.
- [89] J Chris Eilbeck and Magnus Johansson. “The discrete nonlinear Schrödinger equation—20 years on”. In: *Conference on Localization and Energy Transfer in Nonlinear Systems*. 2003, p. 44.
- [90] PG Kevrekidis, KØ Rasmussen, and AR Bishop. “The discrete nonlinear Schrödinger equation: a survey of recent results”. In: *International Journal of Modern Physics B* 15.21 (2001), pp. 2833–2900.
- [91] M Hasenbusch and T Török. “High-precision Monte Carlo study of the 3D XY-universality class”. In: *Journal of Physics A: Mathematical and General* 32.36 (1999), p. 6361.
- [92] Zohar Nussinov. “O (n) Spin Systems—Some General Properties: A Generalized Mermin-Wagner-Coleman Theorem, Ground States, Peierls Bounds, and Dynamics”. In: *arXiv preprint hep-th/0105147* (2001).
- [93] Zohar Nussinov. “Commensurate and incommensurate O (n) spin systems: novel even-odd effects, a generalized Mermin-Wagner-Coleman theorem, and ground states”. In: *arXiv preprint cond-mat/0105253* (2001).
- [94] Massimo Campostrini et al. “Critical behavior of the three-dimensional XY universality class”. In: *Physical Review B* 63.21 (2001), p. 214503.
- [95] I Dukovski, Jonathan Machta, and LV Chayes. “Invaded cluster simulations of the XY model in two and three dimensions”. In: *Physical Review E* 65.2 (2002), p. 026702.
- [96] J Ch Eilbeck, PS Lomdahl, and AC Scott. “The discrete self-trapping equation”. In: *Physica D: Nonlinear Phenomena* 16.3 (1985), pp. 318–338.
- [97] JC Eilbeck. “DISCRETE SELF-TRAPPING EQUATION”. In: *Davydov’s Soliton Revisited: Self-Trapping of Vibrational Energy in Protein* 243 (2013), p. 473.
- [98] KØ Rasmussen et al. “Statistical mechanics of a discrete nonlinear system”. In: *Physical Review Letters* 84.17 (2000), p. 3740.
- [99] RS MacKay and S Aubry. “Proof of existence of breathers for time-reversible or Hamiltonian networks of weakly coupled oscillators”. In: *Nonlinearity* 7.6 (1994), p. 1623.
- [100] Roberto Livi, Roberto Franzosi, and Gian-Luca Oppo. “Self-localization of Bose-Einstein condensates in optical lattices via boundary dissipation”. In: *Physical Review Letters* 97.6 (2006), p. 060401.

- [101] Benno Rumpf. “Simple statistical explanation for the localization of energy in nonlinear lattices with two conserved quantities”. In: *Physical Review E* 69.1 (2004), p. 016618.
- [102] Benno Rumpf. “Transition behavior of the discrete nonlinear Schrödinger equation”. In: *Physical Review E* 77.3 (2008), p. 036606.
- [103] Benno Rumpf. “Stable and metastable states and the formation and destruction of breathers in the discrete nonlinear Schrödinger equation”. In: *Physica D: Nonlinear Phenomena* 238.20 (2009), pp. 2067–2077.
- [104] S Flach, K Kladko, and RS MacKay. “Energy thresholds for discrete breathers in one-, two-, and three-dimensional lattices”. In: *Physical Review Letters* 78.7 (1997), p. 1207.
- [105] Kay Kirkpatrick. “Solitons and Gibbs measures for nonlinear Schrödinger equations”. In: *Mathematical Modelling of Natural Phenomena* 7.2 (2012), pp. 95–112.
- [106] Stefano Iubini, Stefano Lepri, and Antonio Politi. “Nonequilibrium discrete nonlinear Schrödinger equation”. In: *Physical Review E* 86.1 (2012), p. 011108.
- [107] Stefano Iubini et al. “Discrete breathers and negative-temperature states”. In: *New Journal of Physics* 15.2 (2013), p. 023032.
- [108] Stefano Iubini, Antonio Politi, and Paolo Politi. “Relaxation and coarsening of weakly-interacting breathers in a simplified DNLS chain”. In: *Journal of Statistical Mechanics: Theory and Experiment* 2017.7 (2017), p. 073201.
- [109] Stefano Iubini et al. “A Chain, a Bath, a Sink, and a Wall”. In: *Entropy* 19.9 (2017), p. 445.
- [110] Stefano Iubini et al. “Dynamical freezing of relaxation to equilibrium”. In: *Physical Review Letters* 122.8 (2019), p. 084102.
- [111] Thudiyangal Mithun et al. “Weakly nonergodic dynamics in the Gross-Pitaevskii lattice”. In: *Physical Review Letters* 120.18 (2018), p. 184101.
- [112] Thudiyangal Mithun et al. “Dynamical glass and ergodization times in classical Josephson Junction Chains”. In: *Physical Review Letters* 122.5 (2019), p. 054102.
- [113] Carlo Danieli et al. “Dynamical glass in weakly nonintegrable Klein-Gordon chains”. In: *Physical Review E* 100.3 (2019), p. 032217.
- [114] Alexander Yu Cherny, Thomas Engl, and Sergej Flach. “Non-Gibbs states on a Bose-Hubbard lattice”. In: *Physical Review A* 99.2 (2019), p. 023603.
- [115] DM Basko. “Kinetic theory of nonlinear diffusion in a weakly disordered nonlinear Schrödinger chain in the regime of homogeneous chaos”. In: *Physical Review E* 89.2 (2014), p. 022921.
- [116] Lars Onsager. “Statistical hydrodynamics”. In: *Il Nuovo Cimento (1943-1954)* 6.2 (1949), pp. 279–287.
- [117] Richard P Feynman. “Chapter II Application of quantum mechanics to liquid helium”. In: *Progress in low temperature physics*. Vol. 1. Elsevier, 1955, pp. 17–53.

- [118] Alexei A Abrikosov. “On the magnetic properties of superconductors of the second group”. In: *Sov. Phys. JETP* 5 (1957), pp. 1174–1182.
- [119] VL Berezinsky. “Destruction of long range order in one-dimensional and two-dimensional systems having a continuous symmetry group. I. Classical systems”. In: *Zh. Eksp. Teor. Fiz.* 32 (1970), pp. 493–500.
- [120] VL Berezinsky. “Destruction of long-range order in one-dimensional and two-dimensional systems possessing a continuous symmetry group. II. Quantum systems.” In: *Zh. Eksp. Teor. Fiz.* 61 (1972), p. 610.
- [121] J Michael Kosterlitz and DJ Thouless. “Long range order and metastability in two dimensional solids and superfluids.(Application of dislocation theory)”. In: *Journal of Physics C: Solid State Physics* 5.11 (1972), p. L124.
- [122] Pavlos G Lagoudakis and Natalia G Berloff. “A polariton graph simulator”. In: *New Journal of Physics* 19.12 (2017), p. 125008.
- [123] Natalia G Berloff et al. “Realizing the classical XY Hamiltonian in polariton simulators”. In: *Nature Materials* 16.11 (2017), pp. 1120–1126.
- [124] F Rojas, Sanjay Puri, and AJ Bray. “Kinetics of phase ordering in the O (n) model with a conserved order parameter”. In: *Journal of Physics A: Mathematical and General* 34.19 (2001), p. 3985.
- [125] Thomas WB Kibble. “Topology of cosmic domains and strings”. In: *Journal of Physics A: Mathematical and General* 9.8 (1976), p. 1387.
- [126] Tom WB Kibble. “Some implications of a cosmological phase transition”. In: *Physics Reports* 67.1 (1980), pp. 183–199.
- [127] Wojciech H Zurek. “Cosmological experiments in superfluid helium?” In: *Nature* 317.6037 (1985), pp. 505–508.
- [128] Wojciech H Zurek. “Cosmological experiments in condensed matter systems”. In: *Physics Reports* 276.4 (1996), pp. 177–221.
- [129] Dmitry A Garanin and Eugene M Chudnovsky. “Ordered vs. disordered states of the random-field model in three dimensions”. In: *The European Physical Journal B* 88.4 (2015), p. 81.
- [130] Michikazu Kobayashi and Leticia F Cugliandolo. “Quench dynamics of the three-dimensional U (1) complex field theory: Geometric and scaling characterizations of the vortex tangle”. In: *Physical Review E* 94.6 (2016), p. 062146.
- [131] Manoj Kumar et al. “Ordering kinetics in the random-bond X Y model”. In: *Physical Review E* 96.4 (2017), p. 042127.
- [132] MG Vasin and VM Vinokur. “Description of glass transition kinetics in 3D XY model in terms of gauge field theory”. In: *Physica A: Statistical Mechanics and its Applications* 525 (2019), pp. 1161–1169.
- [133] Thomas C Proctor, Dmitry A Garanin, and Eugene M Chudnovsky. “Random fields, topology, and the Imry-Ma argument”. In: *Physical Review Letters* 112.9 (2014), p. 097201.

- [134] Hajime Yoshino, Koji Hukushima, and Hajime Takayama. “Extended droplet theory for aging in short-range spin glasses and a numerical examination”. In: *Physical Review B* 66.6 (2002), p. 064431.
- [135] Arjan Hulsebos. “The Behavior of vortex loops in the 3-d XY model”. In: *Nuclear Physics B-Proceedings Supplements* 34 (1994), pp. 695–697.
- [136] Keijo Kajantie et al. “O (2) symmetry breaking versus vortex loop percolation”. In: *Physics Letters B* 482.1-3 (2000), pp. 114–122.
- [137] Greg Kohring, Robert E Shrock, and Peter Wills. “Role of vortex strings in the three-dimensional O (2) model”. In: *Physical Review Letters* 57.11 (1986), p. 1358.
- [138] Petter Minnhagen and Peter Olsson. “Monte Carlo calculation of the vortex interaction for high-T<sub>c</sub> superconductors”. In: *Physical Review B* 44.9 (1991), p. 4503.
- [139] AV Pochinsky, MI Polikarpov, and BN Yurchenko. “Properties of vortex loops in the 3D XY model”. In: *Physics Letters A* 154.3-4 (1991), pp. 194–196.
- [140] AJ Bray and K Humayun. “Universal amplitudes of power-law tails in the asymptotic structure factor of systems with topological defects”. In: *Physical Review E* 47.1 (1993), R9.
- [141] AJ Bray and K Humayun. “Towards a systematic calculation of the scaling functions for the ordering kinetics of nonconserved fields”. In: *Physical Review E* 48.3 (1993), R1609.
- [142] AJ Bray and AD Rutenberg. “Growth laws for phase ordering”. In: *Physical Review E* 49.1 (1994), R27.
- [143] AD Rutenberg and AJ Bray. “Energy-scaling approach to phase-ordering growth laws”. In: *Physical Review E* 51.6 (1995), p. 5499.
- [144] Sanjay Puri, AJ Bray, and F Rojas. “Ordering kinetics of conserved XY models”. In: *Physical Review E* 52.5 (1995), p. 4699.
- [145] Keekwon Nam, Bongsoo Kim, and Sung Jong Lee. “Coarsening kinetics of a two-dimensional O (2) Ginzburg–Landau model: the effect of reversible mode coupling”. In: *Journal of Statistical Mechanics: Theory and Experiment* 2011.03 (2011), P03013.
- [146] BV Svistunov. “Highly nonequilibrium Bose condensation in a weakly interacting gas”. In: *J. Moscow Phys. Soc* 1 (1991), p. 373.
- [147] Yu M Kagan, BV Svistunov, and GV Shlyapnikov. “Erratum: Kinetics of Bose condensation in an interacting Bose gas [sov. physics-jetp 74, 279–285 (February 1992)]”. In: *JETP* 75.2 (1992), p. 387.
- [148] Yu Kagan and BV Svistunov. “Kinetics of the onset of long-range order during Bose condensation in an interacting gas”. In: *Zh. Eksp. Teor. Fiz* 105 (1994), p. 353.
- [149] Natalia G Berloff and Boris V Svistunov. “Scenario of strongly nonequilibrium Bose-Einstein condensation”. In: *Physical Review A* 66.1 (2002), p. 013603.

- [150] Natalia G Berloff and Paul H Roberts. “Motions in a bose condensate: VI. Vortices in a nonlocal model”. In: *Journal of Physics A: Mathematical and General* 32.30 (1999), p. 5611.
- [151] Natalia G Berloff and Paul H Roberts. “Capture of an impurity by a vortex line in a Bose condensate”. In: *Physical Review B* 63.2 (2000), p. 024510.
- [152] Paul H Roberts and Natalia G Berloff. “The nonlinear Schrödinger equation as a model of superfluidity”. In: *Quantized vortex dynamics and superfluid turbulence*. Springer, 2001, pp. 235–257.
- [153] Natalia G Berloff and Carlo F Barenghi. “Vortex nucleation by collapsing bubbles in Bose-Einstein condensates”. In: *Physical Review Letters* 93.9 (2004), p. 090401.
- [154] Natalia G Berloff and Anthony J Youd. “Dissipative dynamics of superfluid vortices at nonzero temperatures”. In: *Physical Review Letters* 99.14 (2007), p. 145301.
- [155] Hayder Salman and Natalia G Berloff. “Condensation of classical nonlinear waves in a two-component system”. In: *Physica D: Nonlinear Phenomena* 238.15 (2009), pp. 1482–1489.
- [156] Giorgio Krstulovic and Marc Brachet. “Energy cascade with small-scale thermalization, counterflow metastability, and anomalous velocity of vortex rings in Fourier-truncated Gross-Pitaevskii equation”. In: *Physical Review E* 83.6 (2011), p. 066311.
- [157] Natalia G Berloff, Marc Brachet, and Nick P Proukakis. “Modeling quantum fluid dynamics at nonzero temperatures”. In: *Proceedings of the National Academy of Sciences* 111.Supplement 1 (2014), pp. 4675–4682.
- [158] Steven Mathey, Thomas Gasenzer, and Jan M Pawłowski. “Anomalous scaling at nonthermal fixed points of Burgers’ and Gross-Pitaevskii turbulence”. In: *Physical Review A* 92.2 (2015), p. 023635.
- [159] Kirill P Kalinin and Natalia G Berloff. “Polaritonic network as a paradigm for dynamics of coupled oscillators”. In: *Physical Review B* 100.24 (2019), p. 245306.
- [160] I-K Liu et al. “Dynamical equilibration across a quenched phase transition in a trapped quantum gas”. In: *Communications Physics* 1.1 (2018), pp. 1–12.
- [161] Mathilde Hugbart et al. “Population and phase coherence during the growth of an elongated Bose-Einstein condensate”. In: *Physical Review A* 75.1 (2007), p. 011602.
- [162] Stephan Ritter et al. “Observing the formation of long-range order during Bose-Einstein condensation”. In: *Physical Review Letters* 98.9 (2007), p. 090402.
- [163] Chad N Weiler et al. “Spontaneous vortices in the formation of Bose-Einstein condensates”. In: *Nature* 455.7215 (2008), pp. 948–951.
- [164] Giacomo Lamporesi et al. “Spontaneous creation of Kibble-Zurek solitons in a Bose-Einstein condensate”. In: *Nature Physics* 9.10 (2013), pp. 656–660.

- [165] Julian Struck et al. “Quantum simulation of frustrated classical magnetism in triangular optical lattices”. In: *Science* 333.6045 (2011), pp. 996–999.
- [166] Christoph Weiss. “Distinguishing mesoscopic quantum superpositions from statistical mixtures in periodically shaken double wells”. In: *Journal of Physics B: Atomic, Molecular and Optical Physics* 45.2 (2012), p. 021002.
- [167] Christoph Weiss. “Effective time-reversal via periodic shaking”. In: *Journal of Physics: Conference Series*. Vol. 414. 1. IOP Publishing. 2013, p. 012032.
- [168] Can Sun et al. “Observation of the kinetic condensation of classical waves”. In: *Nature Physics* 8.6 (2012), pp. 470–474.
- [169] A. Bohrdt et al. “Scrambling and thermalization in a diffusive quantum many-body system”. In: *New J. Phys* 19 (2017), p. 063001.
- [170] Astrid S de Wijn, B Hess, and B V Fine. “Largest lyapunov exponents for lattices of interacting classical spins”. In: *Physical Review Letters* 109.3 (2012), p. 034101.
- [171] AS De Wijn, B Hess, and B V Fine. “Lyapunov instabilities in lattices of interacting classical spins at infinite temperature”. In: *Journal of Physics A: Mathematical and Theoretical* 46.25 (2013), p. 254012.
- [172] Carlo Danieli et al. “Computational efficiency of numerical integration methods for the tangent dynamics of many-body Hamiltonian systems in one and two spatial dimensions”. In: *arXiv preprint arXiv:1812.01870* (2018).
- [173] GJ Milburn et al. “Quantum dynamics of an atomic Bose-Einstein condensate in a double-well potential”. In: *Physical Review A* 55.6 (1997), p. 4318.
- [174] Augusto Smerzi et al. “Quantum coherent atomic tunneling between two trapped Bose-Einstein condensates”. In: *Physical Review Letters* 79.25 (1997), p. 4950.
- [175] Srikanth Raghavan et al. “Coherent oscillations between two weakly coupled Bose-Einstein condensates: Josephson effects,  $\pi$  oscillations, and macroscopic quantum self-trapping”. In: *Physical Review A* 59.1 (1999), p. 620.
- [176] Anthony J Leggett. “Bose-Einstein condensation in the alkali gases: Some fundamental concepts”. In: *Reviews of Modern Physics* 73.2 (2001), p. 307.
- [177] Michael Albiez et al. “Direct observation of tunneling and nonlinear self-trapping in a single bosonic Josephson junction”. In: *Physical Review Letters* 95.1 (2005), p. 010402.
- [178] Ramaz Khomeriki, Stefano Ruffo, and Sandro Wimberger. “Driven collective quantum tunneling of ultracold atoms in engineered optical lattices”. In: *EPL (Europhysics Letters)* 77.4 (2007), p. 40005.
- [179] Amichay Vardi and James R Anglin. “Bose-Einstein condensates beyond mean field theory: Quantum backreaction as decoherence”. In: *Physical Review Letters* 86.4 (2001), p. 568.
- [180] Martin Holthaus. “Bloch oscillations and Zener breakdown in an optical lattice”. In: *Journal of Optics B: Quantum and Semiclassical Optics* 2.5 (2000), p. 589.

- [181] Wolfgang Muessel et al. “Optimized absorption imaging of mesoscopic atomic clouds”. In: *Applied Physics B* 113.1 (2013), pp. 69–73.
- [182] DB Hume et al. “Accurate atom counting in mesoscopic ensembles”. In: *Physical Review Letters* 111.25 (2013), p. 253001.
- [183] MR Andrews et al. “Direct, nondestructive observation of a Bose condensate”. In: *Science* 273.5271 (1996), p. 84.
- [184] H-J Miesner et al. “Bosonic stimulation in the formation of a Bose-Einstein condensate”. In: *Science* 279.5353 (1998), pp. 1005–1007.
- [185] Kali E Wilson et al. “In situ imaging of vortices in Bose-Einstein condensates”. In: *Physical Review A* 91.2 (2015), p. 023621.
- [186] Cristina Figl et al. “Demonstration and characterization of a detector for minimally destructive detection of Bose condensed atoms in real time”. In: *Applied Optics* 45.15 (2006), pp. 3415–3419.
- [187] André Eckardt, Christoph Weiss, and Martin Holthaus. “Superfluid-insulator transition in a periodically driven optical lattice”. In: *Physical Review Letters* 95.26 (2005), p. 260404.
- [188] H Lignier et al. “Dynamical control of matter-wave tunneling in periodic potentials”. In: *Physical Review Letters* 99.22 (2007), p. 220403.
- [189] C Sias et al. “Resonantly enhanced tunneling of Bose-Einstein condensates in periodic potentials”. In: *Physical Review Letters* 98.12 (2007), p. 120403.
- [190] A Zenesini et al. “Time-resolved measurement of Landau-Zener tunneling in periodic potentials”. In: *Physical Review Letters* 103.9 (2009), p. 090403.
- [191] Herman Feshbach. “Unified theory of nuclear reactions”. In: *Annals of Physics* 5.4 (1958), pp. 357–390.
- [192] S Inouye et al. “Observation of Feshbach resonances in a Bose-Einstein condensate”. In: *Nature* 392.6672 (1998), pp. 151–154.
- [193] JL Roberts et al. “Resonant Magnetic Field Control of Elastic Scattering in Cold R 85 b”. In: *Physical Review Letters* 81.23 (1998), p. 5109.
- [194] Neil R Claussen et al. “Very-high-precision bound-state spectroscopy near a 85 Rb Feshbach resonance”. In: *Physical Review A* 67.6 (2003), p. 060701.
- [195] M Gustavsson et al. “Control of interaction-induced dephasing of Bloch oscillations”. In: *Physical Review Letters* 100.8 (2008), p. 080404.
- [196] CA Sackett et al. “Measurements of collective collapse in a Bose-Einstein condensate with attractive interactions”. In: *Physical Review Letters* 82.5 (1999), p. 876.
- [197] Jordan M Gerton et al. “Direct observation of growth and collapse of a Bose-Einstein condensate with attractive interactions”. In: *Nature* 408.6813 (2000), pp. 692–695.
- [198] Elizabeth A Donley et al. “Dynamics of collapsing and exploding Bose-Einstein condensates”. In: *Nature* 412.6844 (2001), pp. 295–299.

- [199] L Khaykovich et al. “Formation of a matter-wave bright soliton”. In: *Science* 296.5571 (2002), pp. 1290–1293.
- [200] Kevin E Strecker et al. “Formation and propagation of matter-wave soliton trains”. In: *Nature* 417.6885 (2002), pp. 150–153.
- [201] Christoph Eigen et al. “Observation of Weak Collapse in a Bose-Einstein Condensate”. In: *Physical Review X* 6.4 (2016), p. 041058.
- [202] W-K Rhim, Alexander Pines, and John S Waugh. “Violation of the spin-temperature hypothesis”. In: *Physical Review Letters* 25.4 (1970), p. 218.
- [203] Charles P Slichter. *Principles of magnetic resonance*. Vol. 1. Springer Science & Business Media, 2013.
- [204] Sonja Franke-Arnold et al. “Optical ferris wheel for ultracold atoms”. In: *Optics Express* 15.14 (2007), pp. 8619–8625.
- [205] Luigi Amico et al. “Superfluid qubit systems with ring shaped optical lattices”. In: *Scientific Reports* 4 (2014).
- [206] J Bolte, B Müller, and A Schäfer. “Ergodic properties of classical SU (2) lattice gauge theory”. In: *Physical Review D* 61.5 (2000), p. 054506.
- [207] Á Fülöp and T S Biró. “Towards the equation of state of a classical SU (2) lattice gauge theory”. In: *Physical Review C* 64.6 (2001), p. 064902.
- [208] Tamas S Biró, Berndt Müller, and Sergei G Matinyan. “Chaotic Quantization: Maybe the Lord plays dice, after all?” In: *Decoherence and Entropy in Complex Systems*. Springer, 2004, pp. 164–179.
- [209] Teiji Kunihiro et al. “Chaotic behavior in classical Yang-Mills dynamics”. In: *Physical Review D* 82.11 (2010), p. 114015.
- [210] Hideaki Iida et al. “Entropy production in classical Yang-Mills theory from glasma initial conditions”. In: *Physical Review D* 88.9 (2013), p. 094006.
- [211] Hirokazu Fujisaka. “Statistical dynamics generated by fluctuations of local Lyapunov exponents”. In: *Progress of theoretical physics* 70.5 (1983), pp. 1264–1275.
- [212] R Benzi et al. “Characterisation of intermittency in chaotic systems”. In: *Journal of Physics A: Mathematical and General* 18.12 (1985), p. 2157.
- [213] R Benzi et al. “Characterization of the long-time and short-time predictability of low-order models of the atmosphere”. In: *Journal of the atmospheric sciences* 56.20 (1999), pp. 3495–3507.
- [214] Takuma Akimoto et al. “Generalized Lyapunov exponent as a unified characterization of dynamical instabilities”. In: *Physical Review E* 91.1 (2015), p. 012926.
- [215] P-W\_ Anderson and PR Weiss. “Exchange narrowing in paramagnetic resonance”. In: *Reviews of Modern Physics* 25.1 (1953), p. 269.
- [216] Jorge Chávez-Carlos et al. “Quantum and classical Lyapunov exponents in atom-field interaction systems”. In: *Physical Review Letters* 122.2 (2019), p. 024101.

- [217] IC Percival. “Regular and irregular spectra”. In: *Journal of Physics B: Atomic and Molecular Physics* 6.9 (1973), p. L229.
- [218] Y Alhassid and A Novoselsky. “Chaos in the low-lying collective states of even-even nuclei: Quantal fluctuations”. In: *Physical Review C* 45.4 (1992), p. 1677.
- [219] Thomas Guhr, Axel Müller–Groeling, and Hans A Weidenmüller. “Random-matrix theories in quantum physics: common concepts”. In: *Physics Reports* 299.4-6 (1998), pp. 189–425.
- [220] M Falcioni, U Marini Bettolo Marconi, and Angelo Vulpiani. “Ergodic properties of high-dimensional symplectic maps”. In: *Physical Review A* 44.4 (1991), p. 2263.
- [221] Arkady Pikovsky and Antonio Politi. “Dynamic localization of Lyapunov vectors in spacetime chaos”. In: *Nonlinearity* 11.4 (1998), p. 1049.
- [222] Stefano Ruffo. “Lyapunov Spectra in Spatially Extended Systems”. In: *Cellular Automata and Complex Systems*. Springer, 1999, pp. 153–180.
- [223] Arkady Pikovsky and Antonio Politi. “Dynamic localization of Lyapunov vectors in Hamiltonian lattices”. In: *Physical Review E* 63.3 (2001), p. 036207.
- [224] Harald A Posch and Ch Forster. “Lyapunov instability and collective tangent space dynamics of fluids”. In: *International Conference on Computational Science*. Springer. 2002, pp. 1170–1175.
- [225] Tooru Taniguchi and Gary P Morriss. “Localized behavior in the Lyapunov vectors for quasi-one-dimensional many-hard-disk systems”. In: *Physical Review E* 68.4 (2003), p. 046203.
- [226] Hadrien Bosetti and Harald A Posch. “Covariant Lyapunov vectors for rigid disk systems”. In: *Chemical Physics* 375.2 (2010), pp. 296–308.
- [227] Pavel V Kuptsov and Anna V Kuptsova. “Predictable nonwandering localization of covariant Lyapunov vectors and cluster synchronization in scale-free networks of chaotic maps”. In: *Physical Review E* 90.3 (2014), p. 032901.
- [228] Massimo Cencini, Fabio Cecconi, and Angelo Vulpiani. *Chaos: from simple models to complex systems*. World Scientific, 2010.
- [229] Thudiyangal Mithun et al. “Weakly Nonergodic Dynamics in the Gross-Pitaevskii Lattice”. In: *Physical Review Letters* 120.18 (2018), p. 184101.
- [230] Carlo Danieli, D K Campbell, and Sergej Flach. “Intermittent many-body dynamics at equilibrium”. In: *Physical Review E* 95.6 (2017), p. 060202.
- [231] Alfred Zong et al. “Evidence for topological defects in a photoinduced phase transition”. In: *Nature Physics* 15.1 (2019), pp. 27–31.
- [232] Pavel E Dolgirev et al. “Amplitude dynamics of the charge density wave in LaTe 3: Theoretical description of pump-probe experiments”. In: *Physical Review B* 101.5 (2020), p. 054203.
- [233] VJ Emery and SA Kivelson. “Importance of phase fluctuations in superconductors with small superfluid density”. In: *Nature* 374.6521 (1995), pp. 434–437.

- [234] EW Carlson et al. “Classical phase fluctuations in high temperature superconductors”. In: *Physical Review Letters* 83.3 (1999), p. 612.
- [235] George Gruner. *Density waves in solids*. CRC press, 2018.
- [236] Hong Yao et al. “Theory of stripes in quasi-two-dimensional rare-earth tellurides”. In: *Physical Review B* 74.24 (2006), p. 245126.
- [237] BF Hu et al. “Coexistence and competition of multiple charge-density-wave orders in rare-earth tritellurides”. In: *Physical Review B* 90.8 (2014), p. 085105.
- [238] JP Pouget et al. “Neutron-scattering investigations of the Kohn anomaly and of the phase and amplitude charge-density-wave excitations of the blue bronze K 0.3 MoO 3”. In: *Physical Review B* 43.10 (1991), p. 8421.
- [239] B Hennion, JP Pouget, and M Sato. “Charge-density-wave phase elasticity of the blue bronze”. In: *Physical Review Letters* 68.15 (1992), p. 2374.
- [240] Michael E Manley et al. “Supersonic propagation of lattice energy by phasons in fresnoite”. In: *Nature Communications* 9.1 (2018), pp. 1–8.
- [241] M Lavagnini et al. “Evidence for coupling between charge density waves and phonons in two-dimensional rare-earth tritellurides”. In: *Physical Review B* 78.20 (2008), p. 201101.
- [242] RV Yusupov et al. “Single-Particle and Collective Mode Couplings Associated with 1-and 2-Directional Electronic Ordering in Metallic R Te 3 (R= Ho, Dy, Tb)”. In: *Physical Review Letters* 101.24 (2008), p. 246402.
- [243] N Ru and IR Fisher. “Thermodynamic and transport properties of Y Te 3, La Te 3, and Ce Te 3”. In: *Physical Review B* 73.3 (2006), p. 033101.
- [244] Franco Dalfovo et al. “Theory of Bose-Einstein condensation in trapped gases”. In: *Reviews of Modern Physics* 71.3 (1999), p. 463.